JYVÄSKYLÄ STUDIES IN BIOLOGICAL AND ENVIRONMENTAL SCIENCE
306

Elina Dadu

Interactions of α2β1 Integrin and its Ligands, Type I Collagen and Echovirus 1

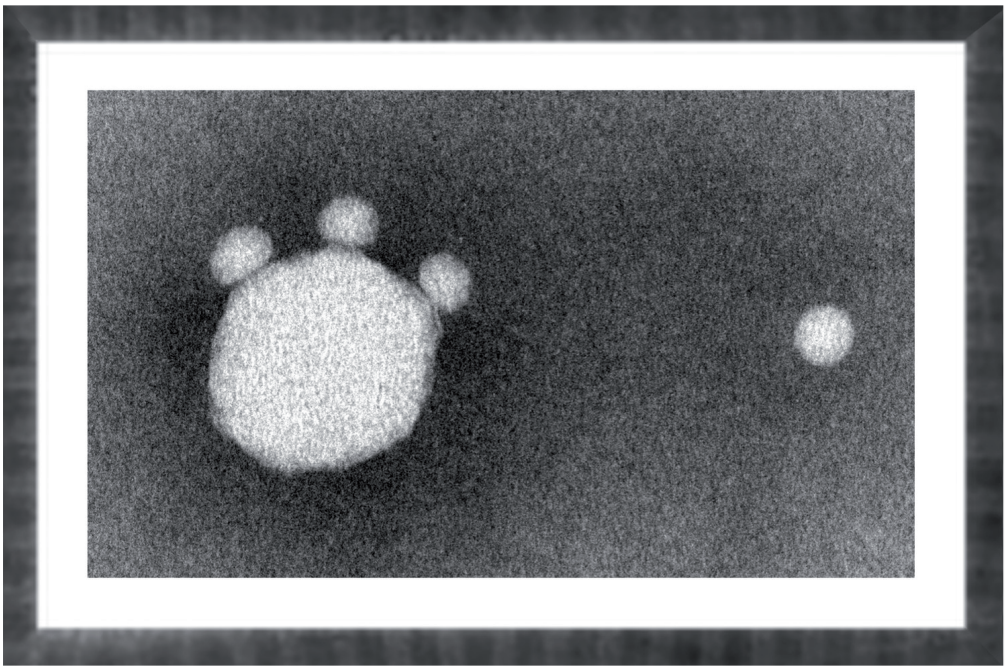

JYVÄSKYLÄN YLIOPISTO

JYVÄSKYLÄ STUDIES IN BIOLOGICAL AND ENVIRONMENTAL SCIENCE 306

Elina Dadu

Interactions of α2β1 Integrin and its Ligands, Type I Collagen and Echovirus 1

Esitetään Jyväskylän yliopiston matemaattis-luonnontieteellisen tiedekunnan suostumuksella
julkisesti tarkastettavaksi yliopiston Ylistönrinteellä salissa YAA303
syyskuun 25. päivänä 2015 kello 12.

Academic dissertation to be publicly discussed, by permission of
the Faculty of Mathematics and Science of the University of Jyväskylä,
in Ylistönrinne, hall YAA303, on September 25, 2015 at 12 o'clock noon.

UNIVERSITY OF JYVÄSKYLÄ

JYVÄSKYLÄ 2015

Interactions of α2β1 Integrin and its Ligands, Type I Collagen and Echovirus 1

JYVÄSKYLÄ STUDIES IN BIOLOGICAL AND ENVIRONMENTAL SCIENCE 306

Elina Dadu

Interactions of α2β1 Integrin and its Ligands, Type I Collagen and Echovirus 1

UNIVERSITY OF JYVÄSKYLÄ

JYVÄSKYLÄ 2015

Editors
Varpu Marjomäki
Department of Biological and Environmental Science, University of Jyväskylä
Pekka Olsbo, Sini Tuikka
Publishing Unit, University Library of Jyväskylä

Jyväskylä Studies in Biological and Environmental Science
Editorial Board

Jari Haimi, Anssi Lensu, Timo Marjomäki, Varpu Marjomäki
Department of Biological and Environmental Science, University of Jyväskylä

Cover picture: Collage of transmission electron microscope images of collagen fibrils, echovirus 1 particles and a lipid vesicle. Picture by Elina Dadu.

URN:ISBN:978-951-39-6288-3
ISBN 978-951-39-6288-3 (PDF)

ISBN 978-951-39-6287-6 (nid.)
ISSN 1456-9701

Jyväskylä University Printing House, Jyväskylä 2015

ABSTRACT

Dadu, Elina
Interactions of α2β1 integrin and its ligands, type I collagen and echovirus 1
Jyväskylä: University of Jyväskylä, 2015, 87 p.
(Jyväskylä Studies in Biological and Environmental Science
ISSN 1456-9701; 306)
ISBN 978-951-39-6287-6 (nid.)
ISBN 978-951-39-6288-3 (PDF)
Yhteenveto: Kollageenireseptori α2β1-integriinin ja sen ligandien, tyypin I kollageenin ja echovirus 1:n, vuorovaikutukset
Diss.

Integrins are a large family of cell membrane receptors that attach cells to their surroundings. A subgroup of the integrins bind collagens, major constituents of extracellular matrix. Type I collagen molecules are the most abundant of them, forming large fibrils in the extracellular matrix. Here, the interactions of collagen receptor integrins and their ligands were investigated. The major type I collagen receptor, α2β1 integrin, was seen to be a functional receptor for type I collagen fibrils. In addition, the effect of integrins on collagen fibril formation was studied *in vitro*. The results suggest that integrins might participate in guiding collagen fibrillogenesis *in vivo*. In addition to collagen, echovirus 1 (EV1) also uses α2β1 integrin as a receptor. EV1 is a human pathogen and belongs to the *Enterovirus B* species. It enters cells via endocytosis and must release its genome and escape the vesicular endocytic structure before it can start the propagation of new virus particles. These early steps of EV1 life cycle were studied. Particularly, interactions of EV1 with lipid membranes and the effect α2β1 integrin has on these interactions were studied. Lipid membrane composition affected the affinity of virus particles to membranes. Intrestingly, flattening of EV1 particles was seen with the particles bound to membranes. The EV1 particles spread along the membranes and the spreading effect was lipid type specific. Presence of integrin enhanced the effect, suggesting that interactions of EV1 and integrin lead to changes in virus structure. These changes could include increased hydrophobicity of the virus surface and greater elasticity of the virus particle. In addition to lipid interaction studies, uncoating or genome release from EV1 particles was investigated using Raman spectroscopy. The observations suggest that uncoating leads to increased porosity of virus particles, and involves a reduction in the α-helical content of the capsid proteins. In conclusion, this thesis reveals new information on interactions of collagen receptor integrins and their ligands. Novel features of virus-lipid interactions were discovered, and the Raman spectroscopic study of EV1 promotes method development in virology.

Keywords: Collagen fibrils; enterovirus; integrin; lipid membranes; molecular interactions; Raman spectroscopy.

Author's address Elina Dadu
Department of Biological and Environmental Science
P.O. Box 35
FI-40014 University of Jyväskylä
Finland
elina.dadu@jyu.fi

Supervisor Professor Janne Ihalainen
Department of Biological and Environmental Science
P.O. Box 35
FI-40014 University of Jyväskylä
Finland

Professor Matti Vuento
Department of Biological and Environmental Science
P.O. Box 35
FI-40014 University of Jyväskylä
Finland

Reviewers Docent Maria Söderlund-Venermo
Department of Virology
P.O. Box 21
00014 University of Helsinki
Finland

Dr Olli Laitinen
University of Tampere
BioMediTech
Biokatu 8, 12
33520 Tampere
Finland

Opponent Reader Roman Tuma
Institute of Molecular and Cellular Biology
Faculty of Biological Sciences
University of Leeds, Leeds, LS2 9JT
United Kingdom

CONTENTS

LIST OF ORIGINAL PUBLICATIONS

The thesis is based on the following original papers, which will be referred to in the text by their Roman numerals I-III.

I Jokinen J.*, Dadu E.*, Nykvist P., Käpylä J., White D.J., Ivaska J., Vehviläinen P., Reunanen H., Larjava H., Häkkinen L. & Heino J. 2004. Integrin-mediated Cell Adhesion to Type I Collagen Fibrils. *Journal of Biological Chemistry* 279: 31956-31963.

II Dadu E., Marjomäki V. & Ihalainen J. 2015. Direct Interactions of Echovirus 1 and Lipid Membranes. Manuscript.

III Ruokola P., Dadu E., Kazmertsuk A., Häkkänen H., Marjomäki V. & Ihalainen J.A. 2014. Raman Spectroscopic Signatures of Echovirus 1 Uncoating. *Journal of Virology* 88: 8504-8513.

* The authors contributed equally to this work.

RESPONSIBILITIES

I I did *in vitro* fibrillogenesis of collagen, purification of αI-GST fusion proteins, collagen binding assays for recombinant α1I and α2I domains, immunoelectron microscopy analysis of α2I domain binding to collagen fibrils, tests of integrin α1I and α2I domains in collagen fibrillogenesis, and cell spreading assays. I analyzed the data and made most of the figures from these experiments and participated in the writing process.

II I planned and conducted the experiments, and analyzed the data. I wrote the article and made the figures.

III I purified and analyzed EV1 for the Raman measurements in solution. I conducted the Raman measurements of EV1 in solution, and analyzed the spectroscopy data. I wrote the article together with other authors, and participated in making the figures of EV1 Raman measurements.

Study I was performed under the supervision of Professor Jyrki Heino and Dr Daniel James White. Studies II and III were conducted under the supervision of Professor Janne Ihalainen. The original paper I is also part of the dissertation of Johanna Jokinen (University of Turku, 2010). The Raman measurements of dry EV1 and 0.9 mg/ml solution of EV1 in original paper III are a part of the licenciate thesis of Päivi Ruokola (University of Jyväskylä, 2013).

ABBREVIATIONS

α2I	I domain of α2 integrin
α1I	I domain of α1 integrin
α2I-GST	Soluble fusion protein of α2I domain and GST
AmI	Amide I area in Raman spectrum
AmII	Amide II area in Raman spectrum
AmIII	Amide III area in Raman spectrum
BDMV	Belladonna mottle mirus
BPMV	Bean pod mottle virus
CARS	Coherent anti-Stokes Raman spectroscopy
Ch	Cholesterol
CHO	Chinese hamster ovary (cell line)
EV1	Echovirus 1
ECM	Extracellular matrix
Ff	Filamentous bacteriophages
Glu	Glutamine
Gly	Glycine
GST	Glutathione-S-transferase
HIV	Human immunodeficiency virus
Hyp	Hydroxyproline
I domain	Inserted domain, the ligand binding domain of integrin α subunit
IR	Infrared
K_d	Dissociation constant
MIDAS	Metal ion dependent adhesion site
MVB	Multivesicular body
PC	Phosphatidyl choline
PDB	Protein Data Bank
PG	Phosphatidyl glycerol
Phe	Phenyl alanine
Pro	Proline
SERS	Surface enhanced Raman spectroscopy
SM	Sphingomyelin
TEM	Transmission electron microscopy
TERS	Tip enhanced Raman spectroscopy
Trp	Tryptophan
TYMV	Turnip yellow mosaic virus
Tyr	Tyrosine
VP	Viral protein

1 INTRODUCTION

The extracellular matrix (ECM) enables the life of multicellular organisms. Cells use it to adhere to each other, to move, and to exchange information. In a significant role are the different collagens, which form fibrils or networks or assist other collagens. The most abundant collagen, type I collagen, forms long, strong fibrils and bundles in the ECM. Integrins are cell membrane receptors that bind cells to the molecules of the ECM or to each other. Each integrin is a heterodimer of one alpha subunit and one beta subunit. A subgroup of integrins, namely α1β1, α2β1, α10β1, and α11β1 integrins, function as collagen receptors. One of the key collagen receptors is α2β1 integrin, whose primary interaction partner in the ECM is type I collagen. Even though *in vivo* type I collagen occurs primarily in fibrils made of numerous collagen monomers, previous studies about integrin binding to collagen have been conducted with monomeric collagen. In this thesis, binding of integrins to collagen fibrils and the potential of integrins to participate in collagen fibrillogenesis were investigated. The results confirm that α2β1 integrin is a functional receptor for type I collagen fibrils, and that integrins may be involved in regulation of collagen fibrillogenesis.

Like the ECM, integrins are also vital to all multicellular organisms and are assumed to have existed as long as them. Several viruses utilize the plasma membrane integrins as a means to enter cells. One example is human echovirus 1 (EV1), which uses the α2β1 integrin to gain access to cells. EV1 is a small, non-enveloped virus with single-stranded RNA genome. It is a human pathogen and it belongs to the species *Enterovirus B*, the genus *Enterovirus*, and the family *Picornaviridae*. It enters the cells via endocytosis. After endocytosis, the vesicular structure matures into a non-acidic multivesicular body (MVB) containing both the virus and the receptor. The virus genome is released from the MVBs through a poorly understood process to the cytoplasm, where the next generation of viruses is produced. The aim of this thesis was to get a deeper understanding on genome release from virus particles and MVBs. To accomplish this goal, the lipid-virus interactions of EV1 were studied. The lipid composition of membranes was observed to affect these interactions. Also, α2β1

integrin was seen to have an effect on the lipid-virus interactions. Interactions of EV1 and other proteins, and the signaling events of the cell, although important for the infection, are out of the scope of this thesis. Further, the genome release event, or uncoating, of EV1 was studied with Raman spectroscopy. This enabled determination of several uncoating-related chemical and structural changes of the virus.

2 REVIEW OF THE LITERATURE

2.1 Integrins mediate binding of the cytoskeleton to extracellular matrix

Integrins are receptors that span the cell membrane and bind to the cytoskeleton inside the membrane and the extracellular matrix (ECM) on the outside. They are crucial molecules to all multicellular organisms and are assumed to have appeared at the same time as cells started to form multicellular organisms (Johnson *et al.* 2009). Within the integrin family in vertebrates, the collagen receptors form a structurally and functionally distinct subgroup (Hynes and Zhao 2000, Chouhan *et al.* 2014). Collagens form a large family of ECM proteins with almost 30 different members (Ricard-Blum 2011). They are grouped together by the presence of at least one triple-helical domain. Like integrins, they have also appeared early in evolution and are very common in the animal kingdom.

2.1.1 Type I collagen

Collagens are defined by the presence of a typical helix structure where three polypeptide chains with a left-handed twist are wound to a triple helix with a right-handed twist (Figure 1) (Bella *et al.* 1994, Prockop and Kivirikko 1995, Shoulders and Raines 2009, Bella 2014). The triple helix gives high tensile strength to collagen molecules, which provide mechanical stability for tissues. The three polypeptides are connected to each other with interstrand hydrogen bonds (Bella *et al.* 1994). Every third amino acid is the smallest of amino acids, glycine (Gly). The tiny amino acid residue (only one hydrogen atom) is placed inside the helix, and it enables the peptides to get very close to each other. In addition to Gly, about 20% of the residues are imino acids, either proline (Pro) or hydroxyproline (Hyp), which stabilizes the twisting helix structure. The hydroxyprolines produced by posttranslational modification are particularly important to the thermal stability of the triple helix, and the effect comes from

the stabilization of stereoelectronically favourable conformation (Shoulders and Raines 2009). The importance of Pro and Gly residues is further highlighted by their suggested effect in reducing unwanted aggregation of collagen molecules. (Prockop and Kivirikko 1995, Shoulders and Raines 2009)

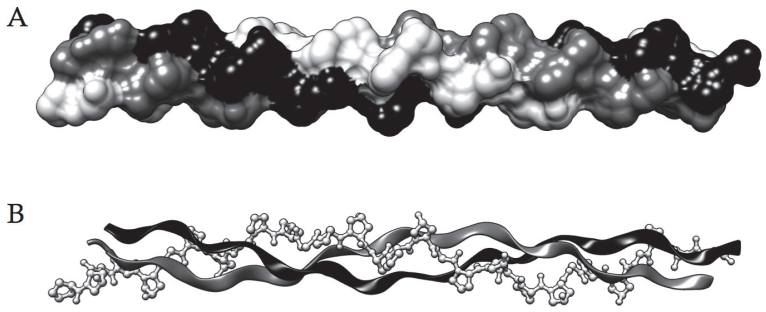

FIGURE 1 Collagen triple helix structure. A) Triple helix is represented as a space-filling model. B) Two of the peptides are drawn as ribbons and one with a ball-and-stick model. The image is based on the x-ray structure of a collagen-like peptide (PDB code 1cag (Bella *et al.* 1994)) and was created with UCSF Chimera. The collagen-like peptide in the figure is about 8 nm long while the length of one collagen monomer is about 300 nm (Kadler *et al.* 1996).

Collagens are divided to subgroups based on their structure and function (Hulmes 2002). Type I collagen belongs to the group of fibril forming collagens along with types II, III, V and XI. Other subgroups are network forming collagens and collagens with interrupted triple helixes. The diameter and degree of order in type I collagen fibrils depend on the tissue (Hulmes 2002, Kadler *et al.* 2008). In the cornea, where optical transparency is necessary, collagen fibrils are narrow (•20 nm) and highly ordered. Contrary to this, the fibrils in mature tendons are very thick (•500 nm), so they can provide the high tensile strength needed in tendons. Type I collagen fibrils also provide structural support to bone, teeth and skin (Hulmes 2002, Kadler *et al.* 2008).

2.1.2 Collagen fibril formation

Cells synthetize monomeric precursors of type I collagen, and secrete them to the extracellular space. The procollagen precursor contains nonhelix propeptides in both ends of the triple helical collagenous domain. Short telopeptides link the propeptides to the triple helical domain (van der Rest and Garrone 1991). After exocytosis, most of the telopeptides are enzymatically removed. This decreases the solubility of collagen monomers leading to spontaneous fibril assembly, which is assisted by the remaining telopeptides (Prockop and Kivirikko 1995, Kuznetsova and Leikin 1999). The interactions with collagen molecules enable the fibril formation, and collagen monomers extracted from tissues form *in vitro* fibrils that have identical periodic structure when compared to fibrils in tissues (Wood 1960a, Wood 1960b, Kadler *et al.*

1996, Kadler *et al.* 2008, Stamov *et al.* 2015). The fibril formation process is illustrated in Figure 2. Figure 2 also shows the striation observed in negatively stained collagen fibres with transmission electron microscopy (TEM). The striation comes from the 300 nm long collagen monomers binding together with repetitive 67 nm steps. The length of the collagen molecules is not equal to a defined number of steps, which leads to gaps between the ends of the monomers. The negative stain locates in the gaps, creating dark stripes (Kadler *et al.* 1996).

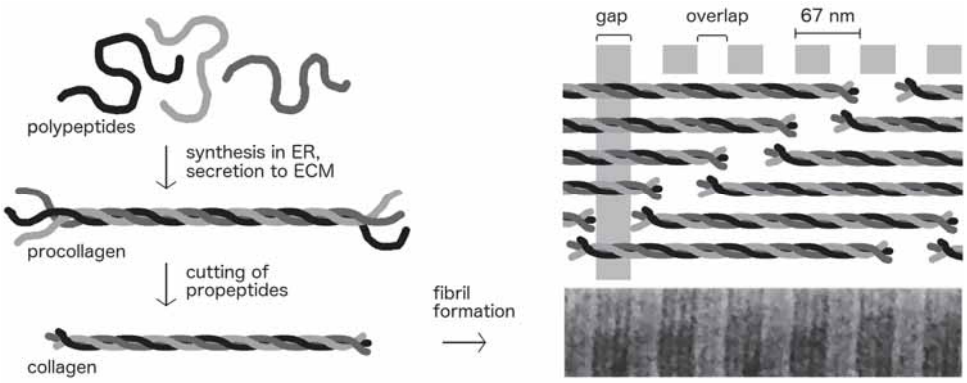

FIGURE 2 Collagen fibril formation and the typical striation of collagen fibril in transmission electron microscopy. Image is based on (Kadler *et al.* 1996).

The molecular organization of fibrils has been extensively studied for decades, with differing interpretations on the crystallinity of fibres, existence of microfibril substructure, and the nucleation of fibrillogenesis (Hulmes and Miller 1979, Piez and Trus 1981, Holmes *et al.* 1992). The current understanding includes nucleation at the start of microfibril formation, after which the microfibrils join, *in vivo* also covalently, to make the fibres. The latest research supports a model where collagen fibrils consist of twisted microfibres wound together in rope-like architecture (Orgel *et al.* 2006, Shoulders and Raines 2009). Recently, high-speed scanning atomic force microscopy has been used to study the dynamics and striation formation of *in vitro* collagen fibrillogenesis (Stamov *et al.* 2015).

The collagen fibrils *in vivo* are stabilized by covalent crosslinking of collagen monomers via N- and C-terminal telopeptides (Orgel *et al.* 2000). Fibrillogenesis also provides stability to the individual collagen molecules themselves (Miles and Ghelashvili 1999). Surprisingly, monomeric type I collagen molecules, whose core function is structural support, have been reported to be unstable at physiological temperature (Leikina *et al.* 2002). The melting time of the triple helix is relatively long, from several hours to days. The collagen molecules are usually quickly incorporated into fibrils after secretion, so most of them do not undergo transition to random coil conformation. The significance of the triple helix instability is, however, unclear.

In addition to the intrinsic factors affecting fibrillogenesis, multiple external factors are also needed for the fibril formation in ECM (Kadler *et al.* 2008). Self-assembly alone can not explain for example the existence of fibrils with tissue-dependent diameters. The extracellular matrix has been found to contain several collagen binding molecules that influence the size of type I collagen fibrils (Danielson *et al.* 1997, Chakravarti *et al.* 1998, Svensson *et al.* 1999). Cell surface receptors have also been noticed to participate in collagen polymerization. This indicates that cells closely control the collagen fibril formation in tissues (Velling *et al.* 2002, Li *et al.* 2003).

2.1.3 Collagen receptor integrins

Integrins are a large family of cell adhesion receptors involved in cell-cell and cell-matrix interactions. They are heterodimers of one alpha and one beta subunit, and some subunits have more than one dimerization partner. The 18 known α subunits and 8 β subunits form together 24 different heterodimers in humans (Heino 2000, Gahmberg *et al.* 2009). All collagen receptor integrins share the common β1 integrin subunit, and there are four unique α subunits resulting in four different heterodimers. The two best known collagen receptors are α1β1 and α2β1 integrins, and α10β1 and α11β1 integrins are the latest additions to the group (Takada and Hemler 1989, Briesewitz *et al.* 1993, Camper *et al.* 1998, Velling *et al.* 1999). The major receptor for type I collagen and other fibril-forming collagens is the α2β1 integrin (Nykvist *et al.* 2000, Tulla *et al.* 2001). The α1β1 is also able to bind to monomers of fibril-forming collagens, although it favors other collagen subtypes (Kern *et al.* 1993, Calderwood *et al.* 1997, Nykvist *et al.* 2000, Tulla *et al.* 2001). Both α1β1 and α2β1 also bind to laminins (Calderwood *et al.* 1997). Less is known about ligand binding preferences of the α10β1 and α11β1 integrins. However, α10 resembles α1 rather than α2 in its ligand binding specificity (Tulla *et al.* 2001) and α11 seems to prefer type I collagen similar to α2 (Zhang *et al.* 2003). Despite the fact that fibril forming collagens are mostly in fibril form *in vivo*, prior to the research included in this dissertation (I), the integrin binding studies with these collagens were conducted with monomeric collagens.

Besides an anchoring function, integrins also transmit signals across the cell membrane regulating many important aspects of cell behavior including proliferation, differentiation, and survival. And while integrins recognise distinct collagen subtypes, they also transmit different signals to the cell. This may be the reason why many cell types express several collagen receptors at the same time. The cellular responses of α1β1 and α2β1 integrins are often opposite to each other (Heino 2000, Heino 2014). The α1β1 integrin is known to stimulate cell proliferation (Pozzi *et al.* 1998, Ekholm *et al.* 2002) and suppress collagen synthesis (Riikonen *et al.* 1995, Langholz *et al.* 1995, Pozzi *et al.* 1998, Gardner *et al.* 1999, Ekholm *et al.* 2002) whereas α2β1 integrin can inhibit cell growth and increase collagen synthesis (Riikonen *et al.* 1995, Langholz *et al.* 1995, Gardner *et al.* 1999, Ivaska *et al.* 1999, Ravanti *et al.* 1999). The properties of α10β1 and α11β1 integrins are not known as thoroughly, but they are known to have roles in the

skeletal and muscle development of the embryo (Tiger *et al.* 2001, Lundgren-Akerlund and Aszodi 2014).

The ligand binding of integrins to collagen is mediated by an independently folding structural domain of the α subunit, the inserted domain (I domain) (Svensson *et al.* 1999, Velling *et al.* 2002, Li *et al.* 2003, White *et al.* 2004). The I domains of collagen receptor integrins are highly conserved structures, but there are small differences that may provide specific ligand binding characteristics for different integrins (Kamata and Takada 1994, Kern *et al.* 1994, Tulla *et al.* 2001, Zhang *et al.* 2003). The strongest known binding site of integrin involves a GFOGER sequence (Gly-Phe-Hyp-Gly-Glu-Arg) on collagen, and two other high affinity binding sites are also located in the collagen monomer with variations to this sequence (Knight *et al.* 2000). The I domain binding to collagen (illustrated in Figure 3) is mediated by coordination of a divalent metal ion (usually magnesium or manganese) by amino acids from both integrin and collagen (Emsley *et al.* 2000). However, also Co^{2+} ions that have been used to obtain the x-ray structure of α2I domain bound to collagen-like peptide (Figure 3) enable the binding of the I domain to collagen (Emsley *et al.* 2000). In integrin, the amino acids participating in the coordination of the metal ion belong to the metal ion-dependent adhesion site (MIDAS motif). In the collagen GFOGER sequence, a negatively charged amino acid, glutamate (Glu), participates to metal ion coordination (Tuckwell *et al.* 1995, Dickeson *et al.* 1997). In addition to the metal ion coordination, the recognition of the triple helix is mediated by amino acids near the α integrin MIDAS motif. In non-collagen receptor integrins without an I domain, a MIDAS motif in an I-like domain of the β subunit is responsible for ligand binding (Takagi 2007).

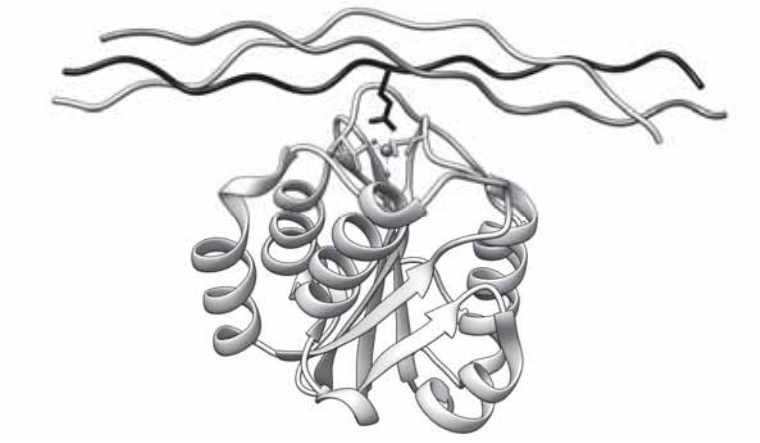

FIGURE 3 Binding of the integrin α2I domain (on the bottom) to collagen triple helix (on the top) is mediated by metal ion coordination. The amino acid residues participating in coordination of the metal ion are shown. Image is based on the x-ray structure of the α2I domain with a collagen-mimetic peptide and a Co^{2+} ion (PDB code 1dzi (Emsley *et al.* 2000)), and was created using UCSF Chimera.

Collagen receptor integrins have three levels of conformational changes related to their activity (Figure 4). The most noticeable of them is the change between the bent and extended conformations (Springer 2002, Takagi *et al.* 2002, Connors *et al.* 2007). The bent form is a conformation with restricted activity or affinity, and the integrin is folded to a globular shape with the ligand-binding domain pointing towards the plasma membrane (Xiong *et al.* 2001, Beglova *et al.* 2002). The extended conformation resembles integrin standing on straight legs with the I domain pointing away from the cell membrane. The opening or closing of the legs also has important effects on affinity and activity (Connors *et al.* 2007, Bennett 2015). The conformation where the receptor is extended and its legs are open is considered the most active conformation with high affinity to ligands. The legs also facilitate the clustering of integrins with each other via interactions of the leg domains, which is correlated with high affinity, and endocytosis of the receptor-ligand complexes (Whittard and Akiyama 2001, Upla *et al.* 2004). Cells can regulate integrin activity with proteins binding to the small cytoplasmic domains of integrins, so called inside-out regulation (Tadokoro *et al.* 2003). The binding of a ligand to the bent conformation can also activate the receptor, so called outside-in activation (Springer and Wang 2004). The corresponding variation in ligand binding affinities comes from active and inactive conformations of the I domains (Emsley *et al.* 2000, Connors *et al.* 2007). However, this traditional interpretation of integrin activation has become more complex when ligands binding to the "inactive" conformation have been discovered (Gahmberg *et al.* 2009). For example echovirus 1 has been reported to bind to the inactive conformation of α2β1 integrin (Jokinen *et al.* 2010). Although the activation with type I collagen ligand does seem to follow the traditional bent/inactive, extended/active rule, the whole story is not that simple.

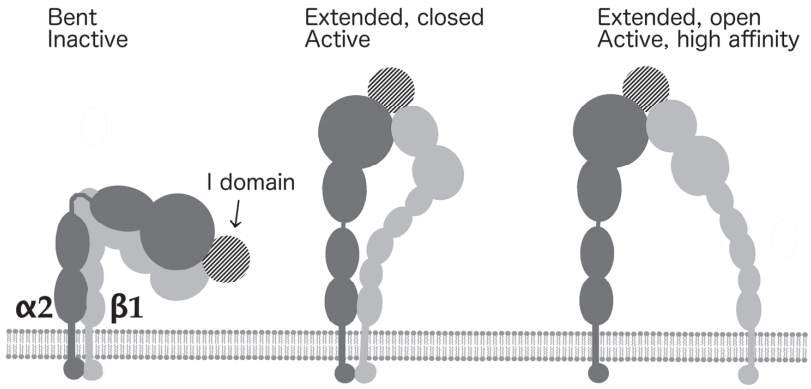

FIGURE 4 The α2β1 integrin conformations and collagen binding affinities. Integrins can be in a bent, inactive/low affinity conformation. Activation correlates with an extended conformation. Further, if integrin legs are separated, the conformation has high activity and affinity to collagen. Image is based on (Springer 2002).

2.2 Echovirus 1 utilizes α2β1 integrin for entering cells

Several viruses use integrins as receptors (Stewart and Nemerow 2007). The human pathogens echovirus 1 and rotaviruses are known to utilise the collagen receptor α2β1 integrin (Bergelson *et al.* 1992, Hewish *et al.* 2000). The α2β1 integrin, also known as VLA-2, platelet glycoprotein Ia/IIa, and CD49b/CD29 (Kehrel 1995), is expressed in several cell types of endothelial and epithelial origins (Mizejewski 1999, Gilcrease 2007).

2.2.1 Enteroviruses

The name echovirus comes from Enteric Cytopathic Human Orphan (ECHO) virus, as echoviruses were originally discovered in the gastrointestinal (enteric) tract and were not immediately associated with diseases. It is currently acknowledged, however, that echoviruses are human pathogens (Hill 1996). They belong to the *Picornavirus* family and the *Enterovirus* genus. The *Enterovirus* genus is divided to 12 species currently named *Enteroviruses A-J* and *Rhinoviruses A-C*, which include many clinically important viruses like echoviruses, coxsackieviruses and polioviruses (Anon. 2014, Anon. 2015, Adams *et al.* 2015). EV1 belongs to the *Enterovirus B* species. Enteroviruses cause a wide range of symptoms that vary from mild infections (flu-like symptoms, rash, herpangina) to aseptic meningitis, heart muscle damage and paralysis (Tuthill *et al.* 2010). They have also been associated with chronic diseases like type 1 diabetes, cardiomyopathies and atherosclerosis (Roivainen *et al.* 1998, Hober and Sauter 2010).

Picornaviruses are small, non-enveloped viruses with single-stranded RNA genomes. They have icosahedral capsids made of 60 copies of identical protomers. Each protomer is comprised of four viral proteins (VP1, VP2, VP3 and VP4). Even though picornaviruses are non-enveloped, two kinds of fatty acid molecules are found in the virus capsids. In the N-terminus of VP4, a covalently linked myristate has been discovered (Chow *et al.* 1987). Buried in the core of the VP1 protein is another fatty acid molecule, most often palmitate, also called the stability-mediating pocket factor (Smyth *et al.* 2003). The fatty acid is important for the proper function of enteroviruses and many antiviral drugs against enteroviruses bind to the same pocket (Muckelbauer *et al.* 1995, Thibaut *et al.* 2012). The 7.5 kb long genome inside the symmetric protein capsid is generally considered to be spatially disordered (Hogle *et al.* 1985), although some genome organization has been seen with rhinovirus (Pickl-Herk *et al.* 2013).

2.2.2 The life cycle of echovirus 1

The life cycle of EV1 starts from binding to the cell surface receptor α2β1 integrin (Bergelson *et al.* 1992). The binding of virus to integrins leads to clustering of the receptors, which triggers endocytosis, and via maturation of

the endosomal structures the virus ends up in non-acidic multivesicular bodies (MVBs) (Marjomäki *et al.* 2002, Pietiäinen *et al.* 2004, Upla *et al.* 2004, Karjalainen *et al.* 2008, Karjalainen *et al.* 2011). The viral RNA is then released from the MVBs to the cytoplasm for replication and propagation of a new virus generation. Finally, the newly formed virions are released through the plasma membrane to start the next cycle of infection. The early steps of the EV1 life cycle and the time scales related to it are illustrated in Figure 5.

EV1 binds to the ligand binding domain (I domain) of the inactive conformation of α2β1 integrin (Jokinen *et al.* 2010). The binding between virus and integrin is strong - it has been shown to be at least ten times stronger (K_d = 1-2 nM) than the binding of integrin and its primary ligand, type I collagen (K_d = 20-40 nM) (Xing *et al.* 2004, Jokinen *et al.* 2010). In poliovirus, often considered a model virus for enteroviruses, receptor binding induces formation of uncoating intermediate virus particles, followed by a rapid penetration through the membrane (Kaplan *et al.* 1990, Yafal *et al.* 1993). The binding of the receptor to EV1, on the contrary, does not induce the formation of uncoating intermediate particles, and the penetration through the membrane happens later than in poliovirus infection (Pietiäinen *et al.* 2004, Xing *et al.* 2004). The EV1 particles are observed in small vesicles within few minutes after binding to the receptor, then in tubulovesicular structures, which mature to MVBs by growing intraluminal vesicles (Karjalainen *et al.* 2011). Maturation of the MVBs takes a couple of hours, and the receptor stays in the MVBs with the virus (Karjalainen *et al.* 2011). Uncoating of the virus particles starts already within half an hour after entry, with the maximum amounts detected from one hour onwards from the start of infection (Marjomäki *et al.* 2002, Soonsawad *et al.* 2014). Breakages in the MVB membranes are detected starting at about the same time as maximum amounts of virus genomes are released from the EV1 particles (Soonsawad *et al.* 2014). After about three hours after entry, genome replication starts and new virions are formed (Pietiäinen *et al.* 2004, Upla *et al.* 2008).

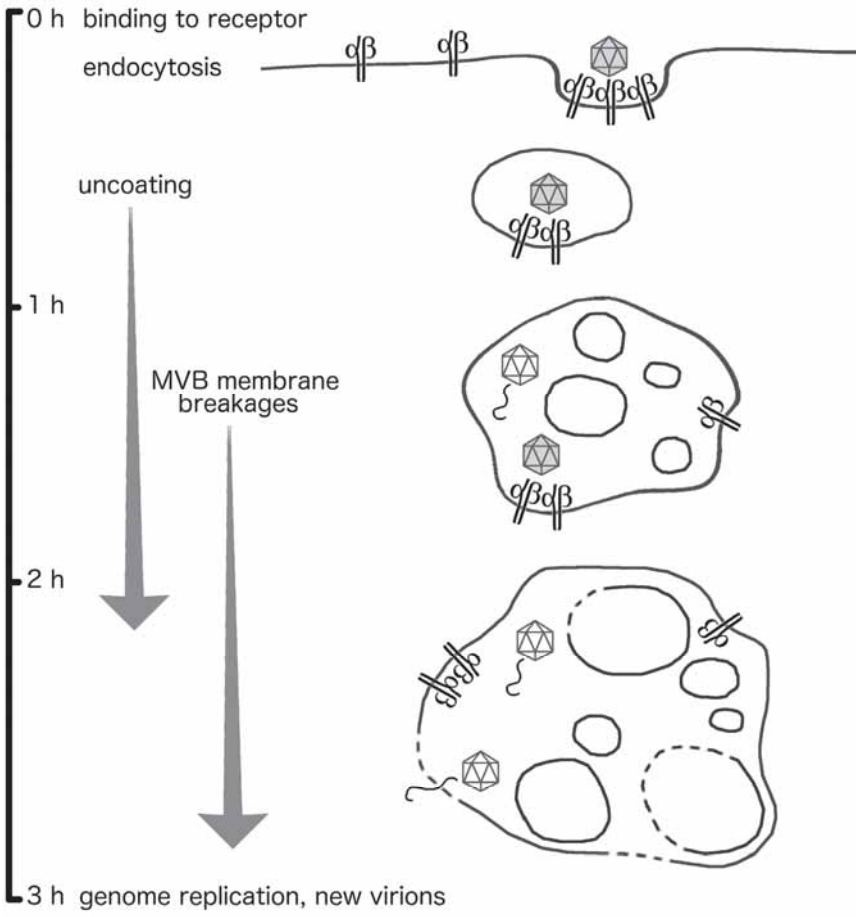

FIGURE 5 A schematic view of the early steps of EV1 life cycle. The life cycle begins with EV1 binding to the α2β1 integrin on the plamsa membrane. The virus-receptor complex is taken into the cell via endocytosis. The vesicular structure matures to a multivesicular body (MVB) by the growth of intraluminal vesicles. The virus genome is released from the MVB to start the propagation of new virus generation in the cytoplasm. The figure is based on (Marjomäki *et al.* 2002, Pietiäinen *et al.* 2004, Karjalainen *et al.* 2011, Soonsawad *et al.* 2014).

Normally in the cell, endocytosis leads to gradual acidification of the endosomes and recycling of the endocytosed material to plasma membrane or the degradation of it in lysosomes. The virus-induced MVB structures resemble normal endosomes to some degree, by for example having intraluminal vesicles. However, the virus-induced MVBs and the intraluminal vesicles within them are much larger (Soonsawad *et al.* 2014). The virus MVBs also have other major differences to endosomes, for example non-acidic pH (Karjalainen *et al.* 2011). Many viruses utilize acidification of endosomes to induce structural changes needed for penetration of the endosomal membrane (Helenius 1984, Suikkanen *et al.* 2003, Li *et al.* 2014). EV1 is an enterovirus, infecting cells in the acidic environment of the gastrointestinal tract. Hence, it is quite logical that it

does not use acidification as a means to trigger structural changes. The non-acidity of virus-induced MVBs has been shown with other enteroviruses as well (Huttunen *et al.* 2014).

2.2.3 Uncoating

The early steps of infection, including binding to receptors, endocytosis pathways, and the uncoating of enteroviruses have been extensively studied. However, knowledge of the physical and chemical details of uncoating or genome release of EV1 particles is still limited. The uncoating of enterovirus particles has been studied by initiating the genome release using heat treatments. For example, temperature manipulations have been concluded to irreversibly convert intact polioviruses to virus particles that resemble naturally occurring uncoating intermediates (Curry *et al.* 1996, Bubeck *et al.* 2005, Lin *et al.* 2011). Uncoating studies using such temperature-manipulated particles have for example revealed the site of ejecting the genome on the virus capsid (Levy *et al.* 2010, Bostina *et al.* 2011).

The main structural changes known to happen in enterovirus uncoating, besides genome release, are the exposure of VP1 N-termini at the capsid surface (Racaniello 1996), and the ejection of the VP4 proteins (Fricks and Hogle 1990). The release of the stability-mediating pocket factor is also considered a prerequisite for the uncoating process, as was shown for bovine enterovirus (Smyth and Martin 2002, Smyth *et al.* 2003). In poliovirus, the N-terminus of VP1 is externalized to the virion surface during the uncoating process that increases the overall hydrophobicity of the particle (Racaniello 1996). Figure 6 illustrates the capsid structure and one separated protomer with different capsid proteins highlighted in different colours. The capsid surface in the intact EV1 is composed of the VP1-3 proteins, and VP4 is buried inside the capsid.

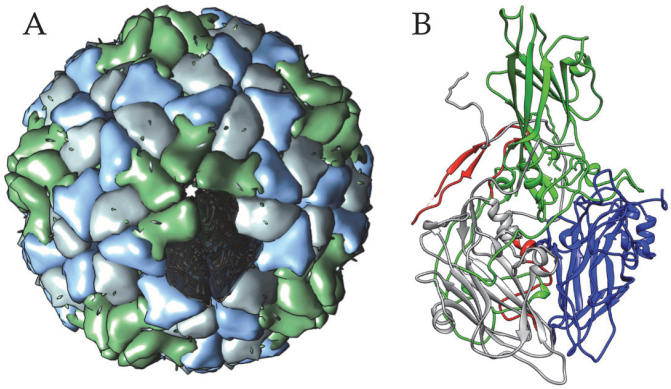

FIGURE 6 EV1 capsid structure. The whole EV1 capsid (A) is composed of 60 protomers. Edges of one protomer are highlighted with black. One protomer (B) is made of four capsid proteins. The capsid proteins are highlighted with different colors (VP1 = green, VP2 = blue, VP3 = gray, VP4 = red). Images are based on the EV1 x-ray structure (PDB code 1ev1 (Filman *et al.* 1998) and were created using UCSF Chimera.

Knowledge about uncoating of EV1 comes mostly from studies with other picornaviruses, mainly poliovirus and rhinovirus. Many features of the uncoating process seem to be common to all picornaviruses studied so far. Uncoating leads to release of the genome through an opening in the capsid, the exact location of which has been under debate (Levy *et al.* 2010, Bostina *et al.* 2011, Strauss *et al.* 2013). The major changes in capsid proteins during uncoating have been extensively studied. The exposure of VP1 N-terminal peptides in uncoating intermediate virions has been observed in at least poliovirus, rhinovirus and coxsackievirus (Fricks and Hogle 1990, Racaniello 1996, Xing *et al.* 2003, Ren *et al.* 2013). The exposed peptides are suggested to bind the virus particle to a lipid membrane separating the virus particle from cytosol - either the plasma membrane before entry or the membrane of the endosomal compartment after entry. The fatty acid molecule buried inside VP1, the pocket factor, has also been linked to uncoating and the stability of the virus particle, and is known to exit the capsid upon uncoating (Smyth and Martin 2002, Smyth *et al.* 2003). A helix in the VP3 protein of coxsackievirus has been seen to undergo change to a β-hairpin upon uncoating and is suggested to be a probe for membranes (Ren *et al.* 2013). Ejection of the VP4 proteins and the myristyl moieties covalently linked to them is commonly observed during uncoating. The VP4 proteins are capable of forming ion channels on membranes (Chow *et al.* 1987, Fricks and Hogle 1990, Danthi *et al.* 2003, Davis *et al.* 2008, Panjwani *et al.* 2014) and the channels they form have been suggested to mediate genome release from endosomal compartments. With poliovirus, they are even suggested to participate in forming umbilical channels attached to the capsids, directly guiding the genome through the membrane (Strauss *et al.* 2013). However, to date such umbilical formations have not been reported with other enteroviruses. The large membrane breakages in EV1-induced MVBs (Soonsawad *et al.* 2014) suggest that at least with EV1 such direct injection of the genome through the MVB membrane might not be necessary. Direct interactions of the virus particles with lipid membranes are likely in the confined space inside the MVBs, with or without the injection of the genome through the membrane.

2.2.4 Lipids in enterovirus life cycle

Virus particles come to contact with lipid membranes at several points of their life cycles, and the importance of host cell lipids to viruses is widely appreciated (den Boon and Ahlquist 2010, Heaton and Randall 2011, Chukkapalli *et al.* 2012). First, the entry to cells is mediated by invagination of the plasma membrane. Then, the virus particle must escape the endosomal vesicles to be able to replicate. Finally, after production of the next generation of viruses, the virus particles must escape the cell one way or another through the plasma membrane.

EV1 endocytosis into the cells has features of macropinocytosis and is characterized by lipid rafts. Clathrin-mediated endocytosis is the most common and the most studied of the endocytic pathways, but multiple other endocytic routes to cells exist, including caveolar trafficking and non-caveolar/non-clathrin

pathways. These pathways differ greatly in their association with lipid rafts. Clathrin does not colocalize with raft lipids, whereas caveolin has a very strong correlation with lipid raft locations (Diaz-Rohrer *et al.* 2014). EV1 entry to cells has been reported to be independent of caveolin, although the endocytic vesicles accumulate caveolin-1 after internalization (Marjomäki *et al.* 2002, Upla *et al.* 2004, Karjalainen *et al.* 2008). Also different entry pathways have been reported for some of the enteroviruses; for example echovirus 7 enters cells via the clathrin-mediated pathway (Kim and Bergelson 2012).

Rafts often induce oligomerization of proteins, for example caveolin and flotillins, and oligomerized proteins are also known to stabilize rafts (Diaz-Rohrer *et al.* 2014). Also EV1 binding is known to induce oligomerization, or clustering, of the integrins located in lipid rafts (Upla *et al.* 2004). Rafts are originally known from polarized endothelial cells, where they are involved in creating differences in lipid composition of the two different sides of the cells (baso-lateral and apical). Later they have been seen to participate in golgi to plasma membrane trafficking also in non-polarized cells (Diaz-Rohrer *et al.* 2014). The rafts in the plasma membrane are generally considered as small (10-200 nm in diameter) and highly dynamic structures, but many other features about their characteristics remain unresolved or under open discussion (Pike 2006, Diaz-Rohrer *et al.* 2014). However, during the recent years, strong evidence about their existence and biological relevance has been reported (Baumgart *et al.* 2007, Toulmay and Prinz 2013). The rafts are often determined by the presence of their main lipid constituents, sphingomyelin and cholesterol, which have a strong affinity to each other. They form microdomains with liquid-ordered phase in phospholipid membranes of liquid-disordered phase (Ipsen *et al.* 1987, Simons and Ikonen 1997, Silvius 2003, de Lange *et al.* 2007, Quinn 2013, Róg and Vattulainen 2014). A model for cholesterol-sphingomyelin association in lipid rafts is illustrated in Figure 7 along with structures of the lipids used in the experimental part of this dissertation.

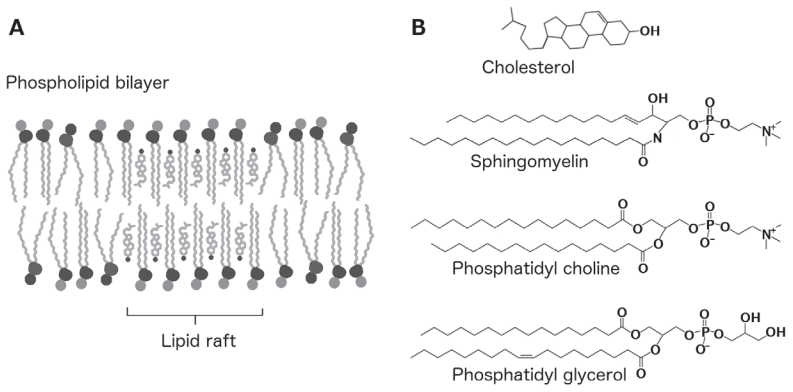

FIGURE 7 Packing of lipids in phospholipid bilayer (A) and the stuctures of selected lipids (B). The rafts shown in (A) are composed of cholesterol and sphingomyelin, and the illustration of the raft is based on (Simons and Ikonen 1997).

In addition to the plasma membrane, cholesterol and sphingomyelin are also enriched in early and recycling endosomes and the intraluminal vesicles of late endosomes (Möbius *et al.* 2003). Generally speaking, the cholesterol content of intracellular membranes increases in the compartments of the secretory pathways from the endoplasmic reticulum to the plasma membrane. Vice versa, the cholesterol content decreases in the compartments of the endocytic pathways from plasma membrane to lysosomes (Diaz-Rohrer *et al.* 2014). The distribution of other lipids also varies in cellular membranes (Bissig and Gruenberg 2013). For example glycosphingolipids are present only in the outer leaflet of the plasma membrane, and phosphatidyl ethanolamine and phosphatidyl serine only in the inner leaflet, and it is generally believed that endosomes share the overall lipid composition. The phosphoinositide composition of the plasma membrane and the endosomes is believed to be different.

Due to the central role of cholesterol in membrane functions, much interest in virus-lipid interaction studies has also been focused on cholesterol (Lu *et al.* 1999, Chatterjee *et al.* 2000, Danthi and Chow 2004, Martín-Acebes *et al.* 2007, Medigeshi *et al.* 2008, Schroeder 2010). Removal of cholesterol from cells has been shown to prevent the entry of several viruses, including EV1 (Heaton and Randall 2011, Siljamäki *et al.* 2013). For an enveloped alphavirus, cholesterol and sphingomyelin have also been reported necessary for optimal endosomal escape (Kielian *et al.* 2010). In addition, RNA viruses are known to manipulate lipid biosynthesis. Lipid metabolism has even been suggested as a target for anti-viral therapies due to its importance to the virus life cycle (Heaton and Randall 2011). For example the polio- and coxsackieviruses traffic cholesterol to replication machinery structures (Wang *et al.* 2011, Chukkapalli *et al.* 2012, Ilnytska *et al.* 2013, Viktorova *et al.* 2014), suggesting a common need for cholesterol-rich membranes in enterovirus replication. Despite the similarities in the need for cholesterol in the replication machinery, all details of interactions with lipids are not common to enteroviruses. For example, differences in the binding of enteroviruses to artificial lipid vesicles have been observed with different enteroviruses (Airaksinen *et al.* 2001). Cryoelectron tomography has shown variation in liposome binding with the two enteroviruses studied to date, poliovirus and rhinovirus. Poliovirus exhibits umbilical protrusions from the capsid that penetrate the lipid membrane and keep the capsid at a 5 nm distance from it (Strauss *et al.* 2013). Rhinovirus, on the other hand, adopted a tight fit with the membrane (Kumar and Blaas 2013). Both interactions were observed with liposomes composed of phospholipids, sphingomyelin and cholesterol, although only poliovirus liposomes had receptors. Other experiments have shown the receptor to be necessary for rhinovirus membrane penetration (Bilek *et al.* 2011).

The studies on molecular interactions of enteroviruses and lipid membranes have concentrated on the VP1 N-terminal peptides and the VP4 proteins, although the rhinovirus RNA has also been suggested to participate in membrane binding (Harutyunyan *et al.* 2014). In molecular dynamics

simulations, the poliovirus VP1 N-terminal peptide does not penetrate the membrane but rather lays on the membrane surface and only perturbs the membrane (Hong *et al.* 2012). Membrane physical properties affect transmembrane helix formation (Barrera *et al.* 2012). Curvature of the vesicles enveloping the viral particles, which may allow additional copies of the N-terminus of VP1 to be inserted into the vesicle membrane or allow more intimate associations of the virus particles with the membrane, generating mechanical forces that trigger RNA release.

2.3 Raman spectroscopy as a tool in virology

For determination of the structural and chemical details involved in specific processes during the virus life cycle, various complementing methods are needed. Traditionally, structures are determined with x-ray crystallography. It gives highly detailed information about the positions of atoms, but the interactions of atoms or molecular groups are missing. In addition, the gained information comes from static structures, and only from those structures that will crystallize. Cryoelectron tomography has been used to solve structures of large proteins or protein complexes, including viruses. Like cystallography, cryoelectron tomography is mostly limited to static structures. Nucleic magnetic resonance (NMR) is another method commonly used for structural studies of proteins. It can measure structures in solution and it can also be used to study dynamic processes, but the large amount of spectral peaks limits it to small proteins. Hence, a method to study dynamic structural and chemical changes in an environment relevant to biological molecules is called for. Raman spectroscopy is a good candidate for complementing the traditional methods used to study virus structures. It cannot be used to solve structures, but it can detect structural changes occurring in the sample. It is a non-destructive spectroscopy method and it can be used with samples of all states of matter, also water solutions (Ferraro *et al.* 2003, Vandenabeele 2013). This is important for biological samples, which can be measured in their natural environment or conditions that resemble those. It makes Raman an ideal probe to study structural alterations and interactions of biomolecules, and dynamics of the systems, without labels or other invasive sample preparation techniques (Lambert *et al.* 2006, Downes and Elfick 2010, Niaura 2014).

2.3.1 Basic principles of Raman scattering

Raman signal is based on inelastic scattering of light, where the energy of the scattered photon changes (Figure 8A) (Ferraro *et al.* 2003, Lambert *et al.* 2006, Vandenabeele 2013). In elastic scattering, or Rayleigh scattering, the scattered photon has the same energy before and after. Inelastic scattering is divided to Stokes and anti-Stokes scattering based on whether the energy of the photon decreases (Stokes) or increases (anti-Stokes). The change in energy comes from

the vibrations of the molecule. This leads to a spectrum with peaks related to the vibrations of the molecule, which correlate strongly with the chemical and structural features of the vibrators (Figure 8B). The method used in the experimental part of this dissertation utilizes anti-Stokes Raman scattering.

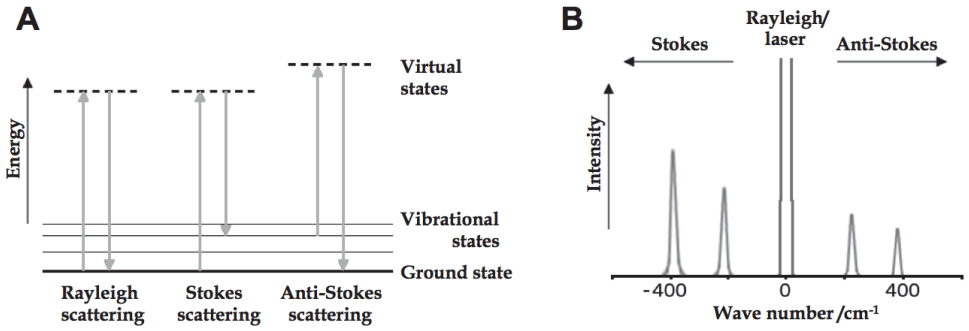

FIGURE 8 Principles of Raman scattering. Energy transitions of electrons during scattering are represented in a Jablonski diagram (A) and the signals from scattering are drawn in a specrum (B). Image is based on (Ferraro *et al.* 2003, Vandenabeele 2013).

2.3.2 Interpretation of Raman spectra

The Raman spectrum of a biological sample is a combination of spectral contributions from the Raman active molecular groups of the sample. This enables a simultaneous study of all the molecular parts participating in the biological process in question. The Raman spectrum of a complex biological molecule or system, like a virus, consists of numerous overlapping peaks or bands with large amount of information (Barth and Zscherp 2002, Tuma 2005, De Gelder *et al.* 2007, Hobro *et al.* 2013, Czamara *et al.* 2015). The complexity of the spectra also makes interpretation of the data non-trivial. The assignment of specific signals in a spectrum with multiple overlapping signals relies on the wealth of published vibrational spectra, from both Raman and infra-red (IR) spectroscopy. As an example, a spectrum of calf thymus DNA is shown in Figure 9. It exhibits the typical spectral features of DNA (Serban *et al.* 2002). Proteins have equally complex spectra, and viruses generally contain both nucleidc acids and proteins, and sometimes also lipids, all contributing to the spectra.

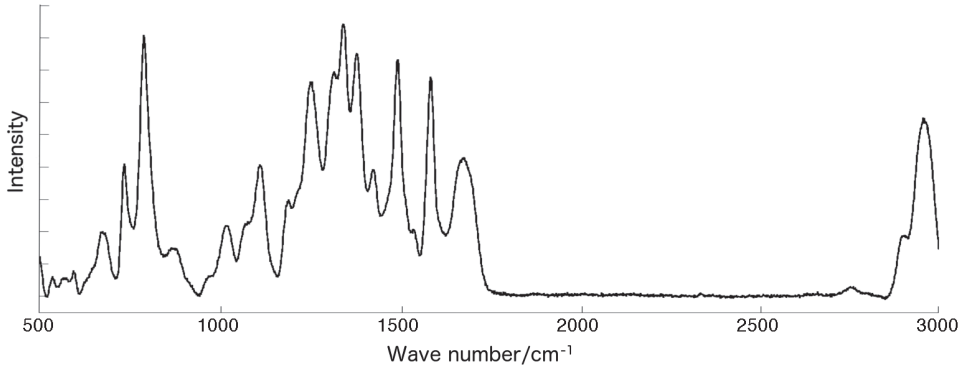

FIGURE 9 Raman spectrum of calf thymus DNA. Courtesy of Heikki Häkkänen.

The Raman signals come from polarizability of electron fields as a result of the photon interacting with the material (Ferraro *et al.* 2003, Vandenabeele 2013). The polarizability of chemical entities differ, and hence some have stronger signals than others. In biological molecules, these are usually chemical groups with double bonds or electronegative atoms. One of the most prominent features in the spectra of proteins are the amide bands originating from the polypeptide chain C=O stretching (amide I band (AmI)) and the coupled C-N and N-H bending motions (amide III band (AmIII)). These are commonly used indicators of protein secondary structures (Tuma 2005, Niaura 2006, Rygula *et al.* 2013). The nomenclature of the amide bands comes from IR spectroscopy, where, unlike in Raman spectroscopy, also an amide II band is visible. Other informative Raman signals come from phosphate groups and aromatic amino acids. The vibrations of for example aromatic amino acids are sensitive to the hydrophobicity of the environment or the hydrogen-bonding status of the residue (Miura *et al.* 1989, Takeuchi 2003, Hernandez *et al.* 2010, Milán-Garcés *et al.* 2013). Local electric fields also affect the signals (Park and Boxer 2002). Hence, changes in the local environment of the molecules affect the position and intensity of the Raman signal making the Raman signals sensitive to secondary structures, ions, charged amino acids, and phosphates in proteins or nucleic acids.

A drawback in Raman spectroscopy is the weakness of Raman signals, which is due to the improbability of inelastic scattering compared to elastic scattering. This leads to a need of relatively high sample concentrations and/or purity. While linear Raman spectroscopy measures the anti-Stokes scattering without modifications to the signal intensities, different Raman methods have been developed to enhance the detection of the weak signals (Downes and Elfick 2010). These include resonance Raman spectroscopy, surface-enhanced and tip-enhanced Raman spectroscopy (SERS and TERS), and coherent anti-Stokes Raman spectroscopy (CARS) (Lambert *et al.* 2006, Downes and Elfick 2010). Resonance Raman spectroscopy enhances the intensities of particular signals in the spectrum and often uses UV light (Robert 2009). CARS uses two lasers with a frequency difference matched to a specific vibration, enabling high

resolution imaging but limiting the spectral information. SERS utilizes local surface plasmons generated from a metallic nanostructure near the sample, leading to enhanced signal intensities (Negri and Dluhy 2013). Raman spectroscopy generally uses visible light laser beams, which enable microscopy with the same resolution as in fluorescence microscopy (Raman microspectroscopy). TERS is based on the same effect as SERS, and it combines Raman with scanning probe microscopy leading to a resolution similar to that of the atomic force microscopy (Domke and Pettinger 2010). Many of these modified Raman methods, along with the linear Raman spectroscopy, have been used for biomedical research, including studying viruses.

2.3.3 Raman studies on viruses

Several Raman spectroscopic studies on viruses have been reported, many of them on plant viruses and bacteriophages. The reported Raman studies on human viruses are limited to a few important pathogens like human immunodeficiency virus (HIV) (Xu and Lu 2005) and hepatitis A (Dinakarpandian *et al.* 1997). The closest relative to EV1 that has been studied with Raman spectroscopy is bovine enterovirus (Kaminaka *et al.* 1999).

Interactions of the genome and the capsid proteins, as well as uncoating, have been the focus of linear or resonance Raman studies with several viruses. The uncoating of bovine enterovirus has been studied with resonance Raman spectroscopy of full and empty virus particles (Kaminaka *et al.* 1999). The study revealed that uncoating leads to reducing hydrogen bonding in the genome and changes in the hydrophobic environment of Trp residues. The other studied viruses vary somewhat from enteroviruses, including for example the plant viruses turnip yellow mosaic virus (TYMV) (Hartman *et al.* 1978), bean pod mottle virus (BPMV) (Li *et al.* 1990, Li *et al.* 1992), and belladonna mottle virus (BDMV) (Prescott *et al.* 1985). These plant viruses have a genome that is bound to the protein capsid in static form. The pH dependent uncoating of BDMV has been seen to involve changes in protonation of cytosine bases and stacking of adenine bases (Prescott *et al.* 1985). The Raman studies of BPMV have revealed for example that the A-form double helix conformation of RNA increases when it is packaged inside virus capsids (Li *et al.* 1992). Also the single-stranded RNA genome of the icosahedral MS2 bacteriophage has been shown to adapt the A-form double helix inside the capsid (Thomas Jr *et al.* 1976).

Other bacteriophages with icosahedral capsids that have been studied include PRD1 and P22. PRD1 is an enveloped virus, and P22 has a head-tail structure with 6 prominent tail spikes. The secondary structures and dynamics involved in genome packaging of these virions have been studied (Fish *et al.* 1980, Aubrey *et al.* 1992, Reilly and Thomas Jr 1994, Tuma *et al.* 1996a, Tuma *et al.* 1996b, Tuma and Thomas Jr 1997). Among other details, the genome packaging has been reported to include expansion of the capsid. Filamentous bacteriophages (Ff) have been extensively studied with Raman spectroscopy (Grygon *et al.* 1988, Overman *et al.* 1994, Overman and Thomas 1995, Overman and Thomas 1998, Tsuboi *et al.* 2003). The studies have revealed for example the

α helical nature of capsid proteins and the organization of the single-stranded DNA genome inside the filamentous capsid.

Many of the latest advancements have focused on the Raman spectroscopic signatures as a means to identify viruses or infected cells. Raman spectroscopy and microspectroscopy have been used to detect cells infected with herpes simplex 1 or adenovirus (Moor *et al.* 2014, Salman *et al.* 2014). Efforts to develop SERS and TERS to analytical methods for virus detection and identification have shown promising results (Reyes-Goddard *et al.* 2008, Hermann *et al.* 2011, Lee *et al.* 2012, Luo *et al.* 2014, Olschewski *et al.* 2015).

AIMS OF THE STUDY

The receptor-ligand interactions play a crucial role in the function of numerous biological and pathological processes. The interactions of integrins and collagens are important in wound healing, angiogenesis, inflammation and thrombosis, and the interactions of integrins and viruses enable the infection with clinically important human pathogens. In addition, key steps in life cycles of viruses are penetration of the cell's membranes and release of the virus genomes. Thus, knowledge on these interactions and molecular phenomena enhances the understanding of many clinically significant processes and increases the possibilities for developing therapeutic approaches. The specific aims of this doctoral thesis were:

I To determine whether the naturally occurring form of type I collagen - fibrils - is a ligand for collagen binding integrins, and to study the potential of integrins as regulators of collagen fibrillogenesis.

II To study echovirus 1 interactions with lipid membranes focusing on the effect of lipid composition and the possible role of the α2I domain of α2β1 integrin in these interactions.

III To define Raman spectroscopic signature of echovirus 1 and use it to study chemical and structural changes occurring in virus particles during uncoating. The study also aims at increasing the utilization of Raman spectroscopy in virology.

3 SUMMARY OF MATERIALS AND METHODS

A detailed description of all materials and methods can be found in the original publications (I-III). An overall view of the materials and methods are summarized in the table below.

TABLE 1 Methods

Method	Publication
Collagen fibrillogenesis	I
Turbidity measurement	I
Cell spreading assay	I
Solid-phase binding assay	I
Protein purification and analysis	I
Transmission electron microscopy	I, II
Immunostaining	I, II
Liposome preparation	II
Dynamic light scattering	II
Virus production, purification and analysis	II, III
Virus particle stability assay	II, III
Raman spectroscopy	II, III
Matlab data analysis	II, III

4 REVIEW OF THE RESULTS

4.1 Integrin α2β1 is a receptor for collagen fibrils

Collagen fibril recognition by integrins was studied by immunoelectron microscopy, solid-phase binding assays and cell spreading assays (I). Collagen fibrils were produced *in vitro* in physiological conditions. In TEM, the produced fibrils mostly exhibited the classical striation seen in type I collagen fibrils *in vivo* and hence were considered to represent the naturally occurring fibrils. The ligand binding domains of two integrins, α1β1 and α2β1, were shown to bind to type I collagen both in the monomeric form and fibrils. Collagen also enabled spreading of α1β1 and α2β1 integrin-expressing cells on monomeric and fibrillar collagen. The primary ligand for type I collagen, α2β1 integrin, was more effective in binding to fibrils than the α1β1 integrin whose primary ligand in ECM is the network-forming collagen type IV. Binding of the α2I domain to collagen fibrils was also visualized with TEM. These findings suggest that α2β1 integrin is a functional cellular receptor for type I collagen fibrils. In addition to this, the effect of integrin αI domains on collagen fibril formation was studied. The effects they had on *in vitro* fibrillogenesis suggest that integrins might participate in collagen fibrillogenesis *in vivo*.

4.1.1 Collagen fibrillogenesis

Collagen molecules that have been extracted from tissues self-assembled back to fibrils under suitable physiological conditions i.e. at neutral pH and at a temperature of +25 - 37 °C (Wood 1960a, Wood 1960b, Kadler *et al.* 1996). This indicates that the interactions of the monomeric molecules with each other are enough to drive the fibril assembly. Fibrillogenesis of bovine dermal collagen was initiated by subjecting a cold monomeric collagen solution to neutral pH and a temperature of +37°C (I). Fibril formation was followed by turbidimetric measurements at 313 nm, demonstrated in Figure 10A.

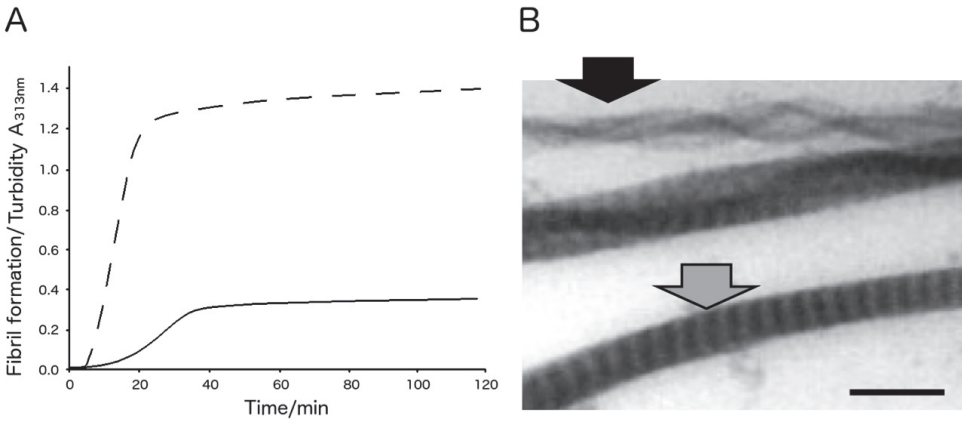

FIGURE 10 Collagen fibril formation. A) Fibrillogenesis was observed with turbidity measurements at 313 nm in physiological conditions (pH 7, +37°C), demonstrated with two collagen concentrations (solid line: 330 µM, dashed line: 1.65 mM). (B) Collagen fibrils in transmission electron microscopy. On the top a very loosely packed fibril (black arrow), on the bottom a tightly packed fibril (grey arrow) and in the middle a fibril with intermediate organization. Scale bar is 300 nm or the length of one collagen monomer.

When the turbidity of the solution showed that the process had reached equilibrium, the quality of the fibrils was investigated with electron microscopy. After 2 h, most of the collagen molecules had formed fibrils, but the fibrils were rather loosely packed. Examples of tightly and loosely packed fibrils observed in TEM are shown in Figure 10B. After 48 h of fibrillogenesis, the majority of fibrils looked like the ones found *in vivo* - they were packed tightly, had similar diameters and the characteristic D-periodic banding pattern (Figure 2 & 10B). A minority of loosely packed bundles of thin fibres remained even after fibril formation had been allowed to progress for 48 h.

4.1.2 Cells expressing α2β1 integrin spread on collagen fibrils

The importance of integrins as receptors for type I collagen fibrils was investigated with cells expressing specific integrins. Wild type chinese hamster ovary (CHO) cells have no receptors for type I collagen. Hence, the effect of specific integrins could be tested by using CHO cells transfected to express specifically those integrins. CHO cells expressing either α1β1 or α2β1 integrins were used (Nykvist *et al.* 2001). These cells were tested in spreading assays on monomeric and fibrillar type I collagen matrices. Results show (I, Fig 2) that cells expressing α2β1 integrin spread on monomeric collagen more effectively than cells expressing α1β1 integrin, as has been previously reported(Tulla *et al.* 2001). The CHO cells expressing α2β1 integrin spread almost as efficiently on collagen fibrils as they did on collagen monomers. Contrary to this, the cells expressing α1β1 integrin were very inefficient in spreading on collagen fibrils. It was thus seen that α2β1 integrin functioned as a receptor for both collagen

monomers and fibrils, and that α1β1 integrin mediated cell spreading almost solely on monomeric collagen and with restricted efficiency.

4.1.3 Dissociation constant determination

The collagen binding properties of recombinant α1I and α2I domains were examined by solid-phase binding assays (I, Fig 7) and electron microscopy (I, Fig 8). The interactions were studied using αI domains produced as glutathione-S-transferase (GST) fusion proteins. In solid-phase binding assay, microtiter plates were first coated with either monomeric or fibrillar type I collagen. The I domains were then allowed to bind to collagen, and the bound fusion proteins were detected with antibody staining utilizing the GST domain. The results were fitted to a Michaelis-Menten equation, and approximate dissociation constants (K_d) were determined to quantify the I domain binding to collagen. The same differences seen with the cell spreading assay were seen also here: the α2I domain bound more efficiently to type I collagen than the α1I domain, and both I domains bound stronger to the monomeric collagen than to the fibrils. The approximate K_d values obtained for binding to collagen are about ten times higher for collagen fibrils than for monomeric collagen, and the difference between the different collagen forms is similar with both I domains (Table 2). The maximum values of the binding curves (I, Fig 7) reach higher numbers with I domains binding to monomeric collagen. This indicates that at saturating I-domain concentrations, fewer I domains were bound to collagen fibrils than to monomeric collagen.

To support the solid-phase binding assays, α2I-domain binding to collagen fibrils was also studied with immunoelectron microscopy. The collagen fibrils formed *in vitro* both tightly packed fibrils and loose fibrils, indistinguishable from each other in the solid-phase binding assay. With TEM it was possible to specifically investigate those I domains that were bound to the tight, striated collagen fibrils. With the immunoelectron microscopy method the numbers of immunolabeled α2I-GST proteins bound per D-period (67 nm) on collagen fibrils were counted from TEM images. The dissociation constant was estimated using different α2I-domain concentrations and by fitting the data to a Michaelis-Menten equation. The obtained value for approximate K_d (•62 nM) was very close to the value obtained from the solid-phase binding assay (•100 nM). The results show that the α2I domain is able to bind to the tightly packed collagen fibrils. The results also confirm the K_d values obtained from the solid-phase binding assay. The approximate dissociation constants are summarized in Table 2.

TABLE 2 Dissociation constants (K_d) of integrin I domains binding to collagen

Integrin	Collagen form	Approximate K_d	Method
α2I	Monomer	10 ± 1 nM	Solid-phase binding assay
α2I	Fibrils	100 ± 10 nM	Solid-phase binding assay
α2I	Fibrils	62 ± 2 nM	TEM
α1I	Monomer	30 ± 3 nM	Solid-phase binding assay
α1I	Fibrils	250 ± 30 nM	Solid-phase binding assay

4.1.4 Integrins affect collagen fibrillogenesis

Both of the studied integrins were seen to bind more efficiently to the monomeric form of type I collagen than to the fibrils. In ECM, type I collagen is typically in fibrils except for the moments between their excretion and fibrillogenesis. With this in mind, the effect of αI-GST fusion proteins on collagen fibrillogenesis was tested (I, Fig 9). Turbidity of a collagen solution at 313 nm increases when monomeric collagen molecules assemble to fibrils, and hence the turbidity measurement can be used to observe the progression of fibrillogenesis. When the α1I domain was added to the collagen solution, it appeared to first accelerate fibrillogenesis, observed as a more rapid increasement of turbidity at the beginning of the experiment when compared to fibrillogenesis without the I domain. However, the final value of turbidity remained at much lower levels with the α1I domain than without it, suggesting that at later stages of fibrillogenesis the α1I domain inhibited the process. The α2I domain inhibited collagen fibril formation from the very beginning in a concentration-dependent manner. Already one α2I domain molecule per two collagen monomers inhibited the fibrillogenesis almost completely. The binding of integrins to collagen is considered to depend on divalent magnesium ions (Staatz *et al.* 1989) and a Mg^{2+} dependency was indeed noticed with the α1I domain - without the ions the α1I domain could not inhibit fibrillogenesis. Contrary to the α1I domain, the α2I domain did not need Mg^{2+} for fibrillogenesis inhibition (I, Fig 9). Hence, the efficient binding of I domains to collagen monomers and the observed effects on fibrillogenesis suggest that integrins might participate in collagen fibril formation.

4.2 Echovirus 1 has direct interactions with lipid membranes

Direct interactions of EV1 with lipid membranes were studied. In addition, the effect of α2β1 integrin on the interactions of EV1 with lipids was studied. For this, sucrose-gradient ultracentrifugation, TEM, and thermal stability assays were used. EV1 was observed to have direct interactions with liposomes composed of only lipids, without the receptor (II). The lipid composition

affected the observed binding: it changed the numbers of bound virus particles, and it had effects on virus particle morphology. The presence of soluble α2 integrin I domain also had effects on virus-lipid interactions by further enhancing the observed morphological changes. This implicates that receptor-virus interactions are important for the direct interactions of EV1 with lipid membranes.

4.2.1 Liposome composition affects virus binding

A comparison of the binding of EV1 particles to lipid membranes with different compositions was done using sucrose-gradient ultracentrifugation (II, Fig 1) and TEM (II, Fig 2). In sucrose gradients after ultracentrifugation, lipid vesicles float near the top of the gradient. The association of proteins or viruses with lipid vesicles can be studied by observing the cofloatation of these molecules with the vesicles (Airaksinen *et al.* 2001, Upla *et al.* 2004) as the free proteins or virus particles move deeper into the gradient. Before the gradient, EV1 was kept at 37°C for 90 min to enable interactions with lipid vesicles (control sample without lipids was treated similarly). Free EV1, detected by immunostaining of the fractionated gradient after centrifugation, penetrated half-way through the sucrose gradient in the used setup. The incubation period reflected the time EV1 spends in cells inside the MVBs before membrane breakages appear (Soonsawad *et al.* 2014). EV1 floated to some extent with all of the lipid vesicles used in the study. Composition of the vesicles affected the cofloatation, with the highest amounts of virus particles floating with phosphatidyl choline (PC) vesicles and the lowest amounts with phosphatidyl glycerol (PG) vesicles (summarized in Table 3). The vesicles composed of both of them (PC:PG) and/or of raft lipids sphingomyelin and cholesterol (SM:Ch and PC:PG:SM:Ch) were in the middle. To test if receptor binding induces structural changes that enhance virus binding to lipid membranes, the effect of the soluble α2I domain on cofloatation of EV1 with lipid vesicles was also studied. The presence of the α2I domain did not increase the numbers of viruses floating with liposomes. On the contrary, the I domain seemed to reduce the floating effect somewhat, as less EV1 signal appeared in the top fractions in samples with the α2I domain than without it. However, the experimental setup using soluble I domains does not accurately represent the conditions occurring *in vivo*, where the integrins are bound to the plasma membrane.

In further experiments, the virus-membrane associations were visualized with TEM and negative staining. EV1 and vesicles of different lipid compositions were investigated. The numbers of free and bound EV1 particles were counted from TEM images (see more details below). In all samples of EV1 with liposomes, some portion of the virus particles were associated with the membranes. The results support the observation from sucrose gradient experiment that the highest numbers of virus particles are bound to PC vesicles and the smallest numbers to PG vesicles, and the vesicles of other lipid compositions have values in between those two.

The lipid vesicle membrane was often seen curved a little at the binding site of the virus particle. In samples of EV1 with PC liposomes (Figure 11A), viruses have the largest contact areas with the membranes. The virus particles were often quite deeply buried within the vesicular structures and some individual virus particles were even seen covered with a bilayer membrane.

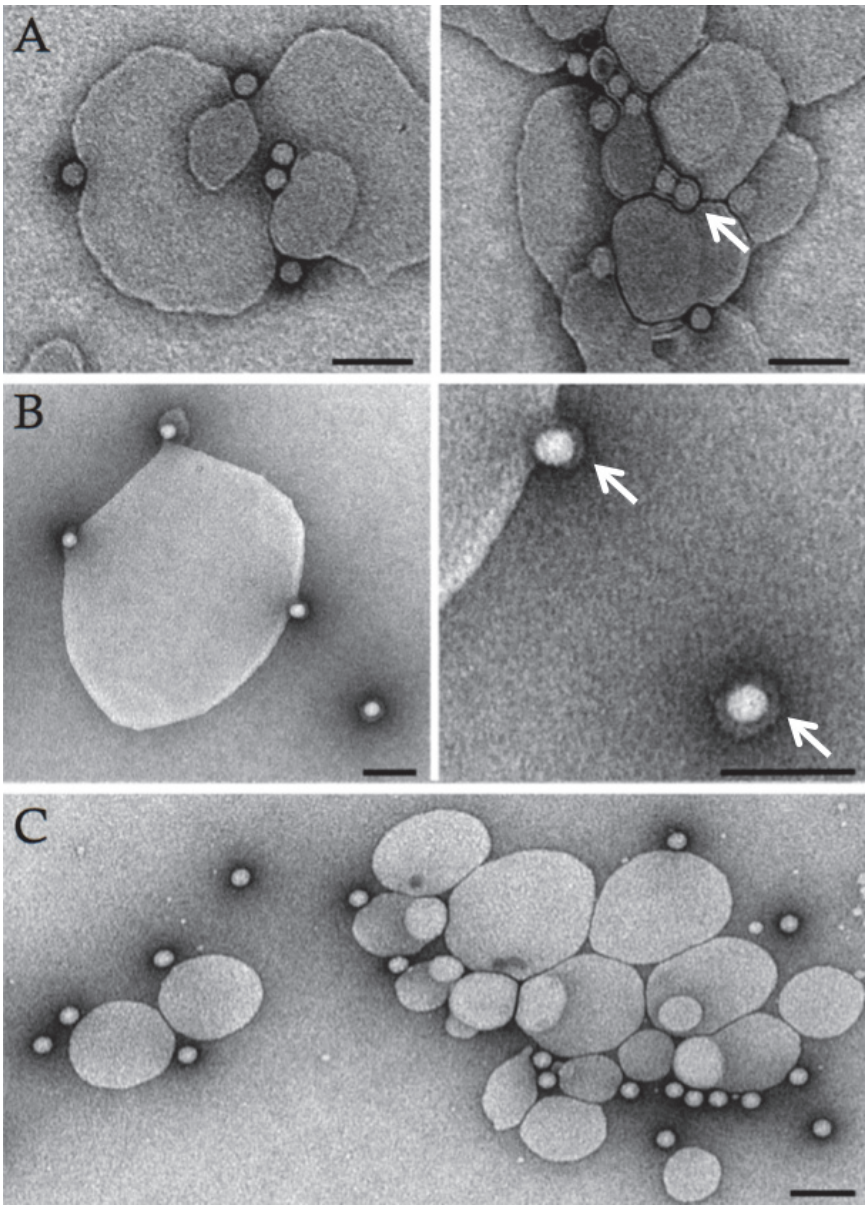

FIGURE 11 TEM images of EV1 and lipid vesicles. EV1 with vesicles of different lipid composition: PC (A), PG (B) and PC:PG:SM:Ch (C). Arrows point to virus particles covered by a lipid layer. Scale bars 100 nm.

Samples of viruses with PG liposomes (Figure 11B), while having the lowest numbers of lipid-associated virus particles, had another interesting feature. Some of the virus particles were observed completely covered with the lipids when next to a vesicle or even when apart from a distinct vesicle, either completely or partially. The lipids surrounging the virus particle seem to form a layer with a non-uniform thickness in contrast to virus particles surrounded by a clear bilayer in samples with PC vesicles. Although the lipid-covered virus particles are in minority, they clearly represent a PG-specific effect.

Samples with lipid vesicles containing raft lipids (Figure 11C) did not exhibit the behaviour seen with the phospholipids; the wrapping of the membrane around the virus particles. The membranes did curve a little at the site of binding, but somewhat less than the phospholipid membranes. The vesicles also appeared more round and symmetrical.

Free virus particles and those associated with lipid membranes were counted from TEM images (Table 3). As in the density-gradient experiment, also here the PC vesicles had the strongest affinity to virus particles. Samples with PG and SM liposomes had less virus particles in close contact with the membrane than samples with other liposomes, and the vesicles with lipid mixtures were again in between the two extremes. The soluble integrin I domain did not increase virus binding to membranes, but instead, similarly to the sucrose gradient experiments, it seemed to slightly reduce it. Table 3 summarizes the results obtained from sucrose-gradient experiments and TEM.

TABLE 3 Binding of EV1 to lipid vesicles

Liposomes	Integrin	Viruses bound to membranes in TEM	Gradient
PC	-	61 ± 15 %	+++
PC	+	63 ± 15 %	
PG	-	40 ± 22 %	+
PG	+	28 ± 16 %	
PC:PG	-	49 ± 20 %	++
PC:PG	+	36 ± 14 %	+
SM	-	32 ± 23 %	
SM	+	23 ± 15 %	
SM/SM:Ch	-		++
PC:PG:SM:Ch	-	39 ± 19 %	++
PC:PG:SM:Ch	+	37 ± 13 %	+

4.2.2 Flattening of the virus particles and the role of integrin

Virus particles are usually considered rather rigid structures with high internal pressure from the genome enforcing the round shape of particles. Hence, it was quite an unexpected observation to see that some of the viruses bound to the PC:PG:SM:Ch membranes were flattened. The flattening was further enhanced if the soluble α2I domain was present in the samples (Figure 12).

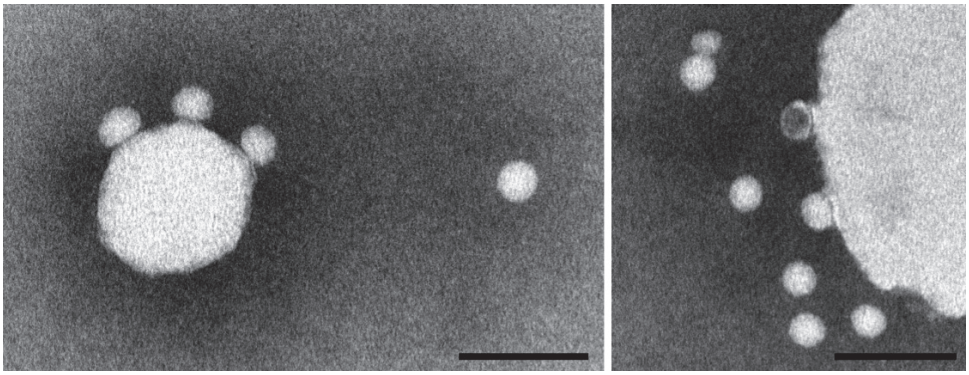

FIGURE 12 Flattened virus particles bound to PC:PG:SM:Ch lipid vesicles with α2I domain present. Free EV1 particles have a normal, round morphology. On the right, one of the virus particles on the membrane is empty (dark middle of the particle). Scale bars 100 nm.

To estimate the magnitude of flattening, diameters of virus particles bound to PC:PG or PC:PG:SM:Ch membranes were measured from TEM images. The ratio of the diameters parallel vs. perpendicular to membrane were calculated and the results are summarized in Table 4. The average diameters parallel to membrane in samples with phospholipid-only membranes were nearly equal to the diameters perpendicular to membrane, representing no flattening. In samples where EV1 particles were binding to PC:PG:SM:Ch membranes without the α2I domain the value was about 110 %. With the α2I domain present in the samples, the average parallel diameter was almost 120 % of the perpendicular diameter, representing significant flattening of the virus particles. This indicates strong and evenly distributed interactions between the virus particle and the lipid membrane. It also suggests that although the integrin I domain did not increase the numbers of EV1 particles binding to membranes, the receptor induces some kind of changes in the virus particles that lead to this enhancement of morphological changes during membrane interactions.

TABLE 4 Flattening of EV1 particles bound to lipid vesicles

Vesicle composition	α2I domain	Parallel/perpendicular diameter %
PC:PG	-	105 ± 9%
PC:PG	+	102 ± 7 %
PC:PG:SM:Ch	-	110 ± 8 %
PC:PG:SM:Ch	+	117 ± 10 %

4.3 Raman spectroscopy of echovirus 1

Raman spectroscopic signature of EV1 was determined (III). In addition to this, Raman spectroscopy of temperature-induced uncoating of EV1 was used to study structural and chemical changes related to EV1 uncoating. The spectra were measured from a relatively dilute solution in order to push the detection limits of Raman spectroscopy in virus studies.

4.3.1 Raman spectroscopic signature of echovirus 1

Raman spectroscopic signals are relatively weak, in comparison to for example absorbance or fluorescence spectroscopy. This calls for high concentrations of samples, and the previously published Raman studies of viruses have used dried viruses or concentrations in the range of 20-100 mg/ml (Hartman *et al.* 1978, Fish *et al.* 1980, Prescott *et al.* 1985, Li *et al.* 1990, Aubrey *et al.* 1992, Li *et al.* 1993, Overman *et al.* 1994, Reilly and Thomas Jr 1994, Overman and Thomas 1995, Tuma *et al.* 1996a). Such concentrations are hard to obtain with many mammalian viruses and the high concentrations increase the possibility of unwanted interactions or aggregation among the virus particles. For these reasons, Raman spectra of EV1 were measured from as dilute solutions as possible, while still obtaining a decent signal to noise ratio. The spectra of viruses in solution were compared to dry virus sample. With concentrations down to 1 mg/ml most of the features of EV1 spectrum were visible. With somewhat higher concentration (4 mg/ml) the spectra were well resolved and the individual signals in the spectra were more reliably assigned to specific features of the virus. As a trade-off for the dilute concentration, relatively long measurement times and higher intensity of the used laser light were needed. The dilute solution also emphasizes the necessity for high virus purity because with small amounts of the studied molecules also small amounts of impurities can obscure the spectra (Ruokola 2013). Impurities can also change virus particle behaviour - for example sucrose, which was used in EV1 purification, is known to stabilize protein structure (Allison *et al.* 1996). For these reasons, the virus was extensively purified with sucrose gradient and dialysis with high molecular weight cut-off filter (III). After this, the virus preparations showed no impurities when studied with TEM, SDS-PAGE, and absorbance and Raman spectroscopy.

The Raman spectrum of Echovirus 1 is represented in Figure 13. It shows a large amount of vibrations that can be assigned reasonably well with the help of previously published Raman spectroscopic data (Tuma *et al.* 1996a, Tuma 2005, De Gelder *et al.* 2007, Hobro *et al.* 2007, Matthäus *et al.* 2008). The strongest signal in the spectrum comes from the aliphatic C-H stretching vibration complex at around 2900 cm^{-1}. For proteins or nucleic acids this is not a very informative signal, and most of the information obtained from virus particles comes from the fingerprint region at 600 - 1800 cm^{-1}. The fingerprint region has a higher sensitivity to structural and chemical nature of particles (Hartman *et al.*

1978, Overman and Thomas 1995) and hence it gained the focus also in the EV1 spectrum.

Some of the main features of EV1 spectrum are pointed out in Figure 13. The amide bands originating from the amide vibrations of the polypeptide backbone are one of the best known spectral features of proteins and they are often used to study the secondary structures of proteins. In EV1 spectrum they are found at typical positions (Tuma 2005) with AmI at 1670 cm^{-1} and AmIII at 1230 - 1300 cm^{-1}. Some of the significant features seen in the spectrum come from vibrations of aromatic amino acids phenylalanine (Phe), tyrosine (Tyr), and tryptophan (Trp). These include anti-symmetric C-C stretching modes at 1580-1615 cm^{-1} and the ring breathing modes at around 1000 cm^{-1}. The C-C stretching modes can give information on for example side-chain conformations. The ring breathing mode of Phe at 1000 cm^{-1} is, however, mostly considered a stabile signal that is not affected by changes in the local environment of the Phe residue. For this reason, it is often used as an internal standard in Raman spectroscopy. Side-chain vibrations of other amino acid residues are located at 600-900 cm^{-1}, and the methyl/methylene vibrations at around 1350 and 1450 cm^{-1}. The signals coming from the virus genome are also visible in the spectrum. Many of them partially overlap with the virus protein vibrations, but some bands can still be specified to RNA. One of the clearest RNA signals is the peak at 811 cm^{-1}, which is considered to be a marker for the A-form double-helix conformation of RNA. The other signals that come from the genome are ring-breathing modes of RNA bases in the region below 800 cm^{-1}, ribose and phosphate signals at 800 - 1100 cm^{-1}, and the stretching vibrations of the bases at 1200-1600 cm^{-1} (Hobro *et al.* 2007, Hobro *et al.* 2013).

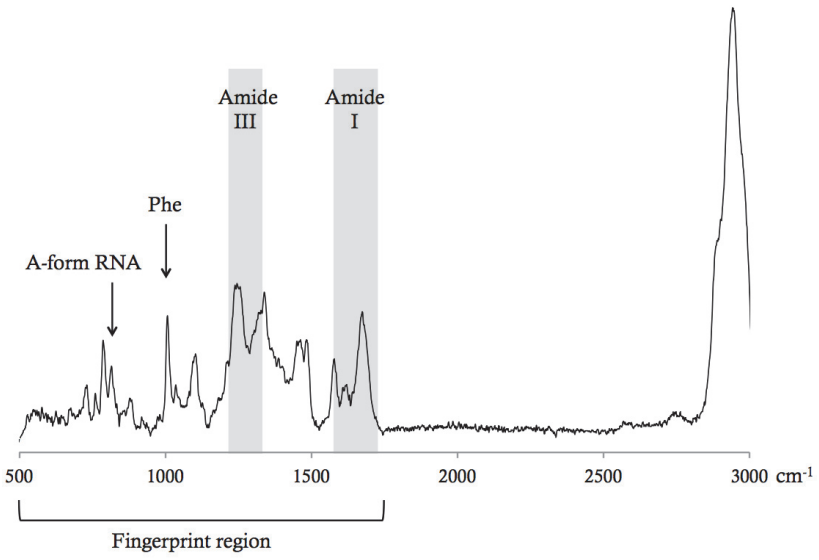

FIGURE 13 Raman spectrum of EV1. Some of the main features are highlighted: the peak at 811 cm^{-1} is a marker for A form double helix RNA, the peak at 1000 cm^{-1} is phenylalanine signal often used as an internal standard, and amide I and III bands give information on the secondary structures of proteins.

4.3.2 Uncoating of echovirus 1

Heat treatments have been used in enterovirus studies to induce uncoating or genome release of the virus particles (Curry *et al.* 1996, Bubeck *et al.* 2005, Lin *et al.* 2011). An uncoating intermediate of EV1 was produced by heating the virus particles at 50°C for 3 min. The heat treatment needed for uncoating was studied with a thermal stability assay. The time and temperature were selected to represent a state where half of the virus particles were releasing their genomes. The uncoating intermediates were compared to untreated viruses and viruses disrupted by a severe heat treatment (10 min at 60°C). The morphology of the resulting particles was confirmed with TEM (III, Fig 3). The Raman spectra of the different particles were measured at room temperature after the heat treatments and used to study chemical and structural changes related to EV1 uncoating.

The Raman spectra of the heat-treated virus particles have clear differences to the spectrum of the intact virus. With most signals in the spectra, a gradual change is observed from the intact virus to the uncoating intermediate, and then to the disrupted particles (III, Fig 5). Due to the complexity of Raman spectra of viruses, many of the changes locate in regions where multiple factors affect the spectra. The source of the changes can in some cases be assigned to a specific feature of the virus, and in the rest at least limited to a few possibilities. One of the largest changes in the spectra are observed in the Amide bands. The AmI signal becomes gradually more intensive at 1670 cm^{-1} and the AmIII signal at around 1240 cm^{-1} indicating increasing amounts of β sheets or coils in the secondary structures of proteins. However, an uncoating intermediate specific reduction in signal intensity is seen at 1650 cm^{-1} within the AmI band (Figure 14), a signal assigned to α helixes. Another change solely specific to the uncoating intermediate is a decrease of signal at 990 cm^{-1}. The peak at 990 cm^{-1} locates at a site where both RNA and protein vibrations attribute to the signal.

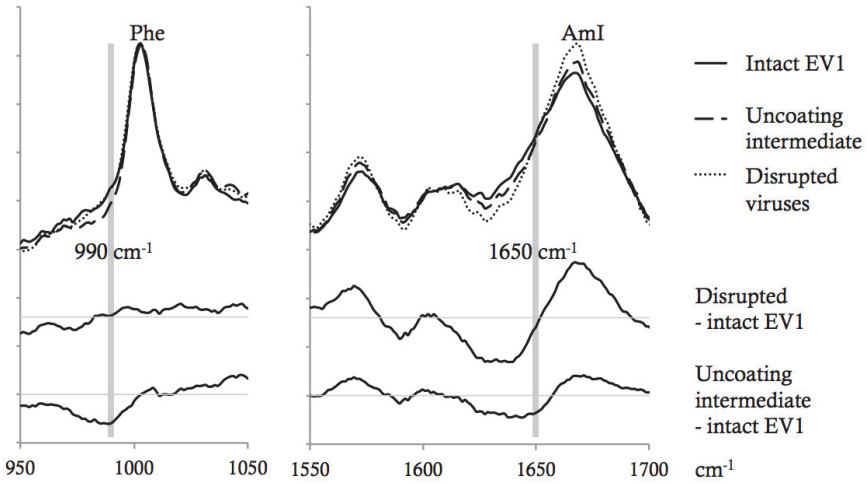

FIGURE 14 Regions of Raman spectra that have changes specific to the uncoating intermediate. These changes locate at 990 and 1650 cm^{-1}, marked with grey vertical lines. The spectra measured from the samples are shown on top, and the differences between the intact EV1 and the heat treated viruses are below them with the horizontal lines representing no difference. The difference spectrum related to the changes in uncoating is on the bottom.

In addition to the major differences in the Raman signals, subtle variations along the spectra are seen. These smaller changes include for example a slight increase of signal at 1710 cm^{-1}. The signal at that location could imply increasement of the protonated state of glutamate (Glu) residues (Barth and Zscherp 2002). However, this should lead to a corresponding reduction of signal of the unprotonated state of Glu at 1390 - 1410 cm^{-1}, which is not easily detected in the spectrum. Other small changes are seen at the typical locations of palmitoyl and myristoyl acid signals (De Gelder *et al.* 2007), which are the fatty acids reported to be part of the enterovirus structure. The fatty acids of EV1 do not exhibit clear, separate peaks in the virus spectra, but the small decreases in signals at 1063 cm^{-1}, 1129 cm^{-1}, and 1296 cm^{-1} could imply that heat-induced changes in fatty acid molecules are visible in the spectra.

Changes in the signals of aromatic amino acids are also seen in the spectra. The Fermi doublet signals of tryptophan (Trp) and tyrosine (Tyr) are commonly used indicators of the local environment of these residues. The Fermi doublets come from the resonance of vibrations of the substituted aromatic rings, and the ratio of the two signals depends on the environment of the aromatic ring (Siamwiza *et al.* 1975). The Trp Fermi doublet is indicative of hydrophobicity of the residue environment, and the Tyr Fermi doublet of the phenole hydrogen bonding. Like the fatty acids, they also do not exhibit clear, separate peaks in the virus spectra. Assignment to specific signals can still be done, with the Tyr Fermi doublet assigned to signals at 829 and 854 cm^{-1}, and the Trp doublet at 1340 and 1360 cm^{-1}. The reduction seen in the signal ratio I_{829}/I_{854} indicates that the phenoxyl groups of Tyr residues have a greater hydrogen bond acceptor role or increasing exposure to solvent after heat treatments (Siamwiza *et al.*

1975). The changes in signals assigned to the Trp doublet suggest an increasingly hydrophilic environment of Trp residues (Miura *et al.* 1988, Schlamadinger *et al.* 2009), although the overlapping RNA signal at 1335 cm^{-1} brings some insecurity to this interpretation. Changes in other signals assigned to Trp residues are also seen. The signal at 880 cm^{-1} is considered to be a marker for Trp hydrogen bonding, with signals at 882-883 cm^{-1} indicating no hydrogen bonding, and at 871 cm^{-1} with strong hydrogen bonding (Miura *et al.* 1988). In the spectrum of the intact EV1 there is a single peak centered at 877 cm^{-1}, and after heat treatments there are two peaks at 873 and 881 cm^{-1}, indicating changes in the Trp hydrogen-bonding status. The frequency of another Trp signal near 1550 cm^{-1} has been reported to indicate changes in side-chain conformation (Miura *et al.* 1989, Kaminaka *et al.* 1999, Takeuchi 2003). In the spectrum of the intact EV1 this signal overlaps with the peak at 1572 cm^{-1}, and heat treatments induce the appearance of a new peak slightly under 1550 cm^{-1}. This suggests a considerable change in conformation of the Trp residues. Changes in this Trp signal have also been noticed in studies of bovine enterovirus uncoating with resonance Raman spectroscopy (Kaminaka *et al.* 1999). A signal at 756 cm^{-1} is also assigned to Trp, and shows heat-induced changes. This complements the interpretation that the heat-treatments cause significant changes to the Trp residues.

Several signals assigned to RNA change due to the heat treatments. One of the biggest changes possibly coming from phosphate groups of RNA is the uncoating-intermediate specific change observed at 990 cm^{-1}. Other signals assigned to RNA are also changing, although not only in the uncoating intermediate but also in the heat-disrupted virus particles. Among them is a signal assigned to the C/U ring breathing modes at 783 cm^{-1} which has been reported to undergo intensity changes due to changes in the environment, particularly in non-helical regions of RNA (Hernández *et al.* 2003, Hobro *et al.* 2007). A slight increase is also seen in the signal of the symmetric phosphate stretching vibration at 811 cm^{-1}, often used as a marker for the A form RNA helix. This suggests that changes happen in the conformation of the RNA backbone. In support of this interpretation is a signal just below 1050 cm^{-1}, assigned to RNA P-O and sugar phosphate C-O stretching, which increases or shifts after heat-treatment, only becoming visible after heat-treatments. Many of the RNA signals overlap at least partially with protein signals, which adds some uncertainty to the interpretation of these signals. Together all these changes suggest that RNA undergoes substantial changes due to the heat treatments. The assignments of Raman signals that changed due to the heat-treatments are summarized in table 5.

TABLE 5 Heat-induced changes in Raman spectra of EV1

Assignment	Signal location (cm^{-1})	Change
Protein secondary structures		
AmIII, β sheets&coils	1240	+
AmIII, α helices	1300	−
AmI, α helices	1650	−
AmI, β sheets&coils	1670	+
Aromatic amino acids		
Tyr Fermi doublet, hydrogen bonding	829, 854	±
Trp	756	±
Trp hydrogen bonding	873 − 881	±
Trp Fermi doublet, hydrophobicity	1340, 1360	±
Trp side chain conformation	1550	+
Genome		
C/U ring breathing, non-helical RNA	783	±
A-form double helix	811	+
RNA phosphate (& amino acids)	990	−
RNA P-O and sugar C-O	1050	+
RNA C-H	1335	+
A/G ring breathing (& Trp)	1575	+
Other		
Protein C-H	1446	−
Protonated Glu	1710	+
Fatty acids	1063, 1129, 1296	−

5 DISCUSSION

Information on the interactions of α2β1 integrin with its ligands, type I collagen and echovirus 1, was obtained. The receptor was shown to efficiently bind to type I collagen in fibril form. Collagen-binding integrins were also seen to participate in collagen fibril formation. The meaning and impact of these findings are discussed in the following. New features of Echovirus 1 interactions with α2β1 integrin were also observed. Virus particles were seen to flatten when in contact with lipid membranes, and the presence of integrin enhanced this effect. Membrane composition also affected the magnitude of the flattening effect, as well as the amounts of membrane-bound EV1 particles. The life cycle of EV1 was further studied by Raman spectroscopy. The Raman signature of EV1 was defined and utilized for investigation of the chemical and structural changes of the virus uncoating process. These findings are discussed in the context of previous knowledge about the EV1 life cycle and molecular interactions.

5.1 Integrins as type I collagen receptors

The main function of type I collagen is to maintain the structure of various tissues. Collagens are, however, also known to dynamically regulate vital cellular functions. Cells use four members of the integrin family to attach to collagen in the extracellular matrix. The results here show for the first time that the major integrin-type collagen receptor, α2β1 integrin, effectively binds tightly packed type I collagen fibrils. The results also suggest, that the integrins might participate in collagen fibrillogenesis, which has been considered a simple self-assembly process.

Collagen fibrils are formed from microfibrils that join together, *in vivo* also covalently (Orgel *et al.* 2000). Due to this it is impossible to extract the microfibrils, which has prolonged the debate on fibril organization and the existence of microfibrillar substructure. Smooth, paraboloidal ends of fibrils have seemingly contradicted the microfibril substructures (Holmes *et al.* 1992).

The collagen fibrils produced for the integrin binding assays were observed in TEM to have smooth ends fitting to the paraboloidal model, or to branch out to smaller fibrils. One fibril might even have one smooth end and one that was branched to small fibrils. Hence, the observations of collagen fibrils in TEM show that microfibril substructure does not disagree with the paraboloidal ends. In addition, the loosely packaged fibrils were seen to be intertwined and commonly branching. Hence, the observations of fibrils in TEM agree with the latest interpretation of fibrils with intertwined rope-like substructure (Orgel *et al.* 2006, Shoulders and Raines 2009).

Integrin binding to collagen fibrils was visualized with immunoelectron microscopy showing that the α2I domain recognizes and binds to classical D-banded collagen fibrils. Characterization of the binding with a solid-phase binding assay revealed that collagen fibril formation leads to weakened binding of the integrins. The α1β1 integrin effectively bound only collagen monomers, and while α2β1 integrin was able to bind the fibrils, the binding to the monomers was stronger. This suggests that fibril formation leads to conformational changes of collagen at the integrin binding site, reducing integrin binding affinity. Fibril formation may also reduce the number of integrin binding sites on collagen by hiding several binding sites inside the collagen fibril. In agreement with the binding assays, α2β1 integrin mediated cell spreading on both collagen fibrils and monomers, while α1β1 integrin mediated spreading of cells only on the monomeric form of type I collagen.

In vitro, the formation of collagen fibrils is a simple self-assembly process. In tissues, collagen molecules have numerous interaction partners and there might be several ways to control the fibril formation (Kadler *et al.* 2008). For example, fibronectin in the ECM has been shown to be necessary for the fibril formation (Velling *et al.* 2002). Also other proteins, such as thrombospondin and decorin, have been observed to affect the kinetics of collagen fibrillogenesis and to regulate the fibril diameter (Danielson *et al.* 1997, Kyriakides *et al.* 1998). It is tempting to hypothesize that receptors such as integrins would also participate in controlling fibril formation. The higher affinity α1β1 and α2β1 integrins have for monomeric collagen compared to collagen fibers suggests that the receptors might collect the newly synthesized collagens and target fibril formation near the plasma membrane. The inhibiting effects of the soluble αI domains on collagen fibrillogenesis supports this possibility. The α2I domains which have high affinity for type I collagen prevented the fibrillogenesis, whereas the α1I domains accelerated the beginning of fibril formation. This suggests distinct regulatory roles for the different integrins. Even though the collagen fibrillogenesis experiment with soluble I domains does not mimic the conditions appearing *in vivo*, where integrins are attached to the cell membrane, the results indicate that α2β1 integrin binding to collagen monomers is stronger than the interactions of collagen molecules with each other. The processes cells use to remodel and relocate collagen fibrils they grow on could involve such receptor-mediated regulation (Schuliga *et al.* 2010).

Together these results show that α2β1 integrin is a functional cellular receptor for type I collagen in fibril form, although it binds more efficiently to the monomeric collagen. The other major collagen receptor, α1β1 integrin, can effectively bind only the monomers, but not fibrils. This complements the previous findings that these two collagen receptors have distinct ligand binding preferences among the different collagen types and other molecules of the ECM, as well as distinct signaling functions (Heino 2000, Nykvist *et al.* 2000, Tulla *et al.* 2001). The observations that integrins bind more efficiently to the monomeric collagen and that the I domains inhibit fibrillogenesis also suggest that integrins may participate in collagen fibril formation.

5.1.1 Impact of the observed interactions of collagen fibrils and integrins

Already prior to the research included in this dissertation (I), the promotion of collagen fibril formation by cells had been reported to depend on both fibronectin and α2β1 integrins (Velling *et al.* 2002, Li *et al.* 2003). The published findings on direct interactions between integrins and collagen fibrils (I) have highlighted the importance of investigating matrix molecule interactions and that oligomerization can affect them, as pointed out by (Chautard *et al.* 2009). After the publication of our findings on integrins and collagen fibrils (I), research about the effects of integrins on fibrillogenesis has been limited. Collagen fibrillogenesis regulation/inhibition has, though, been studied with other collagen receptors, the discoidin domain receptors (Blissett *et al.* 2009, Flynn *et al.* 2010), which are also reported to cooperate with integrins in collagen binding (Zeltz *et al.* 2014). Multiple other aspects of the interactions of integrins and collagen fibrils have, however, been studied since then. Collagen fibril architecture has been studied with emission gun–scanning electron microscopy (Perumal *et al.* 2008). The integrin binding sites were seen partially hidden from the integrins inside the fibril, confirming the same interpretation made from the solid-phase binding assays (I, Fig 7). Due to the observation of the hidden binding sites and mild phenotypes of α2 integrin deficient mice (Zhang *et al.* 2006), the binding of cells to collagen fibrils has been suggested to be enhanced by proteins mediating indirect binding between integrins and collagens in addition to the direct interactions (Zeltz *et al.* 2014). The interactions of collagen-mimetic peptides with cells have further revealed that the triple-helical conformation is important but not crucial for peptide recognition by cells (Khew and Tong 2007). Since the type I collagen monomers are known to be unstable at physiological temperatures (Leikina *et al.* 2002), this begs for the question whether integrins actually recognize also non-helical collagen conformations.

Integrin activation mechanisms and signaling events related to integrin-collagen interactions have been discussed (Nho *et al.* 2006, Connors *et al.* 2007, Nho and Kahm 2010, Jungmann *et al.* 2012). The study of time scales and forces related to α2β1 integrin-mediated cell adhesion to type I collagen have revealed adhesion as a two step process with initial, weak interactions of single receptors followed by a stronger, cooperative receptor binding mode (Taubenberger *et al.*

2007). The developmental state has been seen to affect collagen-integrin interactions (Bergstrom *et al.* 2014). The mechanical tension of collagen matrix has been reported to regulate fibroblast phenotype in an α2β1 integrin-dependent fashion (Eckes *et al.* 2006) and in periodontal ligament fibriblasts α11β1 integrin acts as a mechanosensor and regulates matrix remodeling (Barczyk *et al.* 2013). Fibroblasts have also been shown to recognize whether they are growing on monomeric collagen or fibrils, and change their behaviour accordingly (Xia *et al.* 2008, Schuliga *et al.* 2009). The fibroblasts proliferate faster when grown on monomeric collagen, and secrete more matrix metalloproteinases for proteolysis of collagen when grown on fibrils. Airway smooth muscle cells act similarly and, in addition, have been shown to remodel the fibrils they grow on to a network of larger fibrils (Schuliga *et al.* 2010). The anchoring collagen VII has also been reported to differentiate between monomeric type I collagen and fibrils, but unlike integrins, it binds more efficiently to the fibrils (Villone *et al.* 2008).

The ECM, and the changes in collagen interactions, synthesis or fibril formation are in a central role in several diseases. Alterations in the ECM may both initiate and drive liver and pulmonary fibrosis progression (DeMaio *et al.* 2012, Karsdal *et al.* 2015) and asthma-related modifications in ECM have been reported (Burgess *et al.* 2009). The cell-matrix interactions are important also in intervertebral disks, where surprisingly α1β1 integrin is needed for type I collagen gel contraction (Gilchrist *et al.* 2007). In cancer metastasis, the interactions between integrin and type I collagen are of utmost importance and have been identified as a potential therapeutic target (Johnson *et al.* 2005, Montesano *et al.* 2005, Conti *et al.* 2008, McLane *et al.* 2014). Integrins are also involved in collagen synthesis regulation in the bone (Nabavi *et al.* 2012). For example, the interaction of α2β1 integrin and collagen participates in age-related bone degeneration, shown by abnormally large quantities of collagen fibrils in α2β1 deficient mice (Stange *et al.* 2013).

One of the areas where the information on interactions of integrins and collagen fibrils has had the largest impact is tissue engineering. The development of collagen-based materials for biomedical applications is necessarily based on knowledge on collagen fibril associations with cells and their receptors. Different collagen composite materials and hydrogels have been developed for various biomedical applications, including transplantation of cells (Gruschwitz *et al.* 2010, Farran *et al.* 2010, Oelker and Grinstaff 2012) and nerve guidance structures for spinal cord injury (Abu-Rub *et al.* 2011). Efforts to transplant islet cells to pancreas as a cure for diabetes mellitus relies on islet cells grown in a collagen scaffold (Riopel and Wang 2014). Also different model systems for investigating various patological conditions are built with collagen-based materials including vascular and cardiac muscle models (Elliott *et al.* 2005, Gogly *et al.* 2009, Christalla *et al.* 2012) as well as skin and wound healing models (El Ghalbzouri *et al.* 2005, Fujimura *et al.* 2007, da Cunha *et al.* 2014). Collagen fibril density is relevant to wound healing, and α11β1 integrin mediated spreading of cells has been studied in a dense fibril model (Helary *et*

al. 2012). Due to the central role collagen fibrils have in the cornea and the bone tissue, collagen fibrils have also been included in the development of cell-based regenerative therapies for bone diseases (Kawase *et al.* 2014) and in ocular disease models (Hu *et al.* 2011).

Developing functional tissue models and remedies with a limited number of constituents is a challenging task. Different approaches to accomplish this have included for example creating collagen matrices that are conductive or have adjustable strength (Kumar *et al.* 2013, Sirivisoot *et al.* 2014). An ECM model with layer-by-layer deposition of ECM components has also been prepared (Mhanna *et al.* 2011). The engineered tissues are composed of matrix molecules (often collagen) and cells growing in the matrix. Understanding the interactions between these constituents is very important for the development of functional engineered tissues.

5.2 Life cycle of echovirus 1

Receptors enable infection of cells by viruses, and α2β1 integrin is a receptor for echovirus 1 in addition to the ECM components like collagen. New features were discovered about the interactions of EV1 and α2β1 integrin together with other details related to the early steps of EV1 life cycle. Lipid membranes hold important roles in the life cycle of viruses. Direct interactions of membranes and viruses have been observed with other non-enveloped viruses (Strauss *et al.* 2013), and now also with EV1 (II). The lipid composition was observed to affect both the numbers and morphology of EV1 particles binding directly to vesicles composed of only lipids. Unforseen morphological changes of enteroviruses were detected, and the changes were further enhanced by the presence of soluble integrin I domains. The observed flattening of virus particles, when bound to a membrane, suggests strong interactions between the virus particle surface and the membrane lipids.

EV1 is known to bind strongly to the inactive conformation of α2β1 integrin. One hypothesized model has five integrins binding symmetrically around the capsid resulting in considerable membrane bending (Jokinen *et al.* 2010). The membranes binding to EV1 were seen in TEM to wrap around the virus particles potentially enabling such a binding mode, even though the studied membranes did not contain integrins. Lipid composition of the membrane affected the magnitude of the wrapping around the virus somewhat, but all studied membranes were observed to bend upon virus contact to some degree. The data suggest that the flexibility and charge of the lipids are the most decisive factors for binding to EV1. Phospholipid membranes appeared to be the most flexible and sometimes wrapped the virus particles completely. Membrane composition also affected the amounts of virus particles binding to the membranes. Of the lipids studied here, phosphatidyl choline bound the highest numbers of EV1 particles. PC is present in all membranes in high amounts, but particularly on the cell membrane outer leaflet. It usually has

unsaturated alkyl chains that give membranes fluidity. Perhaps this enables PC membranes to bend around the virus particles more easily than the more rigid membranes comprising the raft lipids cholesterol and sphingomyelin, leading to increasing amounts of virus particles associated with the membranes. However, the other studied phospholipid, phosphatidyl glycerol, while occasionally wrapping around virus particles, had the lowest numbers of bound virus particles. The negative charge on PG might be one explaining factor to this.

Virus particles come to contact with lipid membranes at several points of their life cycles with entry to cells being just one of them. The virus particles also need to escape the endosomal vesicles, and after propagation of the next generation of virus particles, also the host cell. The direct interactions seen with EV1 and membranes might be involved in some or all of them. The last step, the escape from a host cell, is one possibility, since it has been suggested that picornaviruses are not truly non-enveloped viruses. The suggestion comes from an observation that Coxsackievirus B and Hepatitis A virus can be shedded from cells in vesicles (Feng *et al.* 2013, Jackson 2014, Robinson *et al.* 2014). The observations of EV1 wrapped inside phospholipid membranes suggest that if the shedding happens also with EV1, phospholipids might be involved in the process. A tight fit of non-enveloped virus particles and lipid membranes have also been observed in cells infected with simian virus 40 (Kartenbeck *et al.* 1989), which enters the endosomal reticulum by invaginations of the membrane.

For EV1, a potential phase for direct interactions with membranes is the time EV1 particles spend confined inside vesicle structures like the MVBs. The maturation of MVBs is necessary for EV1 infection, including the formation of intraluminal vesicles (Karjalainen *et al.* 2011). The lipid composition of different vesicular structures varies, and the intraluminal vesicles are known to be enriched with cholesterol (Diaz-Rohrer *et al.* 2014). Because of the central importance cholesterol has for many membrane functions, it has commonly been the focus of virus-lipid interactions (Lu *et al.* 1999, Chatterjee *et al.* 2000, Danthi and Chow 2004, Martín-Acebes *et al.* 2007, Medigeshi *et al.* 2008, Schroeder 2010). EV1 has among other viruses been shown to be dependent on cholesterol (Siljamäki *et al.* 2013). The morphological changes, or flattening, of EV1 particles were mostly observed with membranes containing cholesterol and sphingomyelin. If the flattening of EV1 with cholesterol-containing membranes is indeed something that happens also in cells during infection, it might be one reason for cholesterol dependency.

The current data does not show if the flattening happens in cells. It is, however, strong evidence for the strength of direct interactions between the virus surface and the membrane. The flattening was particularly obvious with small vesicles, which are probably less able to allow curvature of the membrane around the virus particle. Virus particles, especially DNA viruses, are generally considered to have high internal pressure from the genome, which is packaged in a very small confined space (Bauer *et al.* 2013). Although empty EV1 capsids

are also roughly spherical, an evenly distributed internal pressure from the genome most likely enforces the spherical particle shape. This suggests that the forces created by the virus binding to the lipid-only membrane must be stronger than the internal pressure from the genome. Such forces require multiple interactions between the interaction partners. Multiple contacts of virus particles and membranes, as well as the importance of membrane curvature, have been suggested also before with poliovirus (Brandenburg *et al.* 2007). Curvature may allow multiple copies of the N-terminus of VP1 to be inserted into the vesicle membrane providing more intimate association of the virus particles with the membrane. Uncoating is known to lead to surfacing of the VP1 N-terminal peptides, and the exposed peptides are suggested to bind the virus to the lipid membrane (Racaniello 1996). However, their position is not static inside the capsid even before uncoating, instead they are dynamically revealed at the virus surface in so called breathing already at physiological temperature (Li *et al.* 1994). This makes multiple VP1 N-terminal peptides available for membrane interactions and potentially enables the tight fit in binding of EV1 to membranes. Similar tight fit to a membrane has also been seen with rhinovirus particles (Kumar and Blaas 2013).

The uncoating of enteroviruses also leads to the ejection of VP4 proteins from inside the capsid (Racaniello 1996). The VP4 proteins are known to form ion channels in the membranes (Chow *et al.* 1987, Fricks and Hogle 1990, Danthi *et al.* 2003, Davis *et al.* 2008, Panjwani *et al.* 2014) and have been suggested to mediate genome penetration from inside the endocytic compartment to the cytosol. The tight binding of EV1 to the membrane might also be a way to introduce the VP4 proteins to the membrane, which could be directly associated with the genome release. As breakages big enough to be observed in TEM have been seen in the membranes of EV1 infected cells (Soonsawad *et al.* 2014), no direct injection of genome through the membrane might be necessary. The feasibility of this interpretation is enhanced by the coinciding of uncoating and the MVB membrane breakages. However, the model where an enterovirus injects its genome directly through the membrane is strongly supported by experiments with poliovirus and rhinovirus. Poliovirus has been seen to exhibit protrusions that penetrate the membrane and could facilitate genome injection (Strauss *et al.* 2013). Rhinovirus, on the other hand, can inject its genome through a liposome membrane to be replicated inside the liposome while mostly maintaining the membrane integrity (Bilek *et al.* 2011). High rhinovirus concentrations did, however, induce membrane breakages, giving room to the possibility of overlapping mechanisms in membrane penetration.

The presence of the soluble α2 integrin I domain in samples with viruses and lipid membranes did not in general enhance the binding of EV1 to membranes. In contrast, the I domain seemed to compete with membrane binding, lowering the numbers of virus particles bound to membranes. The soluble I domain has the possibility to bind to all binding sites on the virus surface, unlike the complete receptors *in vivo*, which are attached to membranes. This might be one reason why the soluble I domains partially

blocked membrane binding of EV1. It might, however, also reflect the processes inside MVBs. The binding of integrins to EV1 is known to be strong (Xing *et al.* 2004) and it might be necessary to disrupt this interaction before membrane binding can occur.

The presence of soluble I domains had also other effects on the membrane interactions of EV1. The flattening effect seen with membranes containing raft lipids was markedly stronger in samples with the I domain. This suggests that α2I domain binding (or releasing of the receptor and virus) changes the virus structure. These changes could involve changes in flexibility of the virus particle or hydrophobicity of the virus surface. The first hypothesis was tested with a temperature stability assay. The largest effect on temperature stability of EV1 came from the α2I domain, which stabilized the virus particles, as seen before (Kazmertsuk *et al.* submitted). The lipid vesicles seemed to lower the virus stability slightly. No clear differences were seen correlating to membrane composition. Some caution must also be taken in the interpretation of the results, as the effects of the lipids on the assay itself are hard to predict. The stability of virus particles at elevated temperatures and the elasticity of the virus particles at physiological temperatures are also not necessarily directly related to each other.

These novel observations of the flattening virus particles call for further investigations. Measurements of the forces involved in flattening with e.g. atomic force microscopy-based molecular force-probes would be highly interesting. Similarly, Raman spectroscopy, or other methods that reveal structural information, would complement the experiments and potentially detect what kind of structural changes and chemical interactions are involved in the membrane interactions.

5.3 Raman spectroscopy of echovirus 1 uncoating

The study on the early steps of EV1 life cycle included also studying the chemical and structural changes related to EV1 uncoating. Uncoating starts already within 30 minutes after entry to cells, detected as empty virus particles inside MVBs (Pietiäinen *et al.* 2004, Soonsawad *et al.* 2014). The uncoating is suggested to involve binding of the virus particle to the MVB membrane and injection of the genome through the lipid bilayer (Strauss *et al.* 2013). The presence of the lipid bilayer is not, however, a sufficient trigger for genome release, and its role in uncoating of EV1 is ambiguous. Fortunately, the uncoating can be studied also without the authentic physiological triggers, using heat treatments (Curry *et al.* 1996, Bubeck *et al.* 2005, Lin *et al.* 2011). They are based on the hypothesis that the mature virus particle is trapped in a metastable structure, and extra energy helps the virus overcome the activation barrier releasing the genome (Hogle 2002).

Three states related to the uncoating of EV1 were produced and characterized with TEM and Raman spectroscopy. These states - intact virions,

uncoating intermediates, and disrupted particles - all appeared as distinct types in both TEM and Raman spectroscopy. The uncoating intermediate virions were visualized in TEM as generally symmetric particles with something protruding from them, and the virions heated at 60 °C had lost structural symmetry and were completely disrupted. Thermal stability assay (Walter *et al.* 2012) confirmed the release of the genome at the temperature used for producing the uncoating intermediate. Raman spectra of these three states were clearly distinct, and Raman markers corresponding to the uncoating of the virion were obtained.

The Raman spectra of EV1 were compared to other published virus spectra. No other linear Raman spectra of picornaviruses were found from literature. The bovine enterovirus and rhinovirus have, however, been studied by surface enhanced Raman scattering (SERS) and ultraviolet resonance Raman spectroscopy (Joisson *et al.* 1993, Shanmukh *et al.* 2006). With these methods, the experimental setup (the substrate material in SERS and the laser wavelength in resonance Raman studies) has an effect on the intensity of the Raman signals, and hence the spectra differ from the linear Raman spectra of EV1. Close similarity of spectra were found with EV1 and BPMV virions (Li *et al.* 1990), which share considerable structural similarity (Li *et al.* 1992).

The amide I band, commonly used in determining the secondary structures of proteins, is one of the most pronounced features of the EV1 spectrum. The wagging mode of water molecules, however, locates at the same wave numbers as the AmI band of proteins. The signals coming from water must thus be very carefully removed to obtain reliable AmI analysis (Sane *et al.* 1999). The AmI band of EV1 is centered at 1668 cm^{-1} and indicates β-sheets as the predominant secondary structure of the virus proteins. This is in agreement with the known secondary structures of the major capsid proteins VP1-3, which all contain an eight-stranded β-barrel fold surrounded with loops and a few α helices (Filman *et al.* 1998). The Raman spectrum of the uncoating intermediate revealed, however, a decrease in the signal at 1653 cm^{-1} indicating reduction in the α-helical secondary structure of proteins. The reduction in the α-helical structure was accompanied by increasing signals assigned to β-sheets and coiled structures (at 1668 and 1240 cm^{-1}), and this effect increased further in the completely disrupted particles. The increasing β-sheet/coil signals thus seem to relate to heat-induced disruption of the virus particles, whereas the decreasing α-helical content is specific to the uncoating intermediate and more likely reflects specific, uncoating-related conformational changes. On the other hand, the increasing amount of flexible loops between domains can serve a critical role in the uncoating process by making the capsid less rigid, enabling other structural changes. Loosening of the capsid structure could also be related to the expansion of the virus particles seen with the uncoating intermediate EV1 particles in TEM. Expansion of capsids has been observed also with rhinovirus prior to genome release (Xing *et al.* 2003).

In addition to expansion, protrusions were detected in virus particles treated at 50°C. The potential constituents of the protrusions are either genome,

capsid proteins, or both. As the capsid structure remained otherwise symmetrical, the potential proteins that could participate in the newly formed structure are probably not VP1-3, which all participate in making the capsid surface in the intact virus. Rather VP4 proteins, which are known to exit the capsid during uncoating, might be involved in the protrusion. The umbilical structures seen to penetrate model membranes in poliovirus are possibly formed by the VP4 proteins (Strauss *et al.* 2013). The protrusions seen here did not resemble umbilical cords, but rather something less structured, suggesting genomic origin. Based on this assumption one would expect to see a pronounced change in the RNA signals of the uncoating intermediate.

Heat-induced changes were indeed observed in signals assigned to RNA. In contrast to the protein signals, the RNA signals are not as easily interpreted as particular structural changes. The RNA signals do suggest, however, a general change in the environment and solvent interactions of the genome. Especially, changes in the signal at 783 cm^{-1} suggest that there are changes in the RNA solvation shell i.e. the water molecules organized around the RNA (Hernández *et al.* 2003, Hobro *et al.* 2007). Changes in RNA signals that are sensitive to changes in the local environment of the molecule can be the result of both the ejection of the genome or the increasing permeability of the capsid. Further, a small increase in the signal at 811 cm^{-1}, considered a marker for the A form double-helix of RNA (Hobro *et al.* 2007, Hobro *et al.* 2013) is noticed after heat treatment at 60°C. This suggests that within the capsid, RNA molecules are somewhat more stabile in other conformations than the A form helix, perhaps as single-stranded RNA. Once the capsid is completely disrupted, the RNA molecules fold more to the A form double helical structure. Most intrestingly, an uncoating specific change in the spectrum is located at 990 cm^{-1}, which is a potential signal for RNA phosphates. The change at this location is no longer seen in the heat-disrupted particles, indicating a change truly related to the uncoating intermediate. The trapping of the genome half-way through the capsid shell could be the source of such a change in the spectrum. Another potential uncoating-specific change in the picornavirus genome has been reported with rhinovirus, where the genome forms an organized layer under the capsid (Pickl-Herk *et al.* 2013). However, further studies would be needed to confidently assign the change at 990 cm^{-1} to a specific change in the EV1 structure. Raman spectroscopy of EV1 while slowly heating the virus could potentially produce a picture of the dynamic changes happening in the virus particles during uncoating. Now the studied particles were heat-treated and then cooled to the measuring temperature (room temperature), enabling the measurement of somewhat static states.

Aromatic amino acids have strong Raman signals that give information on hydrogen bonding, hydrophobicity, and side chain conformation of these residues (Siamwiza *et al.* 1975, Miura *et al.* 1988, Miura *et al.* 1989, Kaminaka *et al.* 1999, Takeuchi 2003, Schlamadinger *et al.* 2009). Heat treatments changed many of these signals. Signals assigned to the Fermi doublets of Tyr and Trp exhibited small changes, indicating changes in hydrogen bonding of Tyr and

hydrophobicity of Trp environment. Also other signals assigned to Trp residues changed, including the 877 cm^{-1} signal that indicates changes in Trp hydrogen bonding status, and the appearing new signal assigned to Trp at around 1550 cm^{-1} that indicates changes in side chain conformations. The changes in the signals of aromatic amino acids support the interpretation obtained from AmI band analysis and TEM, that uncoating leads to loosening of the capsid structure and the subsequent exposure of these residues to water. The observation is also in agreement with the study reported for bovine enterovirus, where the intact and empty virus particles were studied with UV-resonance Raman spectroscopy (Schlamadinger *et al.* 2009). For bovine enterovirus, increasing hydrophobicity of the virus, or moving of Trp residues to increasingly hydrophilic environment is linked with the virus opening process.

The appearance of protonated carboxyl group signals of Glu residues suggests that changes in salt bridges may be involved in the uncoating process. The unprotonated, negatively charged Glu residues can form salt bridges with positively charged amino acid residues, like arginine or lysine. Such electrostatic interactions have been shown to be important stabilizers of virus structures in for example HIV, influenza virus, filamentous viruses, and Bacteriophage hk97 (Dolja *et al.* 1991, Rachakonda *et al.* 2007, He *et al.* 2008, Gertsman *et al.* 2010). The uncoating of enteroviruses is known to involve expelling of the internal protein VP4 (Fricks and Hogle 1990), which participates in three salt bridges that connect it to the other capsid proteins. Thus, the extraction of VP4 from the capsid might be partially controlled by salt bridges. The breakage of salt bridges further supports the model of loosening capsid structure.

Small decreases in signals that could be assigned to myristic and palmitic acids were also observed. The fatty acid covalently bound to VP4 is reported to be myristic acid in enteroviruses (Chow *et al.* 1987), and the stability-mediating pocket factor buried inside VP1 has been identified to most often be palmitic acid in bovine enterovirus (Smyth *et al.* 2003). The release of the stability-mediating pocket factor is known to be involved in uncoating, and the VP4-bound fatty acid is presumably released along with VP4 (Fricks and Hogle 1990). The observed decrease of fatty-acid signals could indicate either changes in the local environment of the fatty acid molecules or their reducing amount at the measured site. Both of these interpretations are in agreement with the previous knowledge on the uncoating process stating that fatty acids are being expelled from the virus particles.

Most of the changes related to uncoating in the Raman spectra of EV1 thus suggest that the heat-induced uncoating leads to increased loosening of the capsid structure, accompanied with increasing permeability. This is supported by the increasing amount of β-sheets or loops, the changes in hydrogen bonding status and hydrophobicity of aromatic amino acid residues, the disconnecting salt bridges, and the changes in fatty acids. These changes can explain the more flexible motion of the capsid constituents that leads to loosening of the capsid structure. This complements the observations made of the virus during

interactions with the lipid membranes, where the capsid also appeared to be a surprisingly flexible structure. In addition to new information on the virus itself, the knowledge of EV1 Raman signature also enables utilization of Raman spectroscopy in more complex situations. These could include for example studying the factors leading to uncoating within cells with Raman microspectroscopy, or monitoring the chemical and conformational changes of uncoating in a time-resolved manner.

6 CONCLUSIONS

The main conclusions of this thesis are:

1. The α2β1 integrin is a functional receptor for type I collagen fibrils. In addition, collagen-binding integrins might participate in collagen fibril formation *in vivo*.
2. EV1 has direct interactions with lipid membranes. Membranes with raft lipids, cholesterol and sphingomyelin, cause virus particles to flatten. The presence of soluble α2 integrin I domain enhances the flattening effect, which suggests that receptor interactions with the virus particle change the virus surface hydrophobicity or make the virus particle more elastic.
3. Raman signature of EV1 was determined. This enables method development and studying of EV1 in more complex systems, for example in cells with Raman microspectroscopy. Chemical and structural changes related to virus uncoating, most importantly loosening of the capsid structure and incresed hydrophobicity, were observed.

Acknowledgements

This work was carried out at the University of Jyväskylä, at the Nanoscience Center and the Department of Biological and Environmental Science, Division of Cell and Molecular Biology. The thesis was supported by the University of Jyväskylä, the Academy of Finland, the National Doctoral Programme in Nanoscience (NGS-NANO), and the Ellen and Artturi Nyyssönen Foundation.

I want to thank my supervisors Professor Janne Ihalainen and Professor Matti Vuento. I especially want to thank Janne for taking me under his wing and providing me with the opportunity to complete my Ph.D. I am grateful to Dr Roman Tuma for kindly agreeing to act as my opponent. I also want to thank the reviewers, Dr Olli Laitinen and Docent Maria Söderlund-Venermo, for their constructive and valuable feedback.

I am grateful for Docent Varpu Marjomäki and her group for the exellent collaboration and sharing their knowledge on echovirus 1. I also want to acknowledge Professor Jyrki Heino, Dr Daniel James While, and Dr Jarmo Käpylä for guiding me through the collagen fibril project, which was my first touch to scienctific research and an exellent foundation to build on.

I have had the privilege to work with many excellent people. Many thanks to all former and present co-workers (too numerous to mention all by name) for making our department such a pleasant place to come to. I am especially grateful to Jonna, Paula and Laura for the discussions, laughters and coffees that so many times carried me through the day.

I express my gratitude for my family and friends for their support and encouragement. Eeli and Tiitus drew my mind off work, and dear friends balanced my life. I thank my parents for always trusting in me, even though I sometimes struggled with that. I am deeply grateful for Eini for her love and support during the previous, busy year of experiments, writing and planning for the future.

YHTEENVETO (RÉSUMÉ IN FINNISH)

Kollageenireseptori α2β1-integriinin ja sen ligandien, tyypin I kollageenin ja echovirus 1:n, vuorovaikutukset

Soluväliaine mahdollistaa monisoluisten eliöiden elämän. Solut kiinnittyvät siihen, liikkuvat sen muodostaman ulkoisen tuen avulla ja vaihtavat sen kautta tietoa toistensa kanssa. Merkittävässä roolissa ovat erilaiset kollageenit, jotka muodostavat säikeitä tai verkkoja tai avustavat muita kollageeneja. Yleisin niistä on tyypin I kollageeni, joka muodostaa suuria, vahvoja säikeitä ja säiekimppuja soluväliaineessa. Solut kiinnittyvät soluväliaineeseen kohdemolekyylille tarkoitetuilla reseptoreilla ja integriinit ovat yksi tärkeä ryhmä tällaisia reseptoreita. Ne muodostuvat kahdesta alayksiköstä (alfa ja beeta), jotka lävistävät solukalvon. Niiden välityksellä solun sisäinen tukiranka yhdistyy soluväliaineeseen ja ne voivat myös välittää tietoa solun sisäpuolen ja ulkopuolen välillä. Neljästä reseptorista muodostuva integriinien alaryhmä, johon kuuluvat α1β1-, α2β1-, α10β1- ja α11β1-integriinit, on erikoistunut kollageeneihin sitoutumiseen. Kollageeneja sitovilla integriineillä on α-alayksikössään ligandeja sitova domeeni, I-domeeni. Yksi tärkeimmistä kollageenia sitovista integriineistä on α2β1-integriini, jonka pääasiallinen vuorovaikutuskumppani soluväliaineessa on tyypin I kollageeni. Vaikka tyypin I kollageeni esiintyy luonnossa lukuisista monomeerisista yksiköistä koostuneina säikeinä, on suurin osa sen ja integriinien välisiin vuorovaikutuksiin liittyvästä tutkimuksesta tehty toisistaan irrotetuilla, monomeerisessa muodossa olevilla kollageenimolekyyleillä. Tässä väitöskirjassa tutkittiin säikeisessä muodossa olevan tyypin I kollageenin ja integriinien välistä vuorovaikutusta. Tutkimalla tiettyjä integriinejä ilmentäviä soluja havaittiin, että erityisesti α2β1-integriiniä ilmentävät solut pystyvät leviämään kollageenisäikeiden päällä. Vuorovaikutuksia tutkittiin myös fuusioproteiineina tuotettujen, muusta integriinistä irrallisten I-domeenien avulla. Määritettiin α1β1- ja α2β1-integriinien I-domeenien sitoutumisen voimakkuus monomeeriselle ja säikeiselle kollageenille kiinteän faasin sitoutumiskokeiden ja elektronimikroskopian avulla. Tulokset osoittivat, että α2β1-integriini on toimiva reseptori tyypin I kollageenisäikeille, mutta sitoutuu silti voimakkaammin monomeerisessa muodossa olevaan kollageeniin. Havaittiin myös, että I-domeenit vaikuttavat kollageenin säikeistymiseen. Tämä viittaa siihen, että integriinit saattavat kudoksissakin osallistua kollageenin säikeistymisen säätelyyn. Väitöskirjassa selvitettiin siten merkittäviä ominaisuuksia kollageenia sitovien integriinien ja tyypin I kollageenisäikeiden välisistä vuorovaikutuksista.

Kuten soluväliaine, myös integriinit ovat elintärkeitä monisoluisille eliöille ja niiden oletetaan olleen olemassa yhtä kauan kuin monisoluiset eliötkin. Viruksilla on siten ollut runsaasti aikaa oppia hyödyntämään solukalvolla olevia integriinejä ja useat virukset käyttävät niitä kiinnittyäkseen soluihin ja päästäkseen niiden sisään. Yksi esimerkki tällaisista viruksista on ihmisen echovirus 1 (EV1), joka käyttää α2β1-integriiniä reseptorinaan. EV1 on pieni, vaipaton RNA-virus, joka kuuluu enterovirusten ryhmään. Enterovirukset ovat kliinises-

ti merkittävä virusryhmä, jotka aiheuttavat ihmisille erilaisia oireita lievistä infektioista halvaantumiseen ja sydänlihastulehdukseen saakka. Muiden enterovirusten tapaan EV1 pääsee solujen sisään endosytoosilla. Siinä solukalvolta kuroutuu solun sisään pieni rakkula, jonka sisällä soluun pääsee myös reseptoriin kiinnittynyt virus. Viruksen pitää kuitenkin vielä vapautua näistä rakkularakenteista ennen kuin uuden virussukupolven muodostuminen voi alkaa. Tiedetään, että EV1-infektiossa alkuperäinen endosytoosirakkula kypsyy monirakkulaiseksi, pH:ltaan neutraaliksi rakkularakenteeksi, joista viruksen perimä vapautuu noin kaksi tuntia infektion alun jälkeen. Tapahtuman yksityiskohtia ei kuitenkaan tunneta kovin tarkasti, eikä tiedetä mitkä tekijät laukaisevat viruksen perimän vapautumisen viruspartikkeleista ja rakkularakenteista. Tässä väitöskirjassa tutkittiin EV1:n perimän vapautumista ja viruksen vuorovaikutuksia lipidikalvojen kanssa. Selvitettiin miten kalvon lipidikoostumus vaikuttaa virusten vuorovaikutukseen kalvojen kanssa. Elektronimikroskopian avulla havaittiin, että jäykille, kolesterolista ja sfingomyeliinistä muodostuneille kalvoille sitoutuvat viruspartikkelit litistyivät hieman. Tämä kertoo voimakkaasta, suorasta vuorovaikutuksesta viruksen ja lipidien välillä. Koska integriinit ovat mukana rakkularakenteissa, joista virus vapautuu, tutkittiin myös integriinin vaikutusta viruksen ja lipidien väliselle vuorovaikutukselle. Havaittiin, että α2β1-integriinin läsnäollessa virusten litistyminen oli voimakkaampaa kuin ilman integriiniä. Tästä pääteltiin, että integriinin läsnäolo aiheutti viruksessa muutoksia, jotka johtivat joko viruksen rakenteen löystymiseen tai sen pinnan kemiallisten ominaisuuksien muuttumiseen siten, että se sitoutui voimakkaammin kalvolipideihin.

EV1:n perimän vapautumista viruspartikkeleista tutkittiin virustutkimuksessa potentiaaliinsa nähden melko vähän hyödynnetyllä menetelmällä, Raman-spektroskopialla. Raman-spektroskopiassa signaali perustuu molekyylien värähdyksiin ja sillä saadaan tietoa molekyyleissä tapahtuvista rakenteellisista ja kemiallisista muutoksista. Perimän vapautuminen viruspartikkelista saadaan puolestaan aikaan myös lämmittämällä viruksia, ilman soluista tulevia normaaleja vapautumista laukaisevia tekijöitä. Tässä väitöskirjatutkimuksessa määritettiin EV1:n Raman-spektroskooppinen sormenjälki ja verrattiin sitä viruksen tunnettuihin rakenteellisiin ja kemiallisiin ominaisuuksiin. Lämpökäsiteltyjen virusten avulla tutkittiin perimän vapautumiseen liittyviä kemiallisia ja rakenteellisia muutoksia. Tulokset viittaavat siihen, että viruspartikkelit muuttuvat perimän vapautuessa huokoisemmiksi. EV1:n Raman-sormenjäljen tunteminen myös mahdollistaa Raman-spektroskopian hyödyntämisen muiden enterovirusten tutkimisessa sekä monimutkaisemmissa koeasetelmissa.

REFERENCES

Anonymous 2014. International Committee on Taxonomy of Viruses. <URL:http://ictvonline.org/virusTaxonomy.asp> [Cited 29.6.2015].

Anonymous 2015. The Picornavirus Pages. <URL:http://www picornaviridae com/> [Cited 29.6.2015].

Abu-Rub M.T., Billiar K.L., van Es M.H., Knight A., Rodriguez B.J., Zeugolis D.I., McMahon S., Windebank A.J. & Pandit A. 2011. Nano-textured self-assembled aligned collagen hydrogels promote directional neurite guidance and overcome inhibition by myelin associated glycoprotein. *Soft Matter* 7: 2770-2781.

Adams M.J., Lefkowitz E.J., King A.M.Q., Bamford D.H., Breitbart M., Davison A.J., Ghabrial S.A., Gorbalenya A.E., Knowles N.J., Krell P., Lavigne R., Prangishvili D., Sanfacon H., Siddell S.G., Simmonds P. & Carstens E.B. 2015. Ratification vote on taxonomic proposals to the International Committee on Taxonomy of Viruses (2015). *Arch Virol* 160: 1837-1850.

Airaksinen A., Somerharju P. & Hovi T. 2001. Variation in Liposome Binding among Enteroviruses. *Virology* 279: 539-545.

Allison S.D., Dong A. & Carpenter J.F. 1996. Counteracting effects of thiocyanate and sucrose on chymotrypsinogen secondary structure and aggregation during freezing, drying, and rehydration. *Biophys J* 71: 2022-2032.

Aubrey K.L., Casjens S.R. & Thomas G.J. 1992. Secondary structure and interactions of the packaged dsDNA genome of bacteriophage P22 investigated by Raman difference spectroscopy. *Biochemistry (N Y)* 31: 11835-11842.

Barczyk M.M., Lu N., Popova S.N., Bolstad A.I. & Gullberg D. 2013. alpha 11 beta 1 integrin-mediated MMP-13-dependent collagen lattice contraction by fibroblasts: Evidence for integrin-coordinated collagen proteolysis. *J Cell Physiol* 228: 1108-1119.

Barrera F.N., Fendos J. & Engelman D.M. 2012. Membrane physical properties influence transmembrane helix formation. *Proceedings of the National Academy of Sciences* 109: 14422-14427.

Barth A. & Zscherp C. 2002. What vibrations tell about proteins. *Q Rev Biophys* 35: 369-430.

Bauer D.W., Huffman J.B., Homa F.L. & Evilevitch A. 2013. Herpes Virus Genome, The Pressure Is On. *J Am Chem Soc* 135: 11216-11221.

Baumgart T., Hammond A.T., Sengupta P., Hess S.T., Holowka D.A., Baird B.A. & Webb W.W. 2007. Large-scale fluid/fluid phase separation of proteins and lipids in giant plasma membrane vesicles. *Proceedings of the National Academy of Sciences* 104: 3165-3170.

Beglova N., Blacklow S.C., Takagi J. & Springer T.A. 2002. Cysteine-rich module structure reveals a fulcrum for integrin rearrangement upon activation. *Nat Struct Mol Biol* 9: 282-287.

Bella J., Eaton M., Brodsky B. & Berman H. 1994. Crystal and molecular structure of a collagen-like peptide at 1.9 A resolution. *Science* 266: 75-81.

Bella J. 2014. A first census of collagen interruptions: Collagen's own stutters and stammers. *J Struct Biol* 186: 438-450.

Bennett J.S. 2015. Regulation of Integrins in Platelets. *Peptide Science* : n/a-n/a.

Bergelson J.M., Shepley M., Chan B., Hemler M. & Finberg R.W. 1992. Identification of the integrin VLA-2 as a receptor for echovirus 1. *Science* 255: 1718-1720.

Bergstrom T., Holmqvist K., Tararuk T., Johansson S. & Forsberg-Nilsson K. 2014. Developmentally regulated collagen/integrin interactions confer adhesive properties to early postnatal neural stem cells. *Biochimica Et Biophysica Acta-General Subjects* 1840: 2526-2532.

Bilek G., Matscheko N.M., Pickl-Herk A., Weiss V.U., Subirats X., Kenndler E. & Blaas D. 2011. Liposomal Nanocontainers as Models for Viral Infection: Monitoring Viral Genomic RNA Transfer through Lipid Membranes. *Journal of Virology* 85: 8368-8375.

Bissig C. & Gruenberg J. 2013. Lipid Sorting and Multivesicular Endosome Biogenesis. *Cold Spring Harbor Perspectives in Biology* 5.

Blissett A.R., Garbellini D., Calomeni E.P., Mihai C., Elton T.S. & Agarwal G. 2009. Regulation of Collagen Fibrillogenesis by Cell-surface Expression of Kinase Dead DDR2. *J Mol Biol* 385: 902-911.

Bostina M., Levy H., Filman D.J. & Hogle J.M. 2011. Poliovirus RNA Is Released from the Capsid near a Twofold Symmetry Axis. *Journal of Virology* 85: 776-783.

Brandenburg B., Lee L.Y., Lakadamyali M., Rust M.J., Zhuang X. & Hogle J.M. 2007. Imaging Poliovirus Entry in Live Cells. *PLoS Biol* 5: e183.

Briesewitz R., Epstein M.R. & Marcantonio E.E. 1993. Expression of native and truncated forms of the human integrin alpha 1 subunit. *Journal of Biological Chemistry* 268: 2989-2996.

Bubeck D., Filman D.J., Cheng N., Steven A.C., Hogle J.M. & Belnap D.M. 2005. The Structure of the Poliovirus 135S Cell Entry Intermediate at 10-Angstrom Resolution Reveals the Location of an Externalized Polypeptide That Binds to Membranes. *Journal of Virology* 79: 7745-7755.

Burgess J.K., Ceresa C., Johnson S.R., Kanabar V., Moir L.M., Nguyen T.T.B., Oliver B.G.G., Schuliga M. & Ward J. 2009. Tissue and matrix influences on airway smooth muscle function. *Pulm Pharmacol Ther* 22: 379-387.

Calderwood D.A., Tuckwell D.S., Eble J., Kühn K. & Humphries M.J. 1997. The Integrin a1 A-domain Is a Ligand Binding Site for Collagens and Laminin. *Journal of Biological Chemistry* 272: 12311-12317.

Camper L., Hellman U. & Lundgren-Åkerlund E. 1998. Isolation, Cloning, and Sequence Analysis of the Integrin Subunit a10, a ß1-associated Collagen Binding Integrin Expressed on Chondrocytes. *Journal of Biological Chemistry* 273: 20383-20389.

Chakravarti S., Magnuson T., Lass J.H., Jepsen K.J., LaMantia C. & Carroll H. 1998. Lumican Regulates Collagen Fibril Assembly: Skin Fragility and

Corneal Opacity in the Absence of Lumican. *The Journal of Cell Biology* 141: 1277-1286.

Chatterjee P.K., Vashishtha M. & Kielian M. 2000. Biochemical Consequences of a Mutation That Controls the Cholesterol Dependence of Semliki Forest Virus Fusion. *Journal of Virology* 74: 1623-1631.

Chautard E., Ballut L., Thierry-Mieg N. & Ricard-Blum S. 2009. MatrixDB, a database focused on extracellular protein-protein and protein-carbohydrate interactions. *Bioinformatics* 25: 690-691.

Chouhan B.S., Käpylä J., Denessiouk K., Denesyuk A., Heino J. & Johnson M.S. 2014. Early Chordate Origin of the Vertebrate Integrin aI Domains. *PLoS ONE* 9: e112064.

Chow M., Newman J.F.E., Filman D., Hogle J.M., Rowlands D.J. & Brown F. 1987. Myristylation of picornavirus capsid protein VP4 and its structural significance. *Nature* 327: 482-486.

Christalla P., Hudson J.E. & Zimmermann W. 2012. The Cardiogenic Niche as a Fundamental Building Block of Engineered Myocardium. *Cells Tissues Organs (Print)* 195: 82-93.

Chukkapalli V., Heaton N.S. & Randall G. 2012. Lipids at the interface of virus–host interactions. *Curr Opin Microbiol* 15: 512-518.

Connors W.L., Jokinen J., White D.J., Puranen J.S., Kankaanpaa P., Upla P., Tulla M., Johnson M.S. & Heino J. 2007. Two synergistic activation mechanisms of alpha 2 beta 1 integrin-mediated collagen binding. *J Biol Chem* 282: 14675-14683.

Conti J.A., Kendall T.J., Bateman A., Armstrong T.A., Papa-Adams A., Xu Q., Packham G., Primrose J.N., Benyon R.C. & Iredale J.P. 2008. The Desmoplastic Reaction Surrounding Hepatic Colorectal Adenocarcinoma Metastases Aids Tumor Growth and Survival via alpha(v) Integrin Ligation. *Clinical Cancer Research* 14: 6405-6413.

Curry S., Chow M. & Hogle J.M. 1996. The poliovirus 135S particle is infectious. *Journal of Virology* 70: 7125-7131.

Czamara K., Majzner K., Pacia M.Z., Kochan K., Kaczor A. & Baranska M. 2015. Raman spectroscopy of lipids: a review. *J Raman Spectrosc* 46: 4-20.

da Cunha C.B., Klumpers D.D., Li W.A., Koshy S.T., Weaver J.C., Chaudhuri O., Granja P.L. & Mooney D.J. 2014. Influence of the stiffness of three-dimensional alginate/collagen-I interpenetrating networks on fibroblast biology. *Biomaterials* 35: 8927-8936.

Danielson K.G., Baribault H., Holmes D.F., Graham H., Kadler K.E. & Iozzo R.V. 1997. Targeted Disruption of Decorin Leads to Abnormal Collagen Fibril Morphology and Skin Fragility. *The Journal of Cell Biology* 136: 729-743.

Danthi P. & Chow M. 2004. Cholesterol Removal by Methyl-ß-Cyclodextrin Inhibits Poliovirus Entry. *Journal of Virology* 78: 33-41.

Danthi P., Tosteson M., Li Q. & Chow M. 2003. Genome Delivery and Ion Channel Properties Are Altered in VP4 Mutants of Poliovirus. *Journal of Virology* 77: 5266-5274.

Davis M.P., Bottley G., Beales L.P., Killington R.A., Rowlands D.J. & Tuthill T.J. 2008. Recombinant VP4 of Human Rhinovirus Induces Permeability in Model Membranes. *Journal of Virology* 82: 4169-4174.

De Gelder J., De Gussem K., Vandenabeele P. & Moens L. 2007. Reference database of Raman spectra of biological molecules. *J Raman Spectrosc* 38: 1133-1147.

de Lange M.J.L., Bonn M. & Müller M. 2007. Direct measurement of phase coexistence in DPPC/cholesterol vesicles using Raman spectroscopy. *Chem Phys Lipids* 146: 76-84.

DeMaio L., Buckley S.T., Krishnaveni M.S., Flodby P., Dubourd M., Banfalvi A., Xing Y., Ehrhardt C., Minoo P., Zhou B., Crandall E.D. & Borok Z. 2012. Ligand-independent transforming growth factor-beta type I receptor signalling mediates type I collagen-induced epithelial-mesenchymal transition. *J Pathol* 226: 633-644.

den Boon J.A. & Ahlquist P. 2010. Organelle-Like Membrane Compartmentalization of Positive-Strand RNA Virus Replication Factories. *Annu Rev Microbiol* 64: 241-256.

Diaz-Rohrer B., Levental K.R. & Levental I. 2014. Rafting through traffic: Membrane domains in cellular logistics. *Biochimica et Biophysica Acta (BBA) - Biomembranes* 1838: 3003-3013.

Dickeson S.K., Walsh J.J. & Santoro S.A. 1997. Contributions of the I and EF Hand Domains to the Divalent Cation-dependent Collagen Binding Activity of the a2ß1 Integrin. *Journal of Biological Chemistry* 272: 7661-7668.

Dinakarpandian D., Shenoy B., Pusztai-Carey M., Malcolm B.A. & Carey P.R. 1997. Active Site Properties of the 3C Proteinase from Hepatitis A Virus (a Hybrid Cysteine/Serine Protease) Probed by Raman Spectroscopy. *Biochemistry (N Y)* 36: 4943-4948.

Dolja V.V., Boyko V.P., Agranovsky A.A. & Koonin E.V. 1991. Phylogeny of capsid proteins of rod-shaped and filamentous RNA plant viruses: Two families with distinct patterns of sequence and probably structure conservation. *Virology* 184: 79-86.

Domke K.F. & Pettinger B. 2010. Studying Surface Chemistry beyond the Diffraction Limit: 10 Years of TERS. *ChemPhysChem* 11: 1365-1373.

Downes A. & Elfick A. 2010. Raman Spectroscopy and Related Techniques in Biomedicine. *Sensors* 10: 1871-1889.

Eckes B., Zweers M.C., Zhang Z.G., Hallinger R., Mauch C., Aumailley M. & Krieg T. 2006. Mechanical tension and integrin alpha 2 beta 1 regulate fibroblast functions. *Journal of Investigative Dermatology Symposium Proceedings* 11: 66-72.

Ekholm E., Hankenson K.D., Uusitalo H., Hiltunen A., Gardner H., Heino J. & Penttinen R. 2002. Diminished Callus Size and Cartilage Synthesis in α1β1 Integrin-Deficient Mice during Bone Fracture Healing. *Am J Pathol* 160: 1779-1785.

El Ghalbzouri A., Jonkman M., Dijkman R. & Ponec M. 2005. Basement membrane reconstruction in human skin equivalents is regulated by

fibroblasts and/or exogenously activated keratinocytes. *J Invest Dermatol* 124: 79-86.

Elliott J., Woodward J., Langenbach K., Tona A., Jones P. & Plant A. 2005. Vascular smooth muscle cell response on thin films of collagen. *Matrix Biology* 24: 489-502.

Emsley J., Knight C.G., Farndale R.W., Barnes M.J. & Liddington R.C. 2000. Structural Basis of Collagen Recognition by Integrin α2β1. *Cell* 101: 47-56.

Farran A.J.E., Teller S.S., Jha A.K., Jiao T., Hule R.A., Clifton R.J., Pochan D.P., Duncan R.L. & Jia X. 2010. Effects of Matrix Composition, Microstructure, and Viscoelasticity on the Behaviors of Vocal Fold Fibroblasts Cultured in Three-Dimensional Hydrogel Networks. *Tissue Engineering Part a* 16: 1247-1261.

Feng Z., Hensley L., McKnight K.L., Hu F., Madden V., Ping L., Jeong S., Walker C., Lanford R.E. & Lemon S.M. 2013. A pathogenic picornavirus acquires an envelope by hijacking cellular membranes. *Nature* 496: 367-371.

Ferraro J.R., Nakamoto K. & Brown C.W. 2003. *Introductory Raman spectroscopy.* Academic Press, Amsterdam,Boston.

Filman D.J., Wien M.W., Cunningham J.A., Bergelson J.M. & Hogle J.M. 1998. Structure Determination of Echovirus 1. *Acta Crystallographica Section D* 54: 1261-1272.

Fish S.R., Hartman K.A., Fuller M.T., King J. & Thomas Jr. G.J. 1980. Investigation of secondary structures and macromolecular interactions in bacteriophage p22 by laser raman spectroscopy. *Biophys J* 32: 234-237.

Flynn L.A., Blissett A.R., Calomeni E.P. & Agarwal G. 2010. Inhibition of Collagen Fibrillogenesis by Cells Expressing Soluble Extracellular Domains of DDR1 and DDR2. *J Mol Biol* 395: 533-543.

Fricks C.E. & Hogle J.M. 1990. Cell-induced conformational change in poliovirus: externalization of the amino terminus of VP1 is responsible for liposome binding. *Journal of Virology* 64: 1934-1945.

Fujimura T., Moriwaki S., Imokawa G. & Takema Y. 2007. Crucial role of fibroblast integrins alpha 2 and beta 1 in maintaining the structural and mechanical properties of the skin. *J Dermatol Sci* 45: 45-53.

Gahmberg C.G., Fagerholm S.C., Nurmi S.M., Chavakis T., Marchesan S. & Grönholm M. 2009. Regulation of integrin activity and signalling. *Biochimica et Biophysica Acta (BBA) - General Subjects* 1790: 431-444.

Gardner H., Broberg A., Pozzi A., Laato M. & Heino J. 1999. Absence of integrin alpha1beta1 in the mouse causes loss of feedback regulation of collagen synthesis in normal and wounded dermis. *Journal of Cell Science* 112: 263-272.

Gertsman I., Fu C., Huang R., Komives E.A. & Johnson J.E. 2010. Critical Salt Bridges Guide Capsid Assembly, Stability, and Maturation Behavior in Bacteriophage HK97. *Molecular & Cellular Proteomics* 9: 1752-1763.

Gilchrist C.L., Chen J., Richardson W.J., Loeser R.F. & Setton L.A. 2007. Functional integrin subunits regulating cell-matrix interactions in the intervertebral disc. *Journal of Orthopaedic Research* 25: 829-840.

Gilcrease M.Z. 2007. Integrin signaling in epithelial cells. *Cancer Lett* 247: 1-25.

Gogly B., Fournier B., Couty L., Naveau A., Brasselet C., Durand E., Coulomb B. & Lafont A. 2009. Gingival fibroblast inhibits MMP-7: Evaluation in an ex vivo aorta model. *J Mol Cell Cardiol* 47: 296-303.

Gruschwitz R., Friedrichs J., Valtink M., Franz C.M., Mueller D.J., Funk R.H.W. & Engelmann K. 2010. Alignment and Cell-Matrix Interactions of Human Corneal Endothelial Cells on Nanostructured Collagen Type I Matrices. *Invest Ophthalmol Vis Sci* 51: 6303-6310.

Grygon C.A., Perno J.R., Fodor S.P. & Spiro T.G. 1988. Ultraviolet resonance Raman spectroscopy as a probe of protein structure in the fd virus. *Biotechniques* 6: 50-55.

Hartman K.A., McDonald-Ordzie P., Kaper J.M., Prescott B. & Thomas G.J. 1978. Studies of virus structure by laser-Raman spectroscopy. 4. Turnip yellow mosaic virus and capsids. *Biochemistry (N Y)* 17: 2118-2123.

Harutyunyan S., Kowalski H. & Blaas D. 2014. The Rhinovirus Subviral A-Particle Exposes 3'-Terminal Sequences of Its Genomic RNA. *Journal of Virology* 88: 6307-6317.

He Y., Liu S., Li J., Lu H., Qi Z., Liu Z., Debnath A.K. & Jiang S. 2008. Conserved Salt Bridge between the N- and C-Terminal Heptad Repeat Regions of the Human Immunodeficiency Virus Type 1 gp41 Core Structure Is Critical for Virus Entry and Inhibition. *Journal of Virology* 82: 11129-11139.

Heaton N.S. & Randall G. 2011. Multifaceted roles for lipids in viral infection. *Trends Microbiol* 19: 368-375.

Heino J. 2014. Cellular Signaling by Collagen-Binding Integrins. In: Gullberg D. (ed.), , Springer Netherlands, pp. 143-155.

Heino J. 2000. The collagen receptor integrins have distinct ligand recognition and signaling functions. *Matrix Biology* 19: 319-323.

Helary C., Rodrigues-Sanchez B., Vigier S. & Guille M.-.G. 2012. Dense fibrillar collagen matrices to analyse extracellular matrix receptor function. *Pathologie Biologie* 60: 7-14.

Helenius A. 1984. Semliki Forest viruspenetration from endosomes: a morphological study. *Biol Cell* 51: 181-185.

Hermann P., Hermelink A., Lausch V., Holland G., Moller L., Bannert N. & Naumann D. 2011. Evaluation of tip-enhanced Raman spectroscopy for characterizing different virus strains. *Analyst* 136: 1148-1152.

Hernandez B., Pfluger F., Adenier A., Kruglik S.G. & Ghomi M. 2010. Vibrational Analysis of Amino Acids and Short Peptides in Hydrated Media. VIII. Amino Acids with Aromatic Side Chains: l-Phenylalanine, l-Tyrosine, and l-Tryptophan. *J Phys Chem B* 114: 15319-15330.

Hernández B., Baumruk V., Leulliot N., Gouyette C., Huynh-Dinh T. & Ghomi M. 2003. Thermodynamic and structural features of ultrastable DNA and RNA hairpins. *J Mol Struct* 651–653: 67-74.

Hewish M.J., Takada Y. & Coulson B.S. 2000. Integrins a2ß1 and a4ß1 Can Mediate SA11 Rotavirus Attachment and Entry into Cells. *Journal of Virology* 74: 228-236.

Hill W.M. 1996. Are echoviruses still orphans? *Br J Biomed Sci* 53: 221-226.

Hober D. & Sauter P. 2010. Pathogenesis of type 1 diabetes mellitus: interplay between enterovirus and host. *Nat Rev Endocrinol* 6: 279-289.

Hobro A.J., Standley D.M., Ahmad S. & Smith N.I. 2013. Deconstructing RNA: optical measurement of composition and structure. *Phys Chem Chem Phys* 15: 13199-13208.

Hobro A.J., Rouhi M., Blanch E.W. & Conn G.L. 2007. Raman and Raman optical activity (ROA) analysis of RNA structural motifs in Domain I of the EMCV IRES. *Nucleic Acids Research* 35: 1169-1177.

Hogle J.M. 2002. Poliovirus Cell Entry: Common Structural Themes in Viral Cell Entry Pathways. *Annu Rev Microbiol* 56: 677-702.

Hogle J., Chow M. & Filman D. 1985. Three-dimensional structure of poliovirus at 2.9 A resolution. *Science* 229: 1358-1365.

Holmes D.F., Chapman J.A., Prockop D.J. & Kadler K.E. 1992. Growing tips of type I collagen fibrils formed in vitro are near-paraboloidal in shape, implying a reciprocal relationship between accretion and diameter. *Proc Natl Acad Sci U S A* 89: 9855-9859.

Hong G., Chen C., Lin M., Krüger J., Becker C.F.W., Fink R.H.A. & Fischer W.B. 2012. Molecular dynamics simulations and conductance studies of the interaction of VP1 N-terminus from Polio virus and gp41 fusion peptide from HIV-1 with lipid membranes. *Mol Membr Biol* 29: 9-25.

Hu S., Cui D., Yang X., Hu J., Wan W. & Zeng J. 2011. The crucial role of collagen-binding integrins in maintaining the mechanical properties of human scleral fibroblasts-seeded collagen matrix. *Molecular Vision* 17: 1334-1342.

Hulmes D.J. & Miller A. 1979. Quasi-hexagonal molecular packing in collagen fibrils. *Nature* 282: 878-880.

Hulmes D.J.S. 2002. Building Collagen Molecules, Fibrils, and Suprafibrillar Structures. *J Struct Biol* 137: 2-10.

Huttunen M., Waris M., Kajander R., Hyypiä T. & Marjomäki V. 2014. Coxsackievirus A9 Infects Cells via Nonacidic Multivesicular Bodies. *Journal of Virology* 88: 5138-5151.

Hynes R.O. & Zhao Q. 2000. The Evolution of Cell Adhesion. *The Journal of Cell Biology* 150: F89-F96.

Ilnytska O., Santiana M., Hsu N., Du W., Chen Y., Viktorova E., Belov G., Brinker A., Storch J., Moore C., Dixon J. & Altan-Bonnet N. 2013. Enteroviruses Harness the Cellular Endocytic Machinery to Remodel the Host Cell Cholesterol Landscape for Effective Viral Replication. *Cell Host & Microbe* 14: 281-293.

Ipsen J.H., Karlström G., Mouritsen O.G., Wennerström H. & Zuckermann M.J. 1987. Phase equilibria in the phosphatidylcholine-cholesterol system. *Biochim Biophys Acta* 27: 162-172.

Ivaska J., Reunanen H., Westermarck J., Koivisto L., Kähäri V. & Heino J. 1999. Integrin a2ß1 Mediates Isoform-Specific Activation of p38 and Upregulation of Collagen Gene Transcription by a Mechanism Involving the a2 Cytoplasmic Tail. *The Journal of Cell Biology* 147: 401-416.

Jackson W.T. 2014. Poliovirus-induced changes in cellular membranes throughout infection. *Current Opinion in Virology* 9: 67-73.

Johnson F., Saigal B., Talpaz M. & Donato N. 2005. Dasatinib (BMS-354825) tyrosine kinase inhibitor suppresses invasion and induces cell cycle arrest and apoptosis of head and neck squamous cell carcinoma and non-small cell lung cancer cells. *Clinical Cancer Research* 11: 6924-6932.

Johnson M.S., Lu N., Denessiouk K., Heino J. & Gullberg D. 2009. Integrins during evolution: Evolutionary trees and model organisms. *Biochimica et Biophysica Acta (BBA) - Biomembranes* 1788: 779-789.

Joisson C., Kuster F., Plaué S. & Regenmortel M.H.V. 1993. Antigenic analysis of bean pod mottle virus using linear and cyclized synthetic peptides. *Arch Virol* 128: 299-317.

Jokinen J., White D.J., Salmela M., Huhtala M., Käpylä J., Sipilä K., Puranen J., Nissinen L., Kankaanpää P., Marjomäki V., Hyypiä T., Johnson M.S. & Heino J. 2010. Molecular mechanism of α 2β 1 integrin interaction with human echovirus 1. *EMBO J* 29: 196-208.

Jungmann O., Nikolovska K., Stock C., Schulz J., Eckes B., Riethmueller C., Owens R.T., Iozzo R.V. & Seidler D.G. 2012. The Dermatan Sulfate Proteoglycan Decorin Modulates alpha 2 beta 1 Integrin and the Vimentin Intermediate Filament System during Collagen Synthesis. *Plos One* 7: e50809.

Kadler K.E., Holmes D.F., Trotter J.A. & Chapman J.A. 1996. Collagen fibril formation. *Biochem J* 316 (Pt 1): 1-11.

Kadler K.E., Hill A. & Canty-Laird E.G. 2008. Collagen fibrillogenesis: fibronectin, integrins, and minor collagens as organizers and nucleators. *Curr Opin Cell Biol* 20: 495-501.

Kamata T. & Takada Y. 1994. Direct binding of collagen to the I domain of integrin alpha 2 beta 1 (VLA-2, CD49b/CD29) in a divalent cation-independent manner. *Journal of Biological Chemistry* 269: 26006-26010.

Kaminaka S., Imamura Y., Shingu M., Kitagawa T. & Toyoda T. 1999. Studies of bovine enterovirus structure by ultraviolet resonance Raman spectroscopy. *J Virol Methods* 77: 117-123.

Kaplan G., Freistadt M.S. & Racaniello V.R. 1990. Neutralization of poliovirus by cell receptors expressed in insect cells. *Journal of Virology* 64: 4697-4702.

Karjalainen M., Rintanen N., Lehkonen M., Kallio K., Mäki A., Hellström K., Siljamäki V., Upla P. & Marjomäki V. 2011. Echovirus 1 infection depends on biogenesis of novel multivesicular bodies. *Cell Microbiol* 13: 1975-1995.

Karjalainen M., Kakkonen E., Upla P., Paloranta H., Kankaanpää P., Liberali P., Renkema G.H., Hyypiä T., Heino J. & Marjomäki V. 2008. A Raft-derived, Pak1-regulated Entry Participates in a2ß1 Integrin-dependent Sorting to Caveosomes. *Molecular Biology of the Cell* 19: 2857-2869.

Karsdal M.A., Manon-Jensen T., Genovese F., Kristensen J.H., Nielsen M.J., Sand J.M.B., Hansen N.B., Bay-Jensen A., Bager C.L., Krag A., Blanchard A., Krarup H., Leeming D.J. & Schuppan D. 2015. Novel insights into the function and dynamics of extracellular matrix in liver fibrosis. *American Journal of Physiology - Gastrointestinal and Liver Physiology* 308: G807-G830.

Kartenbeck J., Stukenbrok H. & Helenius A. 1989. Endocytosis of simian virus 40 into the endoplasmic reticulum. *J Cell Biol* 109: 2721-2729.

Kawase T., Uematsu K., Kamiya M., Nagata M., Okuda K., Burns D.M., Nakata K. & Yoshie H. 2014. Real-time quantitative polymerase chain reaction and flow cytometric analyses of cell adhesion molecules expressed in human cell-multilayered periosteal sheets in vitro. *Cytotherapy* 16: 653-661.

Kehrel B. 1995. Platelet receptors for collagens. *Platelets* 6: 11-16.

Kern A., Briesewitz R., Bank I. & Marcantonio E.E. 1994. The role of the I domain in ligand binding of the human integrin alpha 1 beta 1. *Journal of Biological Chemistry* 269: 22811-22816.

Kern A., Eble J., Golbik R. & Kühn K. 1993. Interaction of type IV collagen with the isolated integrins α1β1 and α2β1. *European Journal of Biochemistry* 215: 151-159.

Khew S.T. & Tong Y.W. 2007. The specific recognition of a cell binding sequence derived from type I collagen by Hep3B and L929 cells. *Biomacromolecules* 8: 3153-3161.

Kielian M., Chanel-Vos C. & Liao M. 2010. Alphavirus Entry and Membrane Fusion. *Viruses* 2: 796-825.

Kim C. & Bergelson J.M. 2012. Echovirus 7 Entry into Polarized Intestinal Epithelial Cells Requires Clathrin and Rab7. *mBio* 3.

Knight C.G., Morton L.F., Peachey A.R., Tuckwell D.S., Farndale R.W. & Barnes M.J. 2000. The Collagen-binding A-domains of Integrins a1ß1 and a2ß1Recognize the Same Specific Amino Acid Sequence, GFOGER, in Native (Triple-helical) Collagens. *Journal of Biological Chemistry* 275: 35-40.

Kumar M. & Blaas D. 2013. Human Rhinovirus Subviral A Particle Binds to Lipid Membranes over a Twofold Axis of Icosahedral Symmetry. *Journal of Virology* 87: 11309-11312.

Kumar V.A., Caves J.M., Haller C.A., Dai E., Liu L., Grainger S. & Chaikof E.L. 2013. Collagen-based substrates with tunable strength for soft tissue engineering. *Biomaterials Science* 1: 1193-1202.

Kuznetsova N. & Leikin S. 1999. Does the Triple Helical Domain of Type I Collagen Encode Molecular Recognition and Fiber Assembly while Telopeptides Serve as Catalytic Domains?: Effect of Proteolytic Cleavage on Fibrillogenesis and on Collagen-Collagen Interaction in Fibres. *Journal of Biological Chemistry* 274: 36083-36088.

Kyriakides T.R., Zhu Y., Smith L.T., Bain S.D., Yang Z., Lin M.T., Danielson K.G., Iozzo R.V., LaMarca M., McKinney C.E., Ginns E.I. & Bornstein P. 1998. Mice That Lack Thrombospondin 2 Display Connective Tissue Abnormalities That Are Associated with Disordered Collagen

Fibrillogenesis, an Increased Vascular Density, and a Bleeding Diathesis. *The Journal of Cell Biology* 140: 419-430.

Lambert P., Whitman A., Dyson O. & Akula S. 2006. Raman spectroscopy: the gateway into tomorrow's virology. *Virology Journal* 3: 51.

Langholz O., Röckel D., Mauch C., Kozlowska E., Bank I., Krieg T. & Eckes B. 1995. Collagen and collagenase gene expression in three-dimensional collagen lattices are differentially regulated by alpha 1 beta 1 and alpha 2 beta 1 integrins. *The Journal of Cell Biology* 131: 1903-1915.

Lee J.H., Oh B.K. & Choi J.W. 2012. Development of a HIV-1 Virus Detection System Based on Nanotechnology. *Sensors (Basel)* 15: 9915-9927.

Leikina E., Mertts M.V., Kuznetsova N. & Leikin S. 2002. Type I collagen is thermally unstable at body temperature. *Proceedings of the National Academy of Sciences* 99: 1314-1318.

Levy H.C., Bostina M., Filman D.J. & Hogle J.M. 2010. Catching a Virus in the Act of RNA Release: a Novel Poliovirus Uncoating Intermediate Characterized by Cryo-Electron Microscopy. *Journal of Virology* 84: 4426-4441.

Li Q., Yafal A.G., Lee Y.M., Hogle J. & Chow M. 1994. Poliovirus neutralization by antibodies to internal epitopes of VP4 and VP1 results from reversible exposure of these sequences at physiological temperature. *Journal of Virology* 68: 3965-3970.

Li S., Sieben C., Ludwig K., Höfer C., Chiantia S., Herrmann A., Eghiaian F. & Schaap I.T. 2014. pH-Controlled Two-Step Uncoating of Influenza Virus. *Biophys J* 106: 1447-1456.

Li S., Van Den Diepstraten C., D'souza S.J., Chan B.M.C. & Pickering J.G. 2003. Vascular Smooth Muscle Cells Orchestrate the Assembly of Type I Collagen via α2β1 Integrin, RhoA, and Fibronectin Polymerization. *Am J Pathol* 163: 1045-1056.

Li T., Johnson J.E. & Thomas G.J., J. 1993. Raman dynamic probe of hydrogen exchange in bean pod mottle virus: base-specific retardation of exchange in packaged ssRNA. *Biophys J* 65: 1963-1972.

Li T., Chen Z., Johnson J.E. & Thomas G.J. 1992. Conformations, interactions, and thermostabilities of RNA and proteins in bean pod mottle virus: investigation of solution and crystal structures by laser Raman spectroscopy. *Biochemistry (N Y)* 31: 6673-6682.

Li T., Chen Z., Johnson J.E. & Thomas G.J. 1990. Structural studies of bean pod mottle virus, capsid and RNA in crystal and solution states by laser Raman spectroscopy. *Biochemistry (N Y)* 29: 5018-5026.

Lin J., Cheng N., Chow M., Filman D.J., Steven A.C., Hogle J.M. & Belnap D.M. 2011. An Externalized Polypeptide Partitions between Two Distinct Sites on Genome-Released Poliovirus Particles. *Journal of Virology* 85: 9974-9983.

Lu Y.E., Cassese T. & Kielian M. 1999. The Cholesterol Requirement for Sindbis Virus Entry and Exit and Characterization of a Spike Protein Region Involved in Cholesterol Dependence. *Journal of Virology* 73: 4272-4278.

Lundgren-Akerlund E. & Aszodi A. 2014. Integrin alpha10beta1: a collagen receptor critical in skeletal development. *Adv Exp Med Biol* 819: 61-71.

Luo S., Sivashanmugan K., Liao J., Yao C. & Peng H. 2014. Nanofabricated SERS-active substrates for single-molecule to virus detection in vitro: A review. *Biosensors and Bioelectronics* 61: 232-240.

Marjomäki V., Pietiäinen V., Matilainen H., Upla P., Ivaska J., Nissinen L., Reunanen H., Huttunen P., Hyypiä T. & Heino J. 2002. Internalization of Echovirus 1 in Caveolae. *Journal of Virology* 76: 1856-1865.

Martín-Acebes M.A., González-Magaldi M., Sandvig K., Sobrino F. & Armas-Portela R. 2007. Productive entry of type C foot-and-mouth disease virus into susceptible cultured cells requires clathrin and is dependent on the presence of plasma membrane cholesterol. *Virology* 369: 105-118.

Matthäus C., Bird B., Miljković M., Chernenko T., Romeo M. & Diem M. 2008. Chapter 10 Infrared and Raman Microscopy in Cell Biology. In: Anonymous Methods in Cell Biology, Academic Press, pp. 275-308.

McLane J.S., Rivet C.J., Gilbert R.J. & Ligon L.A. 2014. A biomaterial model of tumor stromal microenvironment promotes mesenchymal morphology but not epithelial to mesenchymal transition in epithelial cells. *Acta Biomaterialia* 10: 4811-4821.

Medigeshi G.R., Hirsch A.J., Streblow D.N., Nikolich-Zugich J. & Nelson J.A. 2008. West Nile Virus Entry Requires Cholesterol-Rich Membrane Microdomains and Is Independent of avß3 Integrin. *Journal of Virology* 82: 5212-5219.

Mhanna R.F., Voeroes J. & Zenobi-Wong M. 2011. Layer-by-Layer Films Made from Extracellular Matrix Macromolecules on Silicone Substrates. *Biomacromolecules* 12: 609-616.

Milán-Garcés E., Kaptan S. & Puranik M. 2013. Mode-Specific Reorganization Energies and Ultrafast Solvation Dynamics of Tryptophan from Raman Line-Shape Analysis. *Biophys J* 105: 211-221.

Miles C.A. & Ghelashvili M. 1999. Polymer-in-a-box mechanism for the thermal stabilization of collagen molecules in fibers. *Biophys J* 76: 3243-3252.

Miura T., Takeuchi H. & Harada I. 1989. Tryptophan Raman bands sensitive to hydrogen bonding and side-chain conformation. *J Raman Spectrosc* 20: 667-671.

Miura T., Takeuchi H. & Harada I. 1988. Characterization of individual tryptophan side chains in proteins using Raman spectroscopy and hydrogen-deuterium exchange kinetics. *Biochemistry (N Y)* 27: 88-94.

Mizejewski G.J. 1999. Role of integrins in cancer: survey of expression patterns. *Proc Soc Exp Biol Med* 222: 124-138.

Möbius W., Van Donselaar E., Ohno-Iwashita Y., Shimada Y., Heijnen H.F.G., Slot J.W. & Geuze H.J. 2003. Recycling Compartments and the Internal Vesicles of Multivesicular Bodies Harbor Most of the Cholesterol Found in the Endocytic Pathway. *Traffic* 4: 222-231.

Montesano R., Soulie P., Eble J. & Carrozzino F. 2005. Tumour necrosis factor alpha confers an invasive, transformed phenotype on mammary epithelial cells. *J Cell Sci* 118: 3487-3500.

Moor K., Ohtani K., Myrzakozha D., Zhanserkenova O., Andriana B.B. & Sato H. 2014. Noninvasive and label-free determination of virus infected cells by Raman spectroscopy. *J Biomed Opt* 19: 067003-067003.

Muckelbauer J.K., Kremer M., Minor I., Diana G., Dutko F.J., Groarke J., Pevear D.C. & Rossmann M.G. 1995. The structure of coxsackievirus B3 at 3.5 A resolution. *Structure* 3: 653-667.

Nabavi N., Pustylnik S. & Harrison R.E. 2012. Rab GTPase Mediated Procollagen Trafficking in Ascorbic Acid Stimulated Osteoblasts. *Plos One* 7: e46265.

Negri P. & Dluhy R.A. 2013. Ag nanorod based surface-enhanced Raman spectroscopy applied to bioanalytical sensing. *Journal of Biophotonics* 6: 20-35.

Nho R.S. & Kahm J. 2010. beta 1-Integrin-Collagen Interaction Suppresses FoxO3a by the Coordination of Akt and PP2A. *J Biol Chem* 285: 14195-14209.

Nho R.S., Xia H., Diebold D., Kahm J., Kleidon J., White E. & Henke C.A. 2006. PTEN regulates fibroblast elimination during collagen matrix contraction. *J Biol Chem* 281: 33291-33301.

Niaura G. 2006. Raman Spectroscopy in Analysis of Biomolecules. In: Anonymous Encyclopedia of Analytical Chemistry, John Wiley & Sons, Ltd.

Nykvist P., Tu H., Ivaska J., Käpylä J., Pihlajaniemi T. & Heino J. 2000. Distinct Recognition of Collagen Subtypes by a1ß1 and a2ß1Integrins: a1ß1 Mediates Cell Adhesion to Type XIII Collagen. *J Biol Chem* 275: 8255-8261.

Nykvist P., Tasanen K., Viitasalo T., Käpylä J., Jokinen J., Bruckner-Tuderman L. & Heino J. 2001. The Cell Adhesion Domain of Type XVII Collagen Promotes Integrin-mediated Cell Spreading by a Novel Mechanism. *Journal of Biological Chemistry* 276: 38673-38679.

Oelker A.M. & Grinstaff M.W. 2012. Synthesis, Characterization, and In Vitro Evaluation of a Hydrogel-Based Corneal Onlay. *Ieee Transactions on Nanobioscience* 11: 37-45.

Olschewski K., Kammer E., Stockel S., Bocklitz T., Deckert-Gaudig T., Zell R., Cialla-May D., Weber K., Deckert V. & Popp J. 2015. A manual and an automatic TERS based virus discrimination. *Nanoscale* 7: 4545-4552.

Orgel J.P., Wess T.J. & Miller A. 2000. The in situ conformation and axial location of the intermolecular cross-linked non-helical telopeptides of type I collagen. *Structure* 8: 137-142.

Orgel J.P.R.O., Irving T.C., Miller A. & Wess T.J. 2006. Microfibrillar structure of type I collagen in situ. *Proceedings of the National Academy of Sciences* 103: 9001-9005.

Overman S.A. & Thomas G.J. 1998. Amide Modes of the alpha-Helix: Raman Spectroscopy of Filamentous Virus fd Containing Peptide 13C and 2H Labels in Coat Protein Subunits. *Biochemistry (N Y)* 37: 5654-5665.

Overman S.A. & Thomas G.J. 1995. Raman Spectroscopy of the Filamentous Virus Ff (fd, f1, M13): Structural Interpretation for Coat Protein Aromatics. *Biochemistry (N Y)* 34: 5440-5451.

Overman S.A., Aubrey K.L., Vispo N.S., Cesareni G. & Thomas G.J. 1994. Novel Tyrosine Markers in Raman Spectra of Wild-Type and Mutant (Y21M and Y24M) Ff Virions Indicate Unusual Environments for Coat Protein Phenoxyls. *Biochemistry (N Y)* 33: 1037-1042.

Panjwani A., Strauss M., Gold S., Wenham H., Jackson T., Chou J.J., Rowlands D.J., Stonehouse N.J., Hogle J.M. & Tuthill T.J. 2014. Capsid Protein VP4 of Human Rhinovirus Induces Membrane Permeability by the Formation of a Size-Selective Multimeric Pore. *PLoS Pathog* 10: e1004294.

Park E.S. & Boxer S.G. 2002. Origins of the Sensitivity of Molecular Vibrations to Electric Fields: Carbonyl and Nitrosyl Stretches in Model Compounds and Proteins. *J Phys Chem B* 106: 5800-5806.

Perumal S., Antipova O. & Orgel J.P.R.O. 2008. Collagen fibril architecture, domain organization, and triple-helical conformation govern its proteolysis. *Proc Natl Acad Sci U S A* 105: 2824-2829.

Pickl-Herk A., Luque D., Vives-Adrián L., Querol-Audí J., Garriga D., Trus B.L., Verdaguer N., Blaas D. & Castón J.R. 2013. Uncoating of common cold virus is preceded by RNA switching as determined by X-ray and cryo-EM analyses of the subviral A-particle. *Proceedings of the National Academy of Sciences* 110: 20063-20068.

Pietiäinen V., Marjomäki V., Upla P., Pelkmans L., Helenius A. & Hyypiä T. 2004. Echovirus 1 Endocytosis into Caveosomes Requires Lipid Rafts, Dynamin II, and Signaling Events. *Molecular Biology of the Cell* 15: 4911-4925.

Piez K.A. & Trus B.L. 1981. A new model for packing of type-I collagen molecules in the native fibril. *Biosci Rep* 1: 801-810.

Pike L.J. 2006. Rafts defined: a report on the Keystone symposium on lipid rafts and cell function. *Journal of Lipid Research* 47: 1597-1598.

Pozzi A., Wary K.K., Giancotti F.G. & Gardner H.A. 1998. Integrin a1ß1 Mediates a Unique Collagen-dependent Proliferation Pathway In Vivo. *The Journal of Cell Biology* 142: 587-594.

Prescott B., Sitaraman K., Argos P. & Thomas G.J. 1985. Protein-RNA interactions in belladonna mottle virus investigated by laser Raman spectroscopy. *Biochemistry (N Y)* 24: 1226-1231.

Prockop J.D. & Kivirikko K.I. 1995. Collagens: Molecular Biology, Diseases, and Potentials for Therapy. *Annu Rev Biochem* 64: 403-434.

Quinn P.J. 2013. Structure of Sphingomyelin Bilayers and Complexes with Cholesterol Forming Membrane Rafts. *Langmuir* 29: 9447-9456.

Racaniello V.R. 1996. Early events in poliovirus infection: virus-receptor interactions. *Proceedings of the National Academy of Sciences* 93: 11378-11381.

Rachakonda P.S., Veit M., Korte T., Ludwig K., Böttcher C., Huang Q., Schmidt M.F.G. & Herrmann A. 2007. The relevance of salt bridges for the stability of the influenza virus hemagglutinin. *The FASEB Journal* 21: 995-1002.

Ravanti L., Heino J., López-Oti´n C. & Kähäri V. 1999. Induction of Collagenase-3 (MMP-13) Expression in Human Skin Fibroblasts by Three-dimensional Collagen Is Mediated by p38 Mitogen-activated Protein Kinase. *Journal of Biological Chemistry* 274: 2446-2455.

Reilly K.E. & Thomas Jr G.J. 1994. Hydrogen Exchange Dynamics of the P22 Virion Determined by Time-resolved Raman Spectroscopy: Effects of Chromosome Packaging on the Kinetics of Nucleotide Exchanges. *J Mol Biol* 241: 68-82.

Ren J., Wang X., Hu Z., Gao Q., Sun Y., Li X., Porta C., Walter T.S., Gilbert R.J., Zhao Y., Axford D., Williams M., McAuley K., Rowlands D.J., Yin W., Wang J., Stuart D.I., Rao Z. & Fry E.E. 2013. Picornavirus uncoating intermediate captured in atomic detail. *Nat Commun* 4.

Reyes-Goddard J.M., Barr H. & Stone N. 2008. Surface enhanced Raman scattering of herpes simplex virus in tear film. *Photodiagnosis and Photodynamic Therapy* 5: 42-49.

Ricard-Blum S. 2011. The Collagen Family. *Cold Spring Harbor Perspectives in Biology* 3.

Riikonen T., Westermarck J., Koivisto L., Broberg A., Kähäri V. & Heino J. 1995. Integrin a2ß1 Is a Positive Regulator of Collagenase (MMP-1) and Collagen a1(I) Gene Expression. *Journal of Biological Chemistry* 270: 13548-13552.

Riopel M. & Wang R. 2014. Collagen matrix support of pancreatic islet survival and function. *Frontiers in Bioscience-Landmark* 19: 77-90.

Robert B. 2009. Resonance Raman spectroscopy. *Photosynthesis Res* 101: 147-155.

Robinson S.M., Tsueng G., Sin J., Mangale V., Rahawi S., McIntyre L.L., Williams W., Kha N., Cruz C., Hancock B.M., Nguyen D.P., Sayen M.R., Hilton B.J., Doran K.S., Segall A.M., Wolkowicz R., Cornell C.T., Whitton J.L., Gottlieb R.A. & Feuer R. 2014. Coxsackievirus B Exits the Host Cell in Shed Microvesicles Displaying Autophagosomal Markers. *PLoS Pathog* 10: e1004045.

Róg T. & Vattulainen I. 2014. Cholesterol, sphingolipids, and glycolipids: What do we know about their role in raft-like membranes? *Chem Phys Lipids* 184: 82-104.

Roivainen M., Alfthan G., Jousilahti P., Kimpimäki M., Hovi T. & Tuomilehto J. 1998. Enterovirus Infections as a Possible Risk Factor for Myocardial Infarction. *Circulation* 98: 2534-2537.

Ruokola P. 2013. Raman Measurements of Viruses And Their Constituents. .

Rygula A., Majzner K., Marzec K.M., Kaczor A., Pilarczyk M. & Baranska M. 2013. Raman spectroscopy of proteins: a review. *J Raman Spectrosc* 44: 1061-1076.

Salman A., Shufan E., Zeiri L. & Huleihel M. 2014. Characterization and detection of Vero cells infected with Herpes Simplex Virus type 1 using

Raman spectroscopy and advanced statistical methods. *Methods* 68: 364-370.

Sane S.U., Cramer S.M. & Przybycien T.M. 1999. A Holistic Approach to Protein Secondary Structure Characterization Using Amide I Band Raman Spectroscopy. *Anal Biochem* 269: 255-272.

Schlamadinger D.E., Gable J.E. & Kim J.E. 2009. Hydrogen Bonding and Solvent Polarity Markers in the UV Resonance Raman Spectrum of Tryptophan: Application to Membrane Proteins. *J Phys Chem B* 113: 14769-14778.

Schroeder C. 2010. Cholesterol-Binding Viral Proteins in Virus Entry and Morphogenesis. In: Harris J.R. (ed.), , Springer Netherlands, pp. 77-108.

Schuliga M., Ong S.C., Soon L., Zal F., Harris T. & Stewart A.G. 2010. Airway smooth muscle remodels pericellular collagen fibrils: implications for proliferation. *American Journal of Physiology-Lung Cellular and Molecular Physiology* 298: L584-L592.

Schuliga M.J., See I., Ong S.C., Soon L., Camoretti-Mercado B., Harris T. & Stewart A.G. 2009. Fibrillar Collagen Clamps Lung Mesenchymal Cells in a Nonproliferative and Noncontractile Phenotype. *American Journal of Respiratory Cell and Molecular Biology* 41: 731-741.

Serban D., Benevides J.M. & Thomas G.J. 2002. DNA Secondary Structure and Raman Markers of Supercoiling in Escherichia coli Plasmid pUC19. *Biochemistry (N Y)* 41: 847-853.

Shanmukh S., Jones L., Driskell J., Zhao Y., Dluhy R. & Tripp R.A. 2006. Rapid and Sensitive Detection of Respiratory Virus Molecular Signatures Using a Silver Nanorod Array SERS Substrate. *Nano Lett* 6: 2630-2636.

Shoulders M.D. & Raines R.T. 2009. Collagen Structure and Stability. *Annu Rev Biochem* 78: 929-958.

Siamwiza M.N., Lord R.C., Chen M.C., Takamatsu T., Harada I., Matsuura H. & Shimanouchi T. 1975. Interpretation of the doublet at 850 and 830 cm-1 in the Raman spectra of tyrosyl residues in proteins and certain model compounds. *Biochemistry (N Y)* 14: 4870-4876.

Siljamäki E., Rintanen N., Kirsi M., Upla P., Wang W., Karjalainen M., Ikonen E. & Marjomäki V. 2013. Cholesterol Dependence of Collagen and Echovirus 1 Trafficking along the Novela2ß1 Integrin Internalization Pathway. *PLoS ONE* 8: e55465.

Silvius J.R. 2003. Role of cholesterol in lipid raft formation: lessons from lipid model systems. *Biochimica et Biophysica Acta (BBA) - Biomembranes* 1610: 174-183.

Simons K. & Ikonen E. 1997. Functional rafts in cell membranes. *Nature* 387: 569-572.

Sirivisoot S., Pareta R. & Harrison B.S. 2014. Protocol and cell responses in three-dimensional conductive collagen gel scaffolds with conductive polymer nanofibres for tissue regeneration. *Interface Focus* 4: 20130050.

Smyth M.S. & Martin J.H. 2002. Picornavirus uncoating. *Molecular Pathology* 55: 214-219.

Smyth M., Pettitt T., Symonds A. & Martin J. 2003. Identification of the pocket factors in a picornavirus. *Arch Virol* 148: 1225-1233.

Soonsawad P., Paavolainen L., Upla P., Weerachatyanukul W., Rintanen N., Espinoza J., McNerney G., Marjomäki V. & Cheng R.H. 2014. Permeability Changes of Integrin-Containing Multivesicular Structures Triggered by Picornavirus Entry. *PLoS ONE* 9: e108948.

Springer T.A. 2002. Predicted and experimental structures of integrins and β-propellers. *Curr Opin Struct Biol* 12: 802-813.

Springer T.A. & Wang J. 2004. The Three-Dimensional Structure of Integrins and their Ligands, and Conformational Regulation of Cell Adhesion. *Adv Protein Chem* 68: 29-63.

Staatz W.D., Rajpara S.M., Wayner E.A., Carter W.G. & Santoro S.A. 1989. The membrane glycoprotein Ia-IIa (VLA-2) complex mediates the Mg++-dependent adhesion of platelets to collagen. *The Journal of Cell Biology* 108: 1917-1924.

Stamov D.R., Stock E., Franz C.M., Jähnke T. & Haschke H. 2015. Imaging collagen type I fibrillogenesis with high spatiotemporal resolution. *Ultramicroscopy* 149: 86-94.

Stange R., Kronenberg D., Timmen M., Everding J., Hidding H., Eckes B., Hansen U., Holtkamp M., Karst U., Pap T. & Raschke M.J. 2013. Age-related bone deterioration is diminished by disrupted collagen sensing in integrin alpha 2 beta 1 deficient. *Bone* 56: 48-54.

Stewart P.L. & Nemerow G.R. 2007. Cell integrins: commonly used receptors for diverse viral pathogens. *Trends Microbiol* 15: 500-507.

Strauss M., Levy H.C., Bostina M., Filman D.J. & Hogle J.M. 2013. RNA Transfer from Poliovirus 135S Particles across Membranes Is Mediated by Long Umbilical Connectors. *Journal of Virology* 87: 3903-3914.

Suikkanen S., Antila M., Jaatinen A., Vihinen-Ranta M. & Vuento M. 2003. Release of canine parvovirus from endocytic vesicles. *Virology* 316: 267-280.

Svensson L., Aszódi A., Reinholt F.P., Fässler R., Heinegård D. & Oldberg Å. 1999. Fibromodulin-null Mice Have Abnormal Collagen Fibrils, Tissue Organization, and Altered Lumican Deposition in Tendon. *Journal of Biological Chemistry* 274: 9636-9647.

Tadokoro S., Shattil S.J., Eto K., Tai V., Liddington R.C., de Pereda J.M., Ginsberg M.H. & Calderwood D.A. 2003. Talin Binding to Integrin ß Tails: A Final Common Step in Integrin Activation. *Science* 302: 103-106.

Takada Y. & Hemler M.E. 1989. The primary structure of the VLA-2/collagen receptor alpha 2 subunit (platelet GPIa): homology to other integrins and the presence of a possible collagen-binding domain. *The Journal of Cell Biology* 109: 397-407.

Takagi J. 2007. Structural basis for ligand recognition by integrins. *Curr Opin Cell Biol* 19: 557-564.

Takagi J., Petre B.M., Walz T. & Springer T.A. 2002. Global Conformational Rearrangements in Integrin Extracellular Domains in Outside-In and Inside-Out Signaling. *Cell* 110: 599-611.

Takeuchi H. 2003. Raman structural markers of tryptophan and histidine side chains in proteins. *Biopolymers* 72: 305-317.

Taubenberger A., Cisneros D.A., Friedrichs J., Puech P., Muller D.J. & Franz C.M. 2007. Revealing early steps of alpha(2)beta(1) integrin-mediated adhesion to collagen type I by using single-cell force spectroscopy. *Mol Biol Cell* 18: 1634-1644.

Thibaut H.J., De Palma A.M. & Neyts J. 2012. Combating enterovirus replication: State-of-the-art on antiviral research. *Biochem Pharmacol* 83: 185-192.

Thomas Jr G.J., Prescott B., McDonald-Ordzie P.E. & Hartman K.A. 1976. Studies of virus structure by Laser-Raman spectroscopy: II. MS2 phage, MS2 capsids and MS2 RNA in aqueous solutions. *J Mol Biol* 102: 103-124.

Tiger C., Fougerousse F., Grundström G., Velling T. & Gullberg D. 2001. α11β1 Integrin Is a Receptor for Interstitial Collagens Involved in Cell Migration and Collagen Reorganization on Mesenchymal Nonmuscle Cells. *Dev Biol* 237: 116-129.

Toulmay A. & Prinz W.A. 2013. Direct imaging reveals stable, micrometer-scale lipid domains that segregate proteins in live cells. *The Journal of Cell Biology* 202: 35-44.

Tsuboi M., Kubo Y., Ikeda T., Overman S.A., Osman O. & Thomas G.J. 2003. Protein and DNA Residue Orientations in the Filamentous Virus Pf1 Determined by Polarized Raman and Polarized FTIR Spectroscopy. *Biochemistry* 42: 940-950.

Tuckwell D., Calderwood D.A., Green L.J. & Humphries M.J. 1995. Integrin alpha 2 I-domain is a binding site for collagens. *Journal of Cell Science* 108: 1629-1637.

Tulla M., Pentikäinen O.T., Viitasalo T., Käpylä J., Impola U., Nykvist P., Nissinen L., Johnson M.S. & Heino J. 2001. Selective Binding of Collagen Subtypes by Integrin α1I, α2I, and α10I Domains. *Journal of Biological Chemistry* 276: 48206-48212.

Tuma R. 2005. Raman spectroscopy of proteins: from peptides to large assemblies. *J Raman Spectrosc* 36: 307-319.

Tuma R. & Thomas Jr G.J. 1997. Mechanisms of virus assembly probed by Raman spectroscopy: the icosahedral bacteriophage P22. *Biophys Chem* 68: 17-31.

Tuma R., Bamford J.H.K., Bamford D.H. & Thomas J.,George J. 1996a. Structure, Interactions and Dynamics ofPRD1Virus II. Organization of the Viral Membrane and DNA. *J Mol Biol* 257: 102-115.

Tuma R., Bamford J.H.K., Bamford D.H., Russell M.P. & Thomas Jr G.J. 1996b. Structure, Interactions and Dynamics ofPRD1Virus I. Coupling of Subunit Folding and Capsid Assembly. *J Mol Biol* 257: 87-101.

Tuthill T., Groppelli E., Hogle J. & Rowlands D. 2010. Picornaviruses. In: Johnson J.E. (ed.), , Springer Berlin Heidelberg, pp. 43-89.

Upla P., Marjomäki V., Nissinen L., Nylund C., Waris M., Hyypiä T. & Heino J. 2008. Calpain 1 and 2 Are Required for RNA Replication of Echovirus 1. *Journal of Virology* 82: 1581-1590.

Upla P., Marjomäki V., Kankaanpää P., Ivaska J., Hyypiä T., van der Goot F.G. & Heino J. 2004. Clustering Induces a Lateral Redistribution of a2ß1 Integrin from Membrane Rafts to Caveolae and Subsequent Protein Kinase C-dependent Internalization. *Molecular Biology of the Cell* 15: 625-636.

van der Rest M. & Garrone R. 1991. Collagen family of proteins. *The FASEB Journal* 5: 2814-2823.

Vandenabeele P. 2013. *Practical Raman spectroscopy : an introduction.* Wiley, Chichester, West Sussex, U.K.

Velling T., Kusche-Gullberg M., Sejersen T. & Gullberg D. 1999. cDNA Cloning and Chromosomal Localization of Human a11 Integrin: A Collagen-Binding, I Domain-Containing, ß1-Associated Integrin a-Chain Present in Muscle Tissues. *Journal of Biological Chemistry* 274: 25735-25742.

Velling T., Risteli J., Wennerberg K., Mosher D.F. & Johansson S. 2002. Polymerization of Type I and III Collagens Is Dependent On Fibronectin and Enhanced By Integrins a11ß1and a2ß1. *Journal of Biological Chemistry* 277: 37377-37381.

Viktorova E.G., Ford-Siltz L.A., Nchoutmboube J. & Belov G.A. 2014. Fluorescent fatty acid analogs as a tool to study development of the picornavirus replication organelles. *J Virol Methods* 200: 15-21.

Villone D., Fritsch A., Koch M., Bruckner-Tuderman L., Hansen U. & Bruckner P. 2008. Supramolecular interactions in the dermo-epidermal junction zone - Anchoring fibril-collagen VII tightly binds to banded collagen fibrils. *J Biol Chem* 283: 24506-24513.

Walter T.S., Ren J., Tuthill T.J., Rowlands D.J., Stuart D.I. & Fry E.E. 2012. A plate-based high-throughput assay for virus stability and vaccine formulation. *J Virol Methods* 185: 166-170.

Wang X., Diaz A., Hao L., Gancarz B., den Boon J.A. & Ahlquist P. 2011. Intersection of the Multivesicular Body Pathway and Lipid Homeostasis in RNA Replication by a Positive-Strand RNA Virus. *Journal of Virology* 85: 5494-5503.

White D.J., Puranen S., Johnson M.S. & Heino J. 2004. The collagen receptor subfamily of the integrins. *Int J Biochem Cell Biol* 36: 1405-1410.

Whittard J.D. & Akiyama S.K. 2001. Activation of β1 Integrins Induces Cell–Cell Adhesion. *Exp Cell Res* 263: 65-76.

Wood G.C. 1960a. The formation of fibrils from collagen solutions. 2. A mechanism of collagen-fibril formation. *Biochem J* 75: 598-605.

Wood G.C. 1960b. The formation of fibrils from collagen solutions. 3. Effect of chondroitin sulphate and some other naturally occurring polyanions on the rate of formation. *Biochem J* 75: 605-612.

Xia H., Nho R., Kleidon J., Kahm J. & Henke C.A. 2008. Polymerized collagen inhibits fibroblast proliferation via a mechanism involving the formation of a beta 1 integrin-protein phosphatase 2A-tuberous sclerosis complex 2 complex that suppresses S6K1 activity. *J Biol Chem* 283: 20350-20360.

Xing L., Casasnovas J.M. & Cheng R.H. 2003. Structural Analysis of Human Rhinovirus Complexed with ICAM-1 Reveals the Dynamics of Receptor-Mediated Virus Uncoating. *Journal of Virology* 77: 6101-6107.

Xing L., Huhtala M., Pietiäinen V., Käpylä J., Vuorinen K., Marjomäki V., Heino J., Johnson M.S., Hyypiä T. & Cheng R.H. 2004. Structural and Functional Analysis of Integrin a2I Domain Interaction with Echovirus 1. *Journal of Biological Chemistry* 279: 11632-11638.

Xiong J., Stehle T., Diefenbach B., Zhang R., Dunker R., Scott D.L., Joachimiak A., Goodman S.L. & Arnaout M.A. 2001. Crystal Structure of the Extracellular Segment of Integrin aVß3. *Science* 294: 339-345.

Xu Y. & Lu C. 2005. Raman spectroscopic study on structure of human immunodeficiency virus (HIV) and hypericin-induced photosensitive damage of HIV. *Sci China C Life Sci* 48: 117-132.

Yafal A.G., Kaplan G., Racaniello V.R. & Hogle J.M. 1993. Characterization of Poliovirus Conformational Alteration Mediated by Soluble Cell Receptors. *Virology* 197: 501-505.

Zeltz C., Orgel J. & Gullberg D. 2014. Molecular composition and function of integrin-based collagen glues-Introducing COLINBRIs. *Biochimica Et Biophysica Acta-General Subjects* 1840: 2533-2548.

Zhang W., Käpylä J., Puranen J.S., Knight C.G., Tiger C., Pentikäinen O.T., Johnson M.S., Farndale R.W., Heino J. & Gullberg D. 2003. α11β1 Integrin Recognizes the GFOGER Sequence in Interstitial Collagens. *Journal of Biological Chemistry* 278: 7270-7277.

Zhang Z., Bothe I., Hirche F., Zweers M., Gullberg D., Pfitzer G., Krieg T., Eckes B. & Aumailley M. 2006. Interactions of primary fibroblasts and keratinocytes with extracellular matrix proteins: contribution of alpha(2)beta(1) integrin. *J Cell Sci* 119: 1886-1895.

ORIGINAL PUBLICATIONS

I

INTEGRIN-MEDIATED CELL ADHESION TO TYPE I COLLAGEN FIBRILS

by

Jokinen J., Dadu E., Nykvist P., Käpylä J., White D.J., Ivaska J., Vehviläinen P., Reunanen H., Larjava H., Häkkinen L. & Heino J. 2004

Journal of Biological Chemistry 279: 31956-31963

II

DIRECT INTERACTIONS OF ECHOVIRUS 1 AND LIPID MEMBRANES

by

Dadu E., Marjomäki V. & Ihalainen J. 2015

Manuscript

Direct interactions of echovirus 1 and lipid membranes

Elina Dadu, Varpu Marjomäki, and Janne A. Ihalainen

University of Jyvaskyla, Nanoscience Center, Department of Biological and Environmental Sciences, P.O. Box 35, FI-40014 University of Jyvaskyla, Finland.

ABSTRACT

Human Echovirus 1 (EV1) is a small, non-enveloped virus belonging to the *Picornaviridae* family. During infection, it enters cells using α2β1 integrin on the lipid rafts as a receptor, and ends up in non-acidic multivesicular bodies, from where it releases its genome. To get a deeper understanding on the life cycle of EV1 and the escape from these vesicular structures, we studied direct lipid interactions of EV1 and the role of the integrin in them. Lipid interactions of purified EV1 were studied using transmission electron microscopy, density gradient ultracentrifugation and vesicles composed of only lipids. The role of integrin in these interactions was studied using the soluble ligand binding domain (I domain) of α2 integrin. Membrane lipid composition affected the binding equilibrium of the virus particles and the membranes, with the highest binding affinity to phosphatidyl choline (PC) vesicles. EV1 also associated with lipid vesicles containing raft lipids, cholesterol and sphingomyelin, albeit with lower affinity. Interestingly, virus particles flattened along the membrane when binding to vesicles containing raft lipids. The effect was markedly stronger with the soluble α2I domain present, although the I domain did not increase the amounta of the virus particles binding to lipid vesicles. The results suggest that integrin α2I domain presence leads to changes in the virus structure, and those changes correlate with changes in the direct interactions of virus particles and membrane lipids. These changes could include increased hydrophobicity of the virus surface leading to stronger interactions between the virus surface and the lipids, or greater elasticity of the virus particle.

INTRODUCTION

Importance of lipids in life cycle of non-enveloped viruses is widely appreciated [1-3], but the details still remain less studied and are less understood than for example with enveloped viruses. To increase the knowledge on virus-lipid interactions, we have studied human echovirus 1 (EV1) and its interactions with artificial lipid membranes. EV1 is a non-enveloped virus that belongs to the *Picornaviridae* family, and the *Enterovirus* genus. The icosahedral capsid of EV1 is composed of 60 copies of the capsid proteins VP1, VP2, VP3 and VP4, along with some embedded fatty acid molecules, and it holds inside a single-stranded RNA genome. To enter cells, EV1 binds to the cell surface receptor α2β1 integrin [4]. The binding of the virus to the integrins leads to clustering of the receptors, which triggers endocytosis, and via maturation of the endosomal structures, the virus and the integrins end up in non-acidic multivesicular bodies (MVB) [5-9]. It is known that the MVB membranes start breaking at about the same time as the virus genome is released and new virus propagation begins [10]. To our knowledge, the molecular details of the virus escape from the MVBs have not been reported. Here we start to fill this gap by studying the virus-lipid interactions and the role of the ligand binding domain of α2β1 integrin in these interactions.

EV1 binds to the ligand binding domain (I domain) of inactive conformation of the α2β1 integrin [11]. The binding between the virus and the integrin is strong - about ten times stronger than the binding between the integrin and type I collagen, which is the primary ligand of α2β1 integrin [12]. The integrin colocalizes with EV1 at least partially up to 2 h post-infection [6], but it is not known how the receptor-virus interactions relate to the membrane interactions. In poliovirus, a virus often used as an enterovirus model, receptor binding induces uncoating-related structural changes in the virus [13]. With EV1, binding to the receptor does not induce uncoating [7,12]. Poliovirus also penetrates the membrane and reaches the cytoplasm within minutes of attaching to the receptor [14]. EV1, on the other hand, takes hours to reach the cytoplasm [10]. For unknown reasons, EV1 is not only slow but also quite ineffective at this step, and many of the virus particles inside the MVBs never manage to escape them. The knowledge about the uncoating process and the lipid interaction properties originates mostly from studies with polio- and rhinoviruses, and many of the features seem to be common to all of the enteroviruses studied so far. For example, the uncoating involves the VP4 proteins and the VP1 N-termini ejecting from inside the capsid and the VP4s forming channels through the lipid membrane [15-17]. The VP4 proteins have fatty acid molecules covalently attached to them, also assumed to participate in membrane interactions [18,19]. The VP1 N-termini that extrudes from the capsid are proposed to form α-helixes with membrane binding capability [20]. There are a fatty acid molecules (palmitic acids in bovine enterovirus) buried inside the VP1s, called the stability-mediating pocket factors, also suggested to participate in the uncoating process [21,22]. In the VP3, there is a helix in the intact virus that changes to a β-hairpin upon uncoating and it is suggested to be a probe for membranes [23].

Special interest in virus-lipid interactions has been focused on the role of cholesterol, a lipid influencing membrane stability and fluidity [24-29]. The cholesterol-dependence of enterovirus replication machinery has been shown [30]. The EV1 receptor α2β1 integrin is located in the

lipid raft areas, and the virus needs cholesterol and lipid rafts for efficient infection [7,8,31]. We have here observed the morphological changes of EV1 particles interacting with lipid-only membranes with different lipid compositions. In this study, direct interactions between virus particles and membrane lipids are shown. In addition to phospholipids, we have studied the raft-forming lipids, cholesterol and sphingomyelin. The effect of the integrin on the binding affinity and morphology of the EV1 particles binding to the membranes was studied by using the soluble ligand binding domain of the α2 integrin.

MATERIALS AND METHODS

Virus production and purification

Echovirus 1 (Farouk strain, obtained from ATCC) was propagated in a monolayer of GMK cells and purified using a procedure described previously [32,33]. Briefly, the cells infected with EV1 for 24 h were collected and freeze/thawed to lyse cellular structures. Bulk cell debris was removed by centrifugation and the virus was precipitated with PEG-6000 and NaCl. Membranous structures were disruped with detergents and the virus was purified with 10 to 40 % sucrose gradient (3 h 86 000 x g) followed by a density gradient of 29 % (w/w) CsCl in PBS (24 h 154 000 x g). Virions collected from the CsCl gradient were dialyzed against PBS supplemented with 2 mM $MgCl_2$ (PBS/Mg). Finally, dialyzed virions were pelleted by ultracentrifugation, suspended in a small volume of PBS/Mg and stored at 4°C.

Characterization of the purified EV1 virions

Infectivity of the purified viruses was assayed using an end-point-titration method to determine 50% Tissue Culture Infective Dose ($TCID_{50}$) as described previously [32]. Briefly, a monolayer of GMK cells on a 96-well plate were infected with serially diluted virus stock. After a 72-h incubation period the cells were stained using crystal violet supplemented with 10% formalin for 10 min at RT. The detached cells were washed away with water and remaining attached cells were counted as viable and non-infected. The EV1 batches used here had $TCID_{50}$/ml in the range of $5*10^{11}$ - $2*10^{12}$. Protein content of the purified EV1 was determined as previously described [32,34] using an average value of VP1-4 molecular mass (23.5 kDa) and an average value of VP1-4 molar absorptivity (ε_{280} 34440 M^{-1} cm^{-1}). Absorbance was measured with NanoDrop ND-1000 spectrophotometer. The protein concentrations were 4 - 6.5 mg ml^{-1} after subtracting the scattering component. The A_{260}/A_{280} ratio was 1.65-1.71. The protein composition of the purified EV1 was analyzed using 12% SDS-PAGE. All virus batches contained only VP1-4 proteins in a similar manner as in [32].

Preparation and characterization of unilamellar vesicles (liposomes)

Phosphatidyl choline (PC), phosphatidyl glycerol (PG), ovine wool cholesterol (Ch), and porcine brain sphingomyelin (SM) (Avanti Polar Lipids) were dissolved to chloroform and stored at -20°C. Liposomes containing PC, PG, both phospholipids (PC:PG), SM, both raft lipids sphingomyelin and cholesterol (SM:Ch) or all four lipids (PC:PG:SM:Ch) were prepared. Chloroform solutions of the lipids with equimolar ratios were dried for 1-2 h under nitrogen flow

at 45 °C and further for >3 h in a vacuum desiccator. The dry lipids were stored under nitrogen at -20 °C until rehydrated to 100 mg ml^{-1} with PBS/Mg by incubating them at room temperature and 37 °C for minimum of 30 min. Multilamellar vesicles were formed by vortexing during incubation and further by 5 freeze-thaw cycles in liquid nitrogen and at 37 °C. Unilamellar vesicles were formed by extrucion of the multilamellar vesicles 17 times through a membrane with 400-nm pore size (Avanti Polar Lipids Extruder). Liposomes were stored at 4 °C and used within 7 days.

Average diameters of liposomes and the presence of residual chloroform in the liposome preparations were determined from 20 μg/ml of lipid vesicles in PBS/Mg buffer. Average diameters were determined with Beckman Coulter N5 Submicron Particle Size Analyzer to be 185 - 450 nm, depending on the lipid composition. The presence of residual chloroform in liposome preparations was tested using Raman spectroscopy with a home-built Raman setup with a backscattering geometry (described previously [32]) and 5 min exposure and 200 mW laser power. Chloroform has a distinct signal at 668 cm^{-1}, which was not detected in any of the liposome preparations (data not shown).

Flotation of lipids and viruses in sucrose density gradient

The binding of EV1 to liposomes was investigated with sucrose density gradient ultracentrifugation. The α2 integrin ligand binding domain, α2I-GST, was produced as a soluble GST fusion protein in *E. coli* and purified with Gluthathione-Sepharose beads as described by Jokinen *et al.* [35]. Samples were prepared with 14-20 μg of EV1 and 60 μg of liposomes in a total volume of 10 μl. Some of the samples contained additionally 3.4 μg of the soluble α2I-GST. No attempt was made to attach the α2I-GST to the vesicles and it most likely remained soluble in all of the experiments, unless it bound to the virus surface. The samples were incubated at 37 °C for 90 min and then applied on top of 10-40 % (w/v) sucrose gradients (similar to the gradients used for virus purification, described previously [32]). After ultracentrifugation, each gradient was collected from the top to 26 fractions with 500 μl volumes The fractions were held at +60 °C for >1 h to disrupt virus particles and enhance the sensitivity for immunolabeling. The virus was detected from the sucrose gradient fractions with dot blot immunolabeling at room temperature. Briefly, 100 μl of each fraction was loaded onto a nitrocellulose membrane using a dot blot apparatus and allowed to bind to the membrane for 50 min. Samples were sucked through the membrane, and washed thrice with PBS-Tween 0.2 % (á 200 μl). The apparatus was then disassembled and the membrane washed further for 3 min rocking in 20 ml PBS-Tween. Blocking of unspecific binding sites was performed with 3 % BSA in PBS (filtered with 0.45 μm pore size filter) for 50 min. Virus was labeled with rabbit antisera against EV1 [9] in BSA/PBS for 50 min, washed with 3x3 min PBS-Tween, and the secondary antibody (anti-rabbit antibody with conjugated alkaline phosphatase) was allowed to bind for 50 min in BSA/PBS. After washes as above, the membrane was equilibrated into alkaline phosphatase activity (APA) buffer (3x3 min) and the alkaline phosphatase shown with colour reaction of BCIP and NBT in APA buffer. After 1 min the reaction was stopped with dH_2O and an image was taken with BioRad Imager. Intensity of the immunostaining of each dot in the image was determined with ImageJ macro Dot Blot Analyzer [36] (http://rsb.info.nih.gov/ij/macros/toolsets/Dot Blot Analyzer.txt).

Transmission Electron Microscopy

The morphology of the purified virions was visualized by transmission electron microscopy (TEM) and negative staining of the samples with 1% (wt/vol) phosphotungstic acid (Sigma-Aldrich). TEM was also used for visualization of virus-liposome interactions from mixtures of EV1 and liposomes (and in some samples, additionally the soluble α2I) prepared the same way as for the density gradient experiment above. After an incubation of 90 min at 37°C, the samples were diluted 1/20 with PBS/Mg. Formvar-coated EM grids were glow discharged (EMS/SC7620 mini-sputter coater), and samples were deposited on the grids for 1 min, after which the excess sample was blotted away (Whatman 3MM paper). Next, negative stain was added for 1 min and removed as above. Samples dried overnight were imaged with a JEM-1400 (JEOL) transmission electron microscope with a magnification of 20,000 (80 kV). For each sample, 48 images were taken from sample areas that were not too crowded and that had a rather even distribution of virus particles, and yet had the most lipid-associated virus particles. Images covering á 5.44 μm^2 areas were used to count the amount of free and lipid-associated virus particles.

Virus particle stability

The thermal stability of EV1 particles with the lipid vesicles was tested with a thermal stability assay as described previously [32,37], using SYBR green II (Invitrogen) fluorescent dye. The dye becomes fluorescent in contact with RNA released from the virus particles, thus revealing information about the thermal instability of the virus particles in terms of the melting temperature. Samples of EV1, α2I-GST and liposomes were mixed to 10 µl final volume, held at 37°C for 90 min, and then diluted to three parallel samples with 50 µl final volume and a 10X concentration of SYBR green II. The final samples contained 0.7 µg of EV1, 1.1 µg of α2I-GST and 20 µg of liposomes per well. EV1 particles disrupted by incubating the virus at 60°C for 10 min were used as a positive control. The fluorescence was recorded using a Bio-Rad C1000 thermal cycler and raising the temperature from 20 to 90°C by 0.5°C every 10 seconds. The melting temperature acquired from the thermal stability assay represents the temperature where half of the virus particles have released their genome and made it accessible to the SYBR Green II dye.

RESULTS

The flotation of EV1 with the liposomes

Lipid vesicles or their fragments float on top of sucrose gradients in the ultracentrifugation. Proteins or viruses bound to the lipids also float on top of the gradients [8,38,39]. Here, the floating of liposomes was confirmed by visual examination of 6 mg of liposomes in 10-40 % sucrose gradient. Free EV1 particles move deeper into the gradient during ultracentrifugation, detected by dot blot immunostaining in our setup at about the middle of the gradient, in fractions 13-15 (Fig 1). Out of the five liposomes tested, the PC vesicles caused the strongest floating effect of EV1, seen as elevated intensity of EV1 signal in fractions 1-8 from the top of the gradient (Fig 1). The other liposomes also caused floating to some extent, with the PG liposomes having the smallest effect on the EV1 location in the gradient. The effect of the soluble α2I

domain on floating of the virus particles was also studied (data not shown). The presence of the soluble α2I domain did not enhance floating of viruses with liposomes. On the contrary, it seemed to reduce the floating effect a little, as slightly less EV1 signal appeared in the eight topmost fractions in samples with the soluble α2I domain than without it. Thus, all of the lipid vesicles formed contacts with the EV1 particles, and the soluble α2I domain had no major effects on the amounts of the virus particles binding to the lipid membranes.

Visualization of the direct EV1-lipid interactions

The virus-membrane associations were visualized with TEM. Similarily to the density gradient experiment, EV1 interactions were studied with vesicles of different lipid compositions. In all samples of EV1 with liposomes, some portion of the virus particles were associated with the membranes, and the membranes were often slightly curved or dented at the binding site (Fig 2A,C,E-G). In samples of EV1 with PC liposomes, the viruses had large contact areas with the membranes, and were often relatively deeply buried within the vesicular structures. Some individual virus particles were completely covered with a distinct bilayer membrane (Fig 2B). In the TEM images of viruses with PG liposomes, some of the virus particles were surrounded by an additional shade, interpreted as a lipid layer (Fig 2C-D). However, the lipids did not seem to form a distinct bilayer around the viruses, but instead a blob of non-uniform thickness. Although this lipid blob surrounding virus particles was not the case with majority of the viruses, it was a distinct feature in samples of EV1 with PG vesicles.

Free virus particles and those associated with membranes were counted from TEM images (Fig 3). As in the density gradient experiment, also here the PC vesicles had the strongest affinity to virus particles. Samples with the PG and SM liposomes had less virus particles in close contact with the membrane than samples with the other liposomes. Binding of the virus particles to liposomes made of PC:PG or PC:PG:SM:Ch mixtures appeared to be in between the values of PC- and PG-only liposomes. The soluble α2I domain slighty reduced binding of EV1 to membranes, although the effect is not very pronounced and is not seen in all samples. It is necessary to note that the values of EV1 binding to membrane in Fig 3 do not represent the whole virus population, since the TEM images were taken at selected sites. The differences between the samples, however, do reflect the relative binding populations, as the same selection criteria were used for all samples.

Morphological changes of the viruses

One specific feature was observed in the EV1 particles bound to the vesicles composed of all of the four lipids under study (PC:PG:SM:Ch). The virus particles bound to PC:PG:SM:Ch vesicles appeared to be somewhat flattened. These flattened virus particles bound to the PC:PG:SM:Ch vesicles have shorter diameters perpendicular to the plane of the membrane, and longer diameters parallel to the plane of the membrane when compared to virus particles bound to PC:PG vesicles. This feature was further enhanced in samples containing the soluble α2I domain (Fig 4A-B). To estimate the magnitude of flattening, diameters of virus particles bound to PC:PG and PC:PG:SM:Ch membranes were measured from 24 TEM images/sample (60-144 virus particles/sample, Fig 4B). The average virus particle diameter overall was about 28 nm. Flattening of the virus particles is represented as parallel diameter percentage of perpendicular

diameter with respect to the plane of the membrane (Fig 4C). The average parallel diameter bound to PC:PG membranes was found to be nearly equal to the perpendicular diameter, indicating spherical particles. In the case of the PC:PG:SM:Ch membranes without the soluble α2I domain, the parallel diameter was about 110 % of the perpendicular diameter. With the α2I domain present in the samples with EV1 and PC:PG:SM:Ch, the average parallel diameter was almost 120 % of the perpendicular diameter, representing significant flattening of the virus particles. This made the virus particles on average 25.6 nm by 30.2 nm. In figure 4D the relationship of the flattening effect (X/Y %) and the parallel diameters (X) are shown for individual virus particles, and it can be seen that there is a tendency where the flatter the particle, the larger the parallel diameter. The flattening also similarly correlates with decreasing of the perpendicular diameter. Thus, the effect seen is really flattening - simultaneous widening of the virus particle in the direction parallel to membrane and shortening of the diameter perpendicular to membrane. Free EV1 particles from samples without liposomes were also measured with no notable flattening observed (data not shown).

Thermal stability of the virus particles

The effect of the liposomes on the thermal stability of the EV1 particles was studied with the thermal stability assay (Fig 4). Generally, the liposomes lowered the melting temperatures of EV1 by about 2°C, relatively independent of the liposome composition. Small changes between different liposomes were restricted to SM:Ch having slightly smaller effect on the melting temperature than the other liposomes. The change in the melting temperature might be larger with the individual virus particles attached to the membranes than the measurements indicate, as also free virus particles affect the measured melting temperatures. The presence of the soluble α2 integrin I domain had notably larger effect than the liposomes, leading to an 8°C raise in the melting temperature. This is in line with previous observations where the α2 integrin I domain has also increased the thermal stability of EV1 [Kazmertsuk *et al.* submitted]. The liposome effect - lowering the melting temperature by about 2°C - remained the same with and without the soluble integrin I domain. Lipid samples without EV1 were recorded alongside with the virus samples as negative controls, as well as heat-disrupted EV1 samples with liposomes as positive controls of maximum signals with each liposome (data not shown). The liposomes had some effect on the magnitude of SYBR Green fluorescence, especially PG, which increased the background signal.

DISCUSSION

Lipid membranes are intimately involved in several steps of the echovirus life cycle. First, to enter a cell, EV1 attaches to a receptor on the cell membrane. The complex is taken inside the cell in an endocytic vesicle. The vesicle matures into a multivesicular structure, from where the virus genome is released through breakages in the limiting membrane [5,10]. Finally, after the next generation of virus particles have assembled, they are released from the host cell to start another infection cycle.

Membrane interactions of two enteroviruses, poliovirus and rhinovirus, have been investigated with electron tomography. Two very different modes of interaction have been observed with these viruses, with poliovirus binding to the membrane via umbilical extension that holds the main virus particle 5 nm apart from the membrane [40], and rhinovirus binding tightly to the membrane [41]. Our observations reveal that EV1 is able to interact directly and tightly with the membranes without the receptor, similar to rhinovirus.

The composition of lipid membranes is known to be important to viruses. For example, lipid composition of membranes a virus penetrates is known to affect the entry and egress processes [1], and the composition of the intracellular membranes is important to RNA replication of many positive-strand RNA viruses [42]. We observed the effect of lipid composition on the interactions of EV1 and liposomes. Out of the lipids studied here, phosphatidyl choline bound the most virus particles. PC is present in all membranes of the cell, but it is particularly abundant on the outer leaflet of the plasma membrane. It increases fluidity of the membranes due to its unsaturated alkyl chains. Perhaps this enables the PC membranes to wrap around the virus particles more easily than the other membranes, and the increased area of interaction leads to the increased numbers of the membrane-bound virus particles. The other studied phospholipid, phosphatidyl glycerol, was the most inefficient in virus binding based on the sucrose gradient experiment. The most striking difference between these two lipids is the negative charge of PG, compared to the zwitterionic nature with zero net charge of PC. PC also has a different ability to participate in hydrogen bonding with its two ester carbonyls that can act as hydrogen acceptors. Samples that had liposomes containing raft lipids were not seen to wrap around the virus particles. For example the samples containing SM vesicles, which has the same choline head group as PC but quite different behaviour in membranes [43], did not have any membrane embedded virus particles. Though the polar head group is the same as in PC, the ability to form hydrogen bonds is different. SM has an amide bond and a hydroxyl group that can participate in hydrogen bonding wheras PC can only act as hydrogen acceptor. The hydrogen bonding ability of lipid head groups is important, because based on molecular dynamics simulations the externalized VP1 N-termini are suggested to not penetrate the membrane, but lay on the membrane surface and only perturb the membrane [44]. If this is true, the VP1 α-helix has mostly interactions with the head groups instead of the acyl chains of membrane lipids. On the other hand, even if the N-terminal α-helix does penetrate the membrane, the lipid composition is important, as the membrane physical properties have been seen to affect the transmembrane helix formation [45]. Samples of viruses with PG vesicles, while having the lowest affinity, also are the ones where one could see virus particles wrapped completely or partially in a lipid blob. Also PC and PC:PG membranes were occasionally wrapped around the virus particles. It has been suggested, that picornaviruses are not truly non-enveloped viruses, as Coxsackievirus B and Hepatitis A virus have been observed in vesicles shedded from cells [46-48]. Our findings support such a phenomenon and further propose, that phospholipids PC and PG might participate in such behaviour.

In addition to the properties of the individual lipids, sphingomyelin has a strong affinity to cholesterol and the two lipids appear and function together as rafts on the plasma membrane. The lipid rafts are microdomains of liquid ordered phase in phospholipid membranes of liquid

disordered phase [49-53]. These cholesterol and sphingomyelin rich microdomains are involved in many cellular processes. They are originally known from polarized endothelial cells, where they play key roles in regulated traffic of specific lipids to plasma membrane. Cholesterol and sphingomyelin are also enriched in early and recycling endosomes and are necessary for formation of the intraluminal vesicles [54]. Although the MVBs formed during EV1 infection are not acidic and hence not identical to regular endosomes, they have similar intraluminal vesicles, which are also enriched with cholesterol and sphingomyelin [31]. It has been observed that the intraluminal vesicles start breaking at the same time or even earlier than the outer membrane of MVBs [10], so the interaction of EV1 with these intraluminal vesicles might be one step towards escape from MVBs.

In electron microscopy, interaction of viruses and membranes was seen to lead to flattening of virus particles. This suggests strong, direct interactions between the virus and the lipids. Particularly, the effect was seen with membranes where the raft lipids were present. Lipid raft areas are more rigid than the phospholipid membranes of liquid-disordered phase, which might explain why the flattening effect is seen specifically with the raft lipids. The VP1 N-terminal peptides have been observed moving in and out of the virus capsid in so called breathing of the capsid [55], making them available for membrane interactions also in our experiments. If several VP1 N-termini are binding to the membrane simultaneously, that might generate enough force to deform the virus capsid and induce flattening. The VP4 proteins have also been suggested to participate in membrane interactions, forming ion channels on the membrane. On the other hand, they are reported to be completely expelled from the virus capsid during uncoating which would make them an unlikely binding medium between the capsid and the membrane. It is tempting to speculate, however, that the direct interactions seen here could be a way to introduce the VP4 proteins to the membranes.

The presence of the soluble α2 integrin ligand binding domain further increased the flattening effect seen with the lipid raft membranes. This suggests that the virus-integrin interactions lead to changes in the virus structure. Since the soluble integrin I domains seemed to slightly lower the numbers of membrane-bound EV1 particles, it might also be that the receptor-virus connections need to be severed for the structural changes of the virus to happen. In fact, as the integrin binding first stabilizes the virus, observed as the increased melting temperatures (also previously (12, Kazmertsuk *et al.* submitted)), the possible detachment could be one step towards uncoating. However, the actual competition of the I domains and the lipids for the binding with EV1 in these experiments could be due to the soluble nature of the I domains, and thus not present *in vivo*.

Although the liposomes used in this study had average diameters from 185 nm upwards, EV1 patricles were especially often seen bound to small vesicles with only about 100 nm diameters (Fig 2 & 3). The virus particles bound to these smaller vesicles seemed to be more often flattened than the particles bound to larger vesicles. Naturally, the smaller vesicles have higher surface tension and, hence, are more difficult to deform. This might explain why virus particles are flattened more easily with the small vesicles than larger ones - binding of the same strength might more often lead to vesicle deformation instead of virus deformation with larger vesicles

and smaller surface tension. The tendency of smaller vesicles to induce more flattening might also hint to the phenomenon being a part of EV1 interactions with the intraluminal vesicles of MVBs. The area of the MVB intraluminal vesicles in EV1 infected cells have been measured to be on average 1.4-1.45*10^4 nm^2 at 2 to 3.5 h after the start of infection [10], corresponding to about 120 nm diameters of the vesicles. As has been suggested previously for EV1 [11] and poliovirus [14], also our study points to the direction that curvature of the membrane in contact with the viruses may play a part in virus-membrane interactions. RNA viruses are known to manipulate lipid biosynthesis in cells and one goal is suggested to be changing the curvature of the membranes [56]. Curvature could allow multiple copies of the N-terminus of VP1 to be inserted into the vesicle membrane leading to more intimate associations of the virus particles and the membranes.

Thermal stability assay showed that liposomes lower the observed melting temperatures of EV1 by about 2°C. The change in the melting temperature might, however, be larger with the individual virus particles attached to the membranes, as also free virus particles affect the measured melting temperatures. The observed decreasement in the melting temperature might implicate that interactions with lipid membranes destabilizes virus particles. However, some caution must be taken with the interpretation of the thermal stability assay, as the lipids might affect the behaviour of the dye when heated up, and lipids in the hot environment of the observed melting temperatures (44-55°C) also behave quite differently than at physiological temperatures. The soluble integrin I domain lead to an increase in the stability of EV1, as has been seen before [12]Kazmertsuk *et al.* submitted]. The liposome effect - lowering the melting temperature by about 2°C - remained the same with and without the soluble integrin I domain. The increasement of the thermal stability of the virus particles with the soluble I domains seems, at first, to contradict the increased flexibility seen in the flattened virus particles. However, flexibility does not necessarily correlate with thermal instability, and less flexible structures can be more brittle.

In conclusion, the results here demonstrate direct interactions of the EV1 particles with the lipid membranes, which create mechanical forces on the EV1 capsids. This was particularly obvious with the membranes that contained cholesterol and sphingomyelin, which had flattened virus particles attached to them. In addition, the soluble integrin α2I domains enhanced the flattening effect suggesting that receptor interactions induce structural changes in the EV1 particles. To our knowledge, the morphological changes seen here with EV1 have not been observed with other viruses before.

ACKNOWLEDGEMENTS

This research is supported by the Ellen and Artturi Nyyssönen Foundation, and the National Doctoral Programme in Nanoscience (NGS). The authors wish to thank Alli Liukkonen and Heikki Häkkänen for practical help and Artur Kazmertsuk for fruitful discussions. Jyrki Heino and Jarmo Käpylä are acknowledged for the purified α2I-GST protein.

REFERENCES

1. Heaton NS, Randall G: **Multifaceted roles for lipids in viral infection.** *Trends Microbiol* 2011, **19:** 368-375.
2. Chukkapalli V, Heaton NS, Randall G: **Lipids at the interface of virus–host interactions.** *Curr Opin Microbiol* 2012, **15:** 512-518.
3. den Boon JA, Ahlquist P: **Organelle-like membrane compartmentalization of positive-strand RNA virus replication factories.** *Annu Rev Microbiol* 2010, **64:** 241-256.
4. Bergelson JM, Shepley M, Chan B, Hemler M, Finberg RW. **: Identification of the integrin VLA-2 as a receptor for echovirus 1.** *Science* . 1992, 255: 1718-1720.
5. Karjalainen M, Kakkonen E, Upla P, Paloranta H, Kankaanpää P, Liberali P, Renkema GH, Hyypiä T, Heino J, Marjomäki V: **A raft-derived, Pak1-regulated entry participates in a2ß1 integrin-dependent sorting to caveosomes.** *Molecular Biology of the Cell* 2008, **19:** 2857-2869.
6. Karjalainen M, Rintanen N, Lehkonen M, Kallio K, Mäki A, Hellström K, Siljamäki V, Upla P, Marjomäki V: **Echovirus 1 infection depends on biogenesis of novel multivesicular bodies.** *Cell Microbiol* 2011, **13:** 1975-1995.
7. Pietiäinen V, Marjomäki V, Upla P, Pelkmans L, Helenius A, Hyypiä T: **Echovirus 1 endocytosis into caveosomes requires lipid rafts, dynamin II, and signaling events.** *Molecular Biology of the Cell* 2004, **15:** 4911-4925.
8. Upla P, Marjomäki V, Kankaanpää P, Ivaska J, Hyypiä T, van der Goot FG, Heino J: **Clustering induces a lateral redistribution of a2ß1 integrin from membrane rafts to caveolae and subsequent protein kinase C-dependent internalization.** *Molecular Biology of the Cell* 2004, **15:** 625-636.
9. Marjomäki V, Pietiäinen V, Matilainen H, Upla P, Ivaska J, Nissinen L, Reunanen H, Huttunen P, Hyypiä T, Heino J: **Internalization of echovirus 1 in caveolae.** *Journal of Virology* 2002, **76:** 1856-1865.
10. Soonsawad P, Paavolainen L, Upla P, Weerachatyanukul W, Rintanen N, Espinoza J, McNerney G, Marjomäki V, Cheng RH: **Permeability changes of integrin-containing multivesicular structures triggered by picornavirus entry.** *PLoS ONE* 2014, **9:** e108948.
11. Jokinen J, White DJ, Salmela M, Huhtala M, Käpylä J, Sipilä K, Puranen J, Nissinen L, Kankaanpää P, Marjomäki V, Hyypiä T, Johnson MS, Heino J: **Molecular mechanism of α 2β 1 integrin interaction with human echovirus 1.** *EMBO J* 2010, **29:** 196-208.
12. Xing L, Huhtala M, Pietiäinen V, Käpylä J, Vuorinen K, Marjomäki V, Heino J, Johnson MS, Hyypiä T, Cheng RH: **Structural and functional analysis of integrin a2I domain interaction with echovirus 1.** *Journal of Biological Chemistry* 2004, **279:** 11632-11638.
13. Yafal AG, Kaplan G, Racaniello VR, Hogle JM: **Characterization of poliovirus conformational alteration mediated by soluble cell receptors.** *Virology* 1993, **197:** 501-505.
14. Brandenburg B, Lee LY, Lakadamyali M, Rust MJ, Zhuang X, Hogle JM: **Imaging poliovirus entry in live cells.** *PLoS Biol* 2007, **5:** e183.
15. Fricks CE, Hogle JM: **Cell-induced conformational change in poliovirus: Externalization of the amino terminus of VP1 is responsible for liposome binding.** *Journal of Virology* 1990, **64:** 1934-1945.
16. Danthi P, Tosteson M, Li Q, Chow M: **Genome delivery and ion channel properties are altered in VP4 mutants of poliovirus.** *Journal of Virology* 2003, **77:** 5266-5274.
17. Lin J, Cheng N, Chow M, Filman DJ, Steven AC, Hogle JM, Belnap DM: **An externalized polypeptide partitions between two distinct sites on genome-released poliovirus particles.** *Journal of Virology* 2011, **85:** 9974-9983.

18. Panjwani A, Strauss M, Gold S, Wenham H, Jackson T, Chou JJ, Rowlands DJ, Stonehouse NJ, Hogle JM, Tuthill TJ: **Capsid protein VP4 of human rhinovirus induces membrane permeability by the formation of a size-selective multimeric pore.** *PLoS Pathog* 2014, **10:** e1004294.
19. Chow M, Newman JFE, Filman D, Hogle JM, Rowlands DJ, Brown F: **Myristylation of picornavirus capsid protein VP4 and its structural significance.** *Nature* 1987, **327:** 482-486.
20. Racaniello VR: **Early events in poliovirus infection: Virus-receptor interactions.** *Proceedings of the National Academy of Sciences* 1996, **93:** 11378-11381.
21. Smyth MS, Martin JH: **Picornavirus uncoating.** *Molecular Pathology* 2002, **55:** 214-219.
22. Smyth M, Pettitt T, Symonds A, Martin J: **Identification of the pocket factors in a picornavirus.** *Arch Virol* 2003, **148:** 1225-1233.
23. Ren J, Wang X, Hu Z, Gao Q, Sun Y, Li X, Porta C, Walter TS, Gilbert RJ, Zhao Y, Axford D, Williams M, McAuley K, Rowlands DJ, Yin W, Wang J, Stuart DI, Rao Z, Fry EE: **Picornavirus uncoating intermediate captured in atomic detail.** *Nat Commun* 2013, **4:** .
24. Medigeshi GR, Hirsch AJ, Streblow DN, Nikolich-Zugich J, Nelson JA: **West nile virus entry requires cholesterol-rich membrane microdomains and is independent of avß3 integrin.** *Journal of Virology* 2008, **82:** 5212-5219.
25. Schroeder C. Cholesterol-binding viral proteins in virus entry and morphogenesis. In: Harris JR, ed. Vol 51. Springer Netherlands; 2010:77-108. http://dx.doi.org/10.1007/978-90-481-8622-8_3. 10.1007/978-90-481-8622-8_3.
26. Lu YE, Cassese T, Kielian M: **The cholesterol requirement for sindbis virus entry and exit and characterization of a spike protein region involved in cholesterol dependence.** *Journal of Virology* 1999, **73:** 4272-4278.
27. Chatterjee PK, Vashishtha M, Kielian M: **Biochemical consequences of a mutation that controls the cholesterol dependence of semliki forest virus fusion.** *Journal of Virology* 2000, **74:** 1623-1631.
28. Martín-Acebes MA, González-Magaldi M, Sandvig K, Sobrino F, Armas-Portela R: **Productive entry of type C foot-and-mouth disease virus into susceptible cultured cells requires clathrin and is dependent on the presence of plasma membrane cholesterol.** *Virology* 2007, **369:** 105-118.
29. Danthi P, Chow M: **Cholesterol removal by methyl-ß-cyclodextrin inhibits poliovirus entry.** *Journal of Virology* 2004, **78:** 33-41.
30. Ilnytska O, Santiana M, Hsu N, Du W, Chen Y, Viktorova E, Belov G, Brinker A, Storch J, Moore C, Dixon J, Altan-Bonnet N: **Enteroviruses harness the cellular endocytic machinery to remodel the host cell cholesterol landscape for effective viral replication.** *Cell Host & Microbe* 2013, **14:** 281-293.
31. Siljamäki E, Rintanen N, Kirsi M, Upla P, Wang W, Karjalainen M, Ikonen E, Marjomäki V: **Cholesterol dependence of collagen and echovirus 1 trafficking along the Novela2ß1 integrin internalization pathway.** *PLoS ONE* 2013, **8:** e55465.
32. Ruokola P, Dadu E, Kazmertsuk A, Häkkänen H, Marjomäki V, Ihalainen JA: **Raman spectroscopic signatures of echovirus 1 uncoating.** *Journal of Virology* 2014, **88:** 8504-8513.
33. Abraham G, Colonno RJ: **Many rhinovirus serotypes share the same cellular receptor.** *Journal of Virology* 1984, **51:** 340-345.
34. Porterfield JZ, Zlotnick A: **A simple and general method for determining the protein and nucleic acid content of viruses by UV absorbance.** *Virology* 2010, **407:** 281-288.
35. Jokinen J, Dadu E, Nykvist P, Käpylä J, White DJ, Ivaska J, Vehviläinen P, Reunanen H, Larjava H, Häkkinen L, Heino J: **Integrin-mediated cell adhesion to type I collagen fibrils.** *Journal of Biological Chemistry* 2004, **279:** 31956-31963.

36. Carpentier G. **Dot blot analyzer for ImageJ**. . Updated 20082014.
37. Walter TS, Ren J, Tuthill TJ, Rowlands DJ, Stuart DI, Fry EE: **A plate-based high-throughput assay for virus stability and vaccine formulation.** *J Virol Methods* 2012, **185:** 166-170.
38. Airaksinen A, Somerharju P, Hovi T: **Variation in liposome binding among enteroviruses.** *Virology* 2001, **279:** 539-545.
39. Brown DA, Rose JK: **Sorting of GPI-anchored proteins to glycolipid-enriched membrane subdomains during transport to the apical cell surface.** *Cell* 1992, **68:** 533-544.
40. Strauss M, Levy HC, Bostina M, Filman DJ, Hogle JM: **RNA transfer from poliovirus 135S particles across membranes is mediated by long umbilical connectors.** *Journal of Virology* 2013, **87:** 3903-3914.
41. Kumar M, Blaas D: **Human rhinovirus subviral A particle binds to lipid membranes over a twofold axis of icosahedral symmetry.** *Journal of Virology* 2013, **87:** 11309-11312.
42. Wang X, Diaz A, Hao L, Gancarz B, den Boon JA, Ahlquist P. **: Intersection of the multivesicular body pathway and lipid homeostasis in RNA replication by a positive-strand RNA virus.** *Journal of Virology* . 2011, 85: (11)5494-5503.
43. Ramstedt B, Slotte JP: **Sphingolipids and the formation of sterol-enriched ordered membrane domains.** *Biochimica et Biophysica Acta (BBA) - Biomembranes* 2006, **1758:** 1945-1956.
44. Hong G, Chen C, Lin M, Krüger J, Becker CFW, Fink RHA, Fischer WB: **Molecular dynamics simulations and conductance studies of the interaction of VP1 N-terminus from polio virus and gp41 fusion peptide from HIV-1 with lipid membranes.** *Mol Membr Biol* 2012, **29:** 9-25.
45. Barrera FN, Fendos J, Engelman DM: **Membrane physical properties influence transmembrane helix formation.** *Proceedings of the National Academy of Sciences* 2012, **109:** 14422-14427.
46. Jackson WT: **Poliovirus-induced changes in cellular membranes throughout infection.** *Current Opinion in Virology* 2014, **9:** 67-73.
47. Feng Z, Hensley L, McKnight KL, Hu F, Madden V, Ping L, Jeong S, Walker C, Lanford RE, Lemon SM: **A pathogenic picornavirus acquires an envelope by hijacking cellular membranes.** *Nature* 2013, **496:** 367-371.
48. Robinson SM, Tsueng G, Sin J, Mangale V, Rahawi S, McIntyre LL, Williams W, Kha N, Cruz C, Hancock BM, Nguyen DP, Sayen MR, Hilton BJ, Doran KS, Segall AM, Wolkowicz R, Cornell CT, Whitton JL, Gottlieb RA, Feuer R: **Coxsackievirus B exits the host cell in shed microvesicles displaying autophagosomal markers.** *PLoS Pathog* 2014, **10:** e1004045.
49. Quinn PJ: **Structure of sphingomyelin bilayers and complexes with cholesterol forming membrane rafts.** *Langmuir* 2013, **29:** 9447-9456.
50. Silvius JR: **Role of cholesterol in lipid raft formation: Lessons from lipid model systems.** *Biochimica et Biophysica Acta (BBA) - Biomembranes* 2003, **1610:** 174-183.
51. Róg T, Vattulainen I: **Cholesterol, sphingolipids, and glycolipids: What do we know about their role in raft-like membranes?** *Chem Phys Lipids* 2014, **184:** 82-104.
52. Simons K, Ikonen E: **Functional rafts in cell membranes.** *Nature* 1997, **387:** 569-572.
53. de Lange MJL, Bonn M, Müller M: **Direct measurement of phase coexistence in DPPC/cholesterol vesicles using raman spectroscopy.** *Chem Phys Lipids* 2007, **146:** 76-84.
54. Diaz-Rohrer B, Levental KR, Levental I: **Rafting through traffic: Membrane domains in cellular logistics.** *Biochimica et Biophysica Acta (BBA) - Biomembranes* 2014, **1838:** 3003-3013.
55. Li Q, Yafal AG, Lee YM, Hogle J, Chow M: **Poliovirus neutralization by antibodies to internal epitopes of VP4 and VP1 results from reversible exposure of these sequences at physiological temperature.** *Journal of Virology* 1994, **68:** 3965-3970.
56. Viktorova EG, Ford-Siltz LA, Nchoutmboube J, Belov GA: **Fluorescent fatty acid analogs as a tool to study development of the picornavirus replication organelles.** *J Virol Methods* 2014, **200:** 15-21.

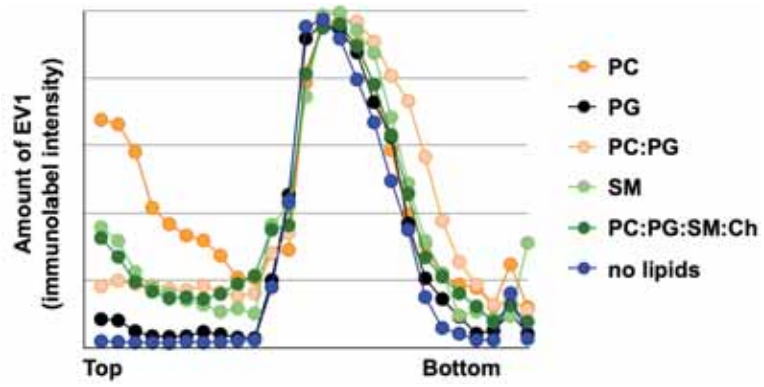

Fig 1. Liposomes cause floating of virus particles in 10 - 40 % sucrose gradient. The location of EV1 particles in the gradient are shown with vesicles of five different compositions. The data represent the mean signals of 2-4 experiments, and individual gradients are normalized to their highest signals.

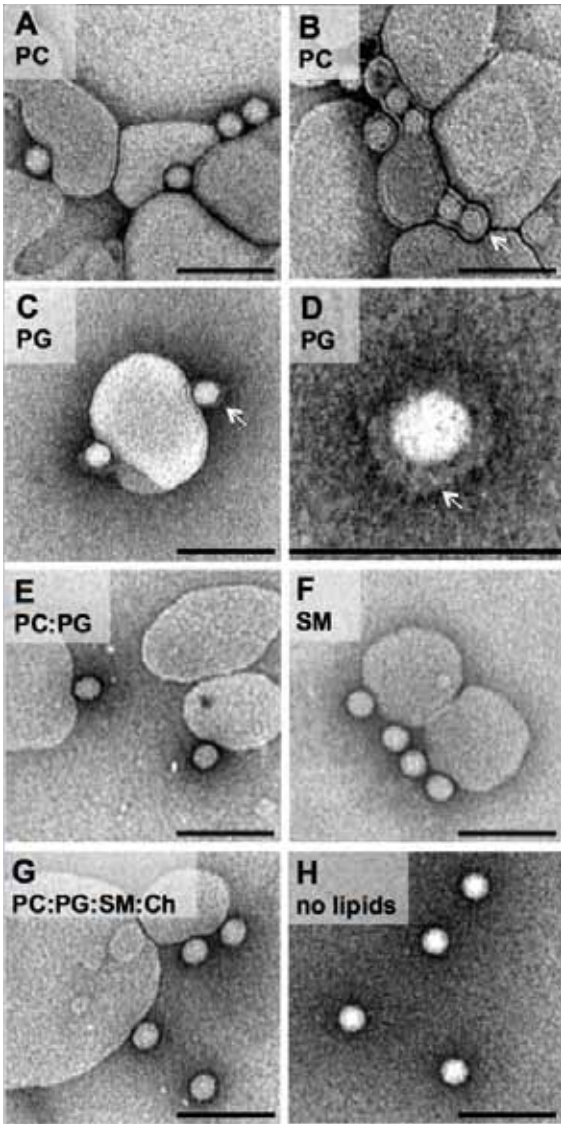

Fig 2. TEM images of EV1 particles and liposomes. Examples of virus particles with liposomes of different lipid compositions: A-B) PC, C-D) PG, E) PC:PG, F) SM, G) PC:PG:SM:Ch, and H) EV1 particles without liposomes. In samples with PC or PG membranes, some of the virus particles were seen wrapped in membrane (arrows), shown in B-D. Scale bars 100 nm.

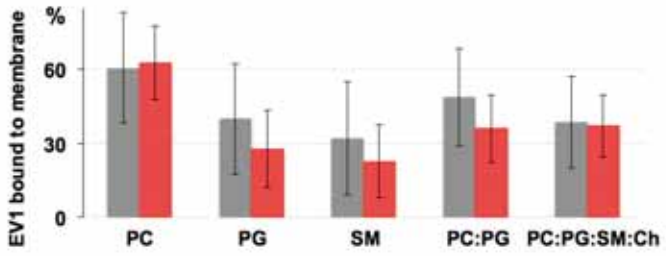

Fig 3. Lipid composition affects the amount of viruses binding to the membranes in TEM. Comparison of samples with (red) and without (gray) the soluble integrin α2I domain. Each bar represents mean percentige of viruses binding to vesicles, calculated from 48 pictures/sample taken at 20 000X magnification, corresponding to 520-1760 virus particles/sample.

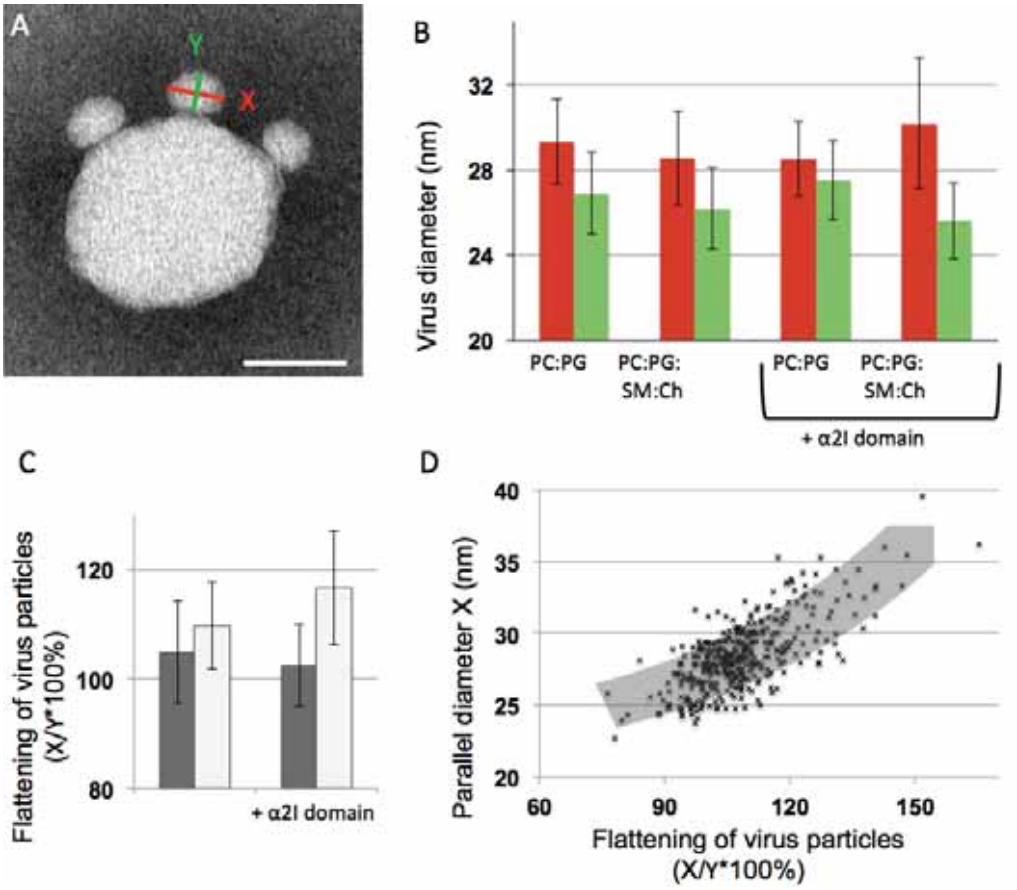

Fig 4. Flattening of the virus particles. Some of the virus particles appear to be flattened and spreading along the lipid membrane, particularly in samples were EV1 particles were incubated with the soluble α2I domain and PC:PG:SM:Ch membranes (A). A) Virus particles bound to a PC:PG:SM:Ch vesicle. Scale bar 50 nm. Flattening was estimated by measuring the virus particle diameters parallel to membrane (X, red) and perpendicular to membrane (Y, green), as shown in figure A. B) Diameters of virus particles (nm) parallel and perpendicular to membrane with PC:PG or PC:PG:SM:Ch and with and without the soluble α2I domain. c) Flattening of the virus particles with the diameters parallel to the membrane represented as % of the diameters perpendicular to the membrane (X/Y %), or the flattening percentage. Samples with PC:PG (grey) and PC:PG:SM:Ch (white) membranes with and without the α2I domain. D) Correlation of the EV1 particle diameter parallel to membrane (nm) and the flattening (X/Y %). The plot in D contains all of the measured virus particles of the diagrams in B and C.

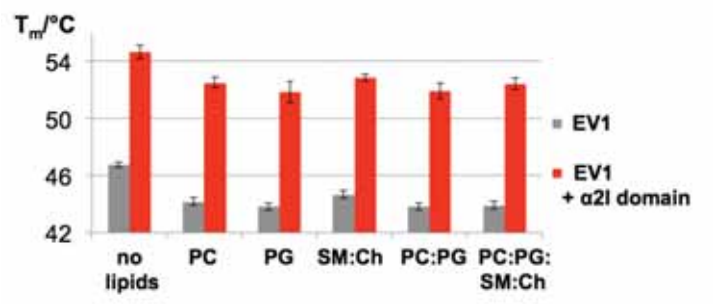

Fig 5. Melting temperatures of EV1 particles from the temperature stability assay. Lipids lower the melting temperature with about 2°C, and the soluble α2I domain raises it with about 8°C.

III

RAMAN SPECTROSCOPIC SIGNATURES OF ECHOVIRUS 1 UNCOATING

by

Ruokola P., Dadu E., Kazmertsuk A., Häkkänen H., Marjomäki V. & Ihalainen J.A. 2014.

Journal of Virology 88: 8504-8513

JVI
JournalsASM.org

Raman Spectroscopic Signatures of Echovirus 1 Uncoating

Päivi Ruokola, Elina Dadu, Artur Kazmertsuk, Heikki Häkkänen, Varpu Marjomäki, Janne A. Ihalainen

Nanoscience Center, Department of Biological and Environmental Science, University of Jyväskylä, Jyväskylä, Finland

ABSTRACT

In recent decades, Raman spectroscopy has entered the biological and medical fields. It enables nondestructive analysis of structural details at the molecular level and has been used to study viruses and their constituents. Here, we used Raman spectroscopy to study echovirus 1 (EV1), a small, nonenveloped human pathogen, in two different uncoating states induced by heat treatments. Raman signals of capsid proteins and RNA genome were observed from the intact virus, the uncoating intermediate, and disrupted virions. Transmission electron microscopy data revealed general structural changes between the studied particles. Compared to spectral characteristics of proteins in the intact virion, those of the proteins of the heat-treated particles indicated reduced α-helix content with respect to β-sheets and coil structures. Changes observed in tryptophan and tyrosine signals suggest an increasingly hydrophilic environment around these residues. RNA signals revealed a change in the environment of the genome and in its conformation. The ionized-carbonyl vibrations showed small changes between the intact virion and the uncoating intermediate, which points to cleavage of salt bridges in the protein structure during the uncoating process. In conclusion, our data reveal distinguishable Raman signatures of the intact, intermediate, and disrupted EV1 particles. These changes indicate structural, chemical, and solute-solvent alterations in the genome and in the capsid proteins and lay the essential groundwork for investigating the uncoating of EV1 and related viruses in real time.

IMPORTANCE

In order to combat virus infection, we need to know the details of virus uncoating. We present here the novel Raman signatures for opened and intact echovirus 1. This gives hope that the signatures may be used in the near future to evaluate the ambient conditions in endosomes leading to virus uncoating using, e.g., coherent anti-Stokes Raman spectroscopy (CARS) imaging. These studies will complement structural studies on virus uncoating. In addition, Raman/CARS imaging offers the possibility of making dynamic live measurements *in vitro* and in cells which are impossible to measure by, for example, cryo-electron tomography. Furthermore, as viral Raman spectra can be overwhelmed with various contaminants, our study is highly relevant in demonstrating the importance of sample preparation for Raman spectroscopy in the field of virology.

Picornaviruses are small, nonenveloped human pathogens able to cause a wide range of illnesses (1). The subgroup enteroviruses include clinically important echoviruses, coxsackieviruses, and poliovirus. These viruses cause a variety of diseases varying from mild infections to aseptic meningitis, heart muscle damage, and paralysis. Enteroviruses have also recently been associated with chronic diseases such as type 1 diabetes, cardiomyopathies, and atherosclerosis (2, 3). Structural details of these viruses have been obtained by means of X-ray crystallography or at a lower resolution by cryo-electron microscopy (4). Various imaging techniques together with biochemical analysis have revealed important information about their entry into cells and the subsequent events leading to uncoating and virus replication (5, 6). However, information on the physicochemical details of genome release events of enteroviral particles is sparse. The uncoating process has been extensively studied by initiating the genome release using heat treatments where intact virions are irreversibly converted to subviral particles that resemble naturally occurring uncoating intermediates (7, 8, 9). Recently, by using such temperature-manipulated particles, a long-standing paradigm of the genome release model from the 5-fold axis was revised (10, 11). However, at present, information on the biochemical events leading to the genome release as well as the initiating environmental trigger of uncoating is lacking (1). Further studies are thus important for addressing one of the events in the enteroviral life cycle, the genome release, and also for the possibility of spotting new potential antiviral targets in related enteroviruses.

Echovirus 1 (EV1) is a picornavirus belonging to a structurally related group of enteroviruses. Common to all picornaviruses, EV1 is an icosahedron-shaped (T=1) assembly of 60 copies of identical protomers comprised of four viral proteins (VP1, VP2, VP3, and VP4), which encapsulate a positive-sense single-stranded RNA genome of approximately 7,500 nucleotides. A 14-carbon saturated fatty acid, myristate, is covalently attached to the N terminus of each picornavirus VP4 capsid protein (12), and it is thought to exit the capsid simultaneously with VP4 during the uncoating process (13). Additionally, studies on poliovirus have shown that the N terminus of VP1 is externalized to the virion surface during the uncoating process, increasing the overall hydrophobicity of the particle (14). Also, the release of the stability-mediating pocket factor, characterized as palmitic acid and located in the core of VP1, is thought to be a prerequisite in the uncoating process, as was shown for bovine enterovirus (15, 16).

Raman spectroscopy provides specific signatures of proteins, nucleic acids, and lipids. It can reveal vast amount of information

Received 20 November 2013 **Accepted** 12 May 2014
Published ahead of print 21 May 2014
Editor: A. Simon
Address correspondence to Janne A. Ihalainen, janne.ihalainen@jyu.fi.

doi:10.1128/JVI.03398-13

about changes taking place in the chemical content of the particles, in the protein secondary structure, and in the physical environment of the particles, which undergo biologically important transformations (17). Raman spectroscopy is a noninvasive characterization technique which uses visible-light laser beams and thus enables microscopic mode with the same resolution as fluorescence microscopy. As the acquisition can be fast, processes in real time can be studied. As Raman spectra are only slightly disturbed by a water environment, information about molecules in their natural habitat or under a wide range of conditions can be obtained. This makes it an ideal probe to study detailed structural alterations and viral protein assembly, interactions, and dynamics, without any labels or other invasive sample preparation methods.

Raman spectroscopic studies on viruses such as turnip yellow mosaic virus (TYMV) (18), bean pod mottle virus (BPMV) (19, 20), and belladonna mottle virus (BDMV) (21) and bacteriophages such as filamentous bacteriophage Ff (22, 23), PRD1 virus (24), and P22 (25–27) have been reported. However, these viruses differ substantially from enteroviruses in several respects. In the plant viruses TYMV, BPMV, and BDMV, the genome is bound to the protein capsid in static form, whereas in the enteroviruses, the interior of the virion is spatially disordered with respect to the symmetric protein shell (28). In addition, the subunit packing is somewhat different between these bromoviruses and enteroviruses (28). The bacteriophage PRD1 is icosahedral but has a lipid envelope. Phage P22 is a nonenveloped, head-tail structured virus, with 6 prominent tail spikes. All such properties influence the Raman spectroscopic character of these viruses.

Detailed Raman spectroscopic signatures from the virus uncoating process of enteroviruses, both *in vivo* and *in vitro*, are missing. For such studies, linear Raman experiments of the initial and final states are a prerequisite. Here, we characterized vibrational spectroscopic properties of intact EV1 virions and investigated the spectral differences arising in the uncoating process of EV1 particles *in vitro*. First, we elucidated the Raman spectroscopic basis of recognition between the intact virion and the disrupted EV1 particle. Further, we determined the Raman signature of the uncoating intermediate, which is obtained by heating the intact, infectious particles at 50°C. Previous studies utilizing heat treatments in order to produce and to investigate uncoating intermediates of enteroviruses have produced a wealth of information. Heating enterovirus particles at 50 to 60°C for various amounts of time has been shown to be able to produce uncoating intermediates (135S) and result in genome ejecting, as well as producing empty (80S) particles indistinguishable from those observed *in vivo* (7, 10, 11). The Raman spectra of the particles that were heat treated at 50°C represent a state where the genome is partially ejected from the capsid, as confirmed by transmission electron microscopy (TEM) and thermal stability assays (29). We conclude that there are clear Raman markers which address the uncoating stage of the virion. The experiments reported here provide a framework for monitoring the sequence of chemical and conformational changes occurring during enterovirus uncoating in a time-resolved manner.

MATERIALS AND METHODS

Cell culture and virus purification. Echovirus 1 (Farouk strain, obtained from the ATCC) was propagated in a monolayer of GMK cells and purified using an overall scheme similar to that described previously (30). To summarize, overnight (24-h)-infected cells were collected and repeatedly freeze-thawed (3 cycles) to lyse cellular structures. Bulk cell debris was removed by centrifugation (4,500 × *g* for 15 min). To precipitate protein, 8% (wt/vol) polyethylene glycol 6000 (PEG 6000) (Sigma-Aldrich) and 2.2% (wt/vol) NaCl were added to the supernatant and stirred overnight (24 h) at 4°C. Precipitated material was collected by centrifugation (8,000 × *g* for 40 min) and suspended in R buffer (10 mM Tris-HCl [pH 7.5], 200 mM NaCl, 50 mM $MgCl_2$, 10% [wt/vol] glycerol). To disrupt membranous structures, 0.3% (wt/vol) sodium deoxycholate (Sigma-Aldrich) and 0.6% (vol/vol) Nonidet P-40 substitute (Sigma-Aldrich) were added to the suspension and incubated for 30 min at 4°C. The resulting mixture was clarified by centrifugation (3,500 × *g* for 15 min) and divided equally (<1.5 ml/gradient) on top of 10-ml linear density gradients of 10 to 40% (wt/vol) sucrose in R buffer. The gradients were subsequently ultracentrifuged (86,000 × *g* for 3 h at 4°C) and fractioned from the top into 500-μl aliquots. Based on optical density measurement at 260 nm (NanoDrop 1000; Thermo Scientific), three virion-containing fractions (fractions 11, 12, and 13) were pooled and diluted to 10 ml in phosphate-buffered saline (PBS) supplemented with 2 mM $MgCl_2$. The diluted fractions were dialyzed three times against 1 liter of PBS supplemented with 2 mM $MgCl_2$ using 50,000-molecular-mass-cutoff Spectra/Por Float-A-Lyzer cellulose ester membranes (Spectrum Laboratories). Finally, dialyzed virions were pelleted by ultracentrifugation (93,000 × *g* for 2 h at 4°C) and suspended in a small volume of PBS supplemented with 2 mM $MgCl_2$. All measured samples were dissolved in the aforementioned PBS buffer. Virions were stored at −80°C.

Infectivity of the purified EV1 virions. Infectivity of the purified virus batch was assayed using the endpoint titration method to determine the 50% tissue culture infective dose ($TCID_{50}$). The $TCID_{50}$ was calculated as described previously (31), positioning the $TCID_{50}$ between the last infected and first noninfected well. Briefly, a monolayer of GMK cells seeded at 5×10^4 ml^{-1} on a 96-well plate were infected with serially diluted virus stock (starting from a 10^{-5} dilution). The progression of the infection was followed daily by light microscopy. After 72 h of incubation, the cells were stained using crystal violet supplemented with 10% formalin (for 10 min at room temperature [RT]). The detached cells were washed off with water, and remaining attached cells were counted as viable and noninfected. For the EV1 batches used in the experiments, the $TCID_{50}$ was found to be 6.1×10^{11} to 1.5×10^{12} virus particles/ml.

Protein content and composition of purified EV1. The protein content of purified EV1 was determined using a method described by Porterfield and Zlotnick (32), where an average value of molecular mass (23.5 kDa) and an average molar absorptivity value (ε_{280}, 34,440 M^{-1} cm^{-1}) for VP1 to -4 were used for the calculations. Protein concentrations of the batches were 0.9 to 3.8 mg ml^{-1} after subtraction of the scattering component (6.9% of the baseline subtracted absorption signal at 260 nm). The A_{260}/A_{280} ratio was 1.65. The absorption spectrum was recorded with a PerkinElmer Lambda 850 spectrophotometer using a 10.0-mm optical path quartz cuvette (Hellma Analytics). The protein composition of purified EV1 was analyzed using 12% SDS-PAGE. The sample lane was loaded with 5 μg of EV1, and PageRuler Plus (Thermo Scientific) was used as a molecular weight marker.

Thermal stability. The thermal stability of the purified EV1 particles was assayed using the method described by Walter et al. (29). The fluorescence signal was recorded using a Bio-Rad C1000 thermal cycler, and the final sample mixture contained 1 μg of EV1 and a 10× concentration of SYBR green II (Invitrogen). All samples were equilibrated at 20°C for 10 min before thermal stability measurements were started. For the full temperature range scan, the fluorescence signal was recorded at 10-s intervals with 0.5°C increments. In additional measurements, the designated temperature was kept constant for 3 min (50°C) or 10 min (60°C), and after heat treatment, the sample was cooled back to 20°C, at which point the fluorescence reading was taken or the sample was loaded to an EM grid.

Transmission electron microscopy. The morphology of the heated and nonheated virions was visualized by negative staining with 1% (wt/

vol) phosphotungstic acid (Sigma-Aldrich). The Formvar-coated EM grids were glow discharged (EMS/SC7620 mini-sputter coater), and samples were deposited on the grids for 15 s, after which the excess sample was blotted away (Whatman 3MM). Next, negative stain was added for 1 min and removed as before. Samples dried at least overnight were imaged with a JEM-1400 (JEOL) transmission electron microscope with a magnification of ×50,000 (80 kV).

Raman spectroscopy. For all Raman viral experiments, aliquots of 6 to 10 μl with a sample concentration of 0.9 mg ml^{-1} for dried samples and 3.8 mg ml^{-1} for aqueous samples were either deposited on a CaF_2 window or sealed in a glass capillary (SMI capillaries, P5070-902; American Dade). Heating of the aqueous samples was performed in a water bath, either at 50°C for 3 min or at 60°C for 10 min. The dried sample was allowed to dry for 15 min at ambient temperature. The Raman spectra were measured with a home-built Raman setup in a backscattering geometry. In this setup, a laser beam of solid-state laser (CNI) with an excitation wavelength of 532 nm was focused onto the sample with a spot diameter of 3 μm using a microscope objective (Plan Neofluar 10×/0.30; Zeiss). Raman scattering was recorded using a charge-coupled device (CCD) camera (Newton DU940P-BV; Andor) attached to an imaging spectrograph (Acton Spectra Pro 2500i) with an entrance slit of 50 μm and a grating of 600 grooves/mm. Raman spectra were accumulated using 30 10-s exposures. Laser powers of 45 mW for dried and 200 mW for aqueous samples were used. From each scan, a dark spectrum was subtracted. The reference spectra of water, buffer solution, empty capillary, and CaF_2 window were detected with the same settings and subtracted from the sample spectra. The fluorescence background was defined by fitting a polynomial curve to the measured spectrum from the points where no Raman signal is expected to be present and subtracted from the data. After this procedure, no spectral signatures other than those of viral constituents were obtained.

Spectra of the aqueous samples at a concentration of 3.8 mg ml^{-1} represent means of measurements from three different EV1 batches normalized to the Phe peak at 1,003 cm^{-1} with a floating average with a span of three data points (2.7 cm^{-1}). In addition, the differences between room temperature and heated samples were analyzed in four separated spectral sections, 610 to 945 cm^{-1}, 945 to 1,145 cm^{-1}, 1,145 to 1,520 cm^{-1}, and 1,520 to 1,800 cm^{-1}, which were normalized to the mean signals of each section and smoothed with a floating average with a span of seven data points (10 cm^{-1}).

Radial distribution and positioning of salt bridges in EV1. The atom coordinates were gathered from the EV1 protomer (PDB entry 1EV1) using UCSF Chimera (33) Build 1.8. Salt bridges were identified manually, scoring only arginine and lysine as salt bridge-forming residues with carboxylic oxygen of Glu and Asp. In the case of many possible connections (<3.5 Å), the closest was chosen, resulting in one connection per residue.

RESULTS

Sample purity and heat-induced uncoating of EV1. The Raman analysis of viral particles imposes a demand for highly homogenous and pure samples. The sucrose gradient purification scheme used here resulted in a single, clearly visible band. The fractioned gradient showed a local absorbance maximum at 260 nm in fraction 12, while five top fractions also showed high optical density; no visible banding was observed (Fig. 1A). After dialysis, the collected fractions (fractions 11 to 13) were analyzed for protein composition using 12% SDS-PAGE. Figure 1C shows that the purified EV1 was contaminant-free in the molecular mass range of 250 to 10 kDa, while the prominent capsid proteins, VP1 to -3, banded next to 35- to 25-kDa markers, as expected. To quantify the protein concentration of a virus sample, a UV-visible (UV-Vis) spectroscopic method introduced by Porterfield and Zlotnick (32) was used. In our hands, the above-mentioned spectroscopic approach has been found to be in reasonable agreement with the more traditional Bradford assay (data not shown). The method incorporates scattering correction into the resulting absorption spectrum, with 6.9% of the total signal. This subsequently affects the A_{260}/A_{280} ratio, which was 1.65 for dialyzed particles (Fig. 1B). In literature, the reported A_{260}/A_{280} ratios for enteroviruses vary considerably (34–36), partially due to differences in genome contents but also resulting from uncorrected spectra. However, as the genome-to-protein ratio (i.e., the A_{260}/A_{280} ratio) does not reflect virion integrity, EV1 was visualized by TEM and was found to consist of a highly homogenous population of intact particles approximately 25 nm in diameter (Fig. 1D).

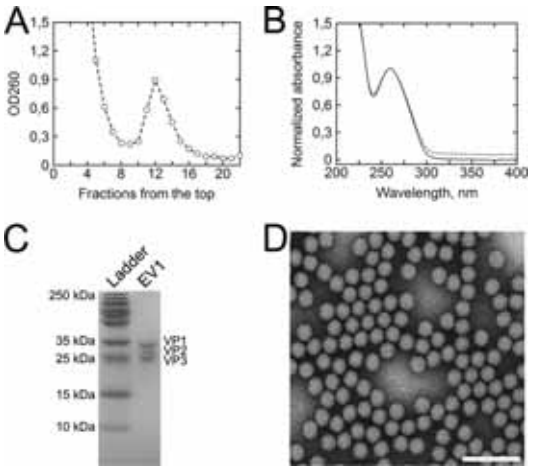

FIG 1 The scheme used to purify EV1 produces a homogenous population of intact virions. (A) A sucrose gradient fractioned from the top shows clear separation in optical density (OD_{260}) between bulk, low-density material and EV1 virions. Fractions 11, 12, and 13 were collected for further purification. (B) Absorption spectrum of dialyzed EV1 (dashed line) and light scattering-corrected spectrum (solid line) normalized at 260 nm for better comparison between the two. The scattering component was calculated to be 6.9% of the total signal, and the A_{260}/A_{280} ratio was 1.65. (C) SDS-PAGE analysis of the purified EV1 samples shows no protein contaminants in the range of 250 to 10 kDa, while bands of the prominent viral proteins VP1 to -3 appear between the 35-kDa and 25-kDa markers. (D) EV1 particles contrasted by negative staining and visualized by TEM show homogenous population of intact virions approximately 25 nm in diameter. Scale bar, 100 nm.

Since the EV1 capsid proved to be nonpermeable to the SYBR green II dye (Fig. 2A), thermal stability assay was used along with TEM to evaluate the extent of genome egress from intact EV1 particles. Figure 2A indicates that the melting temperature (T_m) for intact EV1 particles is 51°C. Noting that SYBR green II signal begins to increase around 40°C and accumulates over approximately 3 min of effective heating time prior to the 51°C T_m mark, 3 min of heating at 50°C was used to produce the so-called uncoating intermediate particles (Fig. 2B). The population of these genome-releasing virions was visualized by TEM (Fig. 3). After 3 min of heating at 50°C, the great majority of the visualized particles were connected to an electron-dense protrusion (Fig. 3B). Additionally, Fig. 3A and B show that both the intact (20°C) virions and partially disrupted virions (50°C) are structurally organized and symmetrical. Similar particles were obtained earlier using polioviruses (11). Heating the intact EV1 virions at 60°C

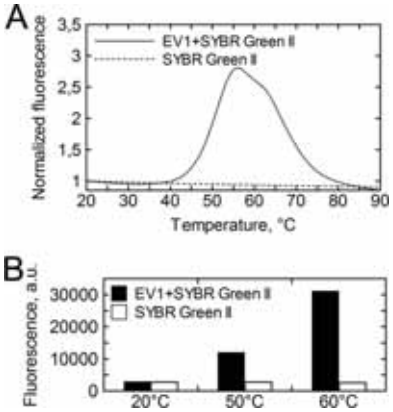

FIG 2 Thermal stability analysis of intact EV1 virions. (A) Fluorescence traces of SYBR green II in the presence of EV1 show a steep increase starting from around 40°C and a midpoint at 51°C (solid line). SYBR green II by itself shows no fluorescence increase as a function of temperature (dashed line). The fluorescence is normalized with respect to the initial fluorescence. (B) EV1 was incubated with SYBR green II at 50°C and 60°C for 3 and 10 min, respectively, and cooled back to 20°C for fluorescence measurement. At 20°C EV1 is not permeable to the dye, whereas temperature-induced genome egress is detected as an increase in fluorescence. The white bars represent the behavior of SYBR green II alone when subjected to the described treatment.

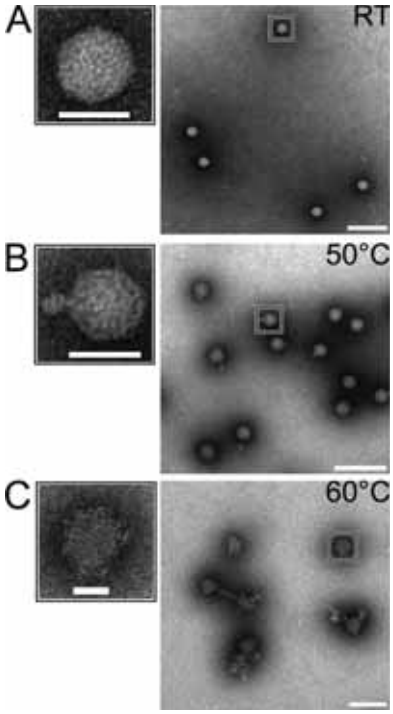

FIG 3 TEM images of negative stained EV1. (A) Intact EV1 virion. (B) EV1 heated at 50°C for 3 min shows an electron-dense protrusion from an otherwise structured particle. (C) Heating for 10 min at 60°C results in complete particle disruption. Scale bars, 25 nm and 100 nm (left and right images, respectively).

resulted in a complete particle disruption (Fig. 3C). Overall, homogenously genome-deprived but structurally intact EV1 particles were challenging to produce by heat treatment alone (data not shown). The heat-induced chemical and structural alterations in the particles treated at 20°C, 50°C, and 60°C were then further probed by Raman spectroscopy.

Raman analysis of viral particles. The Raman spectrum of the intact virion (Fig. 4) shows a large number of vibrations that can be assigned reasonably well using values in the literature, as expressed in Tables 1 and 2 for proteins and RNA, respectively (17, 24, 37, 38, 39). The most prominent vibrational region at 2,900 cm^{-1} originates from aliphatic C-H vibrations. Here, however, we concentrated on the fingerprint region from 600 to 1,800 cm^{-1}, where most previous biological applications of Raman spectroscopy have been performed, as it has higher sensitivity to the structural and chemical nature of particles (for examples, see references 18 and 23). The best-known spectral features found at typical positions (17) in the Raman spectra of the virus are the amide I (Am I) and Am III bands at around 1,670 cm^{-1} and in the region between 1,230 and 1,300 cm^{-1}, respectively. The anti-symmetric C-C stretching modes of aromatic amino acids (Phe, Tyr, and Trp) locate in the region of 1,580 to 1,615 cm^{-1} and the ring breathing modes of aromatic amino acids at around 1,000 cm^{-1}. Other side chain vibrations emerge at around 600 to 900 cm^{-1}, and the methyl/methylene vibration bands are located at around 1,350 and 1,450 cm^{-1}. Many RNA vibrations partially overlap the protein bands, although a large number of vibrations can still be specified. The ring breathing modes of RNA bases appear in the region below 800 cm^{-1}, ribose and phosphate signals between 800 and 1,100 cm^{-1}, and the stretching vibrations of the bases at higher wave numbers (1,200 to 1,600 cm^{-1}) (39, 40).

Raman spectra of viral particles in the buffer environment show clear similarities with spectra of the dried particles (Fig. 4B), and basically all spectral features can be observed from the solution with a concentration as low as 0.9 mg ml^{-1}. However, the details of the spectra were more clearly distinguished from the noise level of our experiment at a virus concentration of 3.8 mg ml^{-1}, which was therefore used in the characterization of the heat-induced changes of the viral particles.

By detecting Raman spectra of the particles treated with different temperatures, we aimed to detect chemical and structural changes between the intact virus particle and an uncoating intermediate virion particle, as well as with an endpoint structure where the virion particle was disrupted by heat treatment (morphology of particles obtained with TEM [see above; Fig. 3]). As shown in Fig. 5, the Raman spectra of the particles that had been heat treated at 50°C and 60°C deviate clearly from that of the intact virion. As the heat treatment changes the form (Fig. 3) and possibly also the solvent shell of the particles, the scattering and fluorescence properties of the particles differ. This creates challenges in baseline determination and normalization of the spectra, and therefore, the Raman spectra were dissected in four individual spectral regions from 610 to 1,800 cm^{-1}. Figure 5A to D show the differences between the particles. In most cases, a gradual change of Raman spectra from intact to 50°C-treated and then to 60°C-

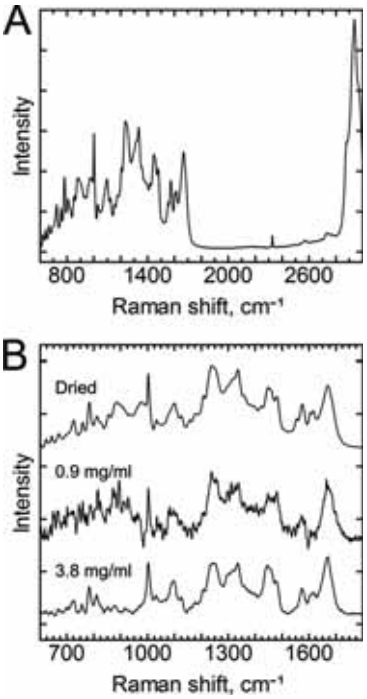

FIG 4 Comparison of the Raman spectra of dried and aqueous EV1 particles. (A) Full Raman spectra of dried intact EV1 virions. The most prominent vibrational region originates from the aliphatic C-H stretching vibrations shown at around 2,900 cm^{-1}, which, however, has a low information content regarding the structural details of the virion particles. The fingerprint region is located between 700 and 1,800 cm^{-1}. The sharp band at 2,331 cm^{-1} originates from N_2. (B) Fingerprint regions of dried EV1 virion (top line) and of aqueous EV1 at 0.9 mg ml^{-1} and 3.8 mg ml^{-1} (middle and bottom lines, respectively). Laser excitation at 532 nm and laser powers of 45 mW for dried and 200 mW for the aqueous viral samples were used with 30 exposures of 10 s in each measurement. The spectra were normalized to that of the Phe vibration at 1,003 cm^{-1}, and the baseline was shifted for better comparison of the spectra. All spectra were measured at ambient temperature.

TABLE 1 Obtained frequencies of the vibrations of proteins found in this study

Assignment[a]	Frequency (cm^{-1})		
	Dried sample	Aqueous sample	Heat-induced effect
Phe	623	620	+
Tyr	644	642	
C-S	670	668	
Trp	758	756	+
Tyr	826, 855	829, 854	− (829)/+ (854)
Trp	887	873–883	− (60°C)
AmIII	960–978	952–977	
Phe	1,003	1,003	
Phe	1,031	1,031	
CC, CH	1,071-1,096	1,073-1,098	+
Nonaromatic side chains	1,127	1,122-1,128	+ (1,120)/− (1,130)
CH_3	1,156-1,176	1,160-1,178	
Phe, Tyr	1,208	1,205-1,210	
Am III	1,230-1,300	1,230-1,300	+ (1,240)/− (1,300)
Trp, CH3	1,318-1,378	1,322-1,383	
Asp, Glu-COO^-	1,390-1,404	1,390-1,402	+ (60°C)
CH_2	1,446-1,458	1,446-1,458	−
Trp	1,555, 1573	1,549, 1,572	+
Phe		1,588-1,594	−
Phe, Trp	1,605	1,603	
Tyr, Trp	1,613, 1,618	1,612, 1,616	
Am I	1,669	1,668	+
Asp, Glu-COOH		1,710	+ (50°C)

[a] The assignment is based on previous studies (17, 24, 37, 38). Am, amide.

treated particles was observed. This effect can be expected according to the TEM analysis as well (Fig. 3), which shows basically a full disruption of the particles after 60°C heat treatment.

The largest changes in the spectra were observed in signals assigned to the amide bands, the methyl/methylene signal at 1,446 cm^{-1}, and RNA signals at 750 to 800 cm^{-1}, although many changes are located in regions where multiple factors affect the spectra. Interestingly, the 1,446 cm^{-1} band, reflecting C-H vibrations from the proteins, is more affected than the corresponding band for RNA molecules at 1,478 cm^{-1}. Thus, the ratio between 1,446 and 1,478 cm^{-1} conveniently indicates changes of signals between proteins and genome, respectively, in the viral particles. The Am I and Am III regions, shown in Fig. 5, reveal information on the changes in the secondary structure of the coat proteins in the heat-treated particles. The differences between the spectra are the most pronounced at 1,630 to 1,650 cm^{-1} and 1,670 cm^{-1} (Fig. 5D). Broadening of the Am I peak is greatest in the spectrum of the intact virus. On the lower-energy side of the Am I vibration, the 1,572 cm^{-1} band, which originates from ring breathing modes, both from Trp as well as from adenine and guanine of RNA (39, 41), shows higher intensity in the heated particles, especially in the spectra of the particles treated at 60°C.

Most of the heat-induced changes grow gradually as the heat treatment becomes more intense. Some of the changes, however, are evident only after heat treatment at 50°C, namely, the decrease of signals at 990 and 1,650 cm^{-1}. At around 990 cm^{-1}, there are RNA vibrations from ribose phosphate (39) and protein-derived signals from proline, arginine, and tyrosine residues, as well as the nearby phenyl alanine signal at 1,003 cm^{-1} (37). At 1,650 cm^{-1}, the signal originates from the amide bonds of proteins (17).

TABLE 2 Obtained frequencies assigned to the RNA molecule from the intact virus particles

Assignment[a]	Frequency (cm^{-1})		
	Dried sample	Aqueous sample	Heat-induced effect
A ring stretching (726)	726	722-727	
C/U breathing/stretching (787)	783	783	
O-P-O symmetric stretching (813)	811	811	+ (60°C)
Ribose-phosphate, C-O stretching (919)		914-921	−
Ribose-phosphate, C-O stretching (977)		969-980	−
P-O stretch, sugar phosphate; C-O stretching (1,047)	1,044	1,044sh[b]	+
PO_2^- symmetric stretch (1,097)	1,091-1,100	1,090-1,100	
U/C ring stretching (1,253)	1,252	1,250	
C/A ring stretching (1,300)	1,300	1,300	−
A, G, U (1,336)	1,336	1,335	+
U/C ring stretching (1,460)	1,460	1,458	−
A/G ring stretching (1,485)	1,480	1,478	+
A/G ring stretching (1,578)	1,576	1,578	+

[a] The assignment is based on the study by Hobro et al. (39).
[b] sh, shoulder.

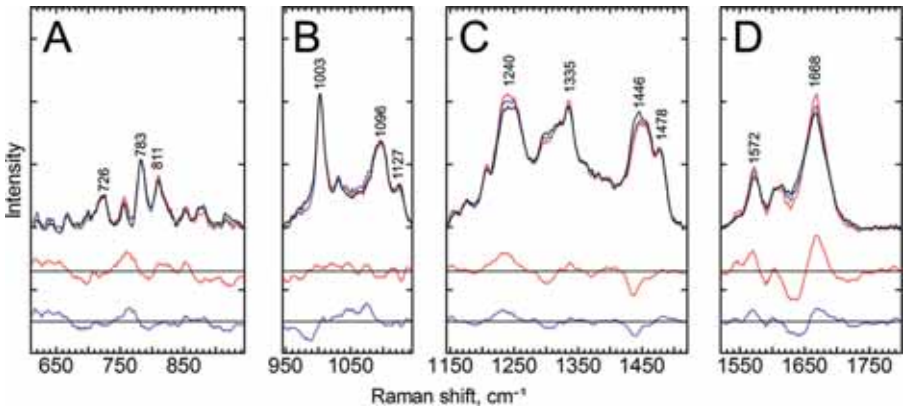

FIG 5 Raman spectra of aqueous EV1 particles at room temperature. The top lines show the Raman spectra of intact EV1 (RT, black line), intermediate particles (50°C, blue line), and disrupted particles (60°C, red line). Below are the 2-fold-magnified difference spectra corresponding to the temperature intervals between 60°C and RT (red) and between 50°C and RT (blue). The spectra were divided into individual sections and normalized to the mean signals of each section, and the baselines were shifted for better visualization. (A) 610 to 945 cm^{-1}; (B) 945 to 1,245 cm^{-1}; (C) 1,245 to 1,520 cm^{-1}; (D) 1,520 to 1,800 cm^{-1}. Marked vibrations from lower to higher frequency are as follows: 726 cm^{-1}, RNA; 783 cm^{-1}, RNA; 811 cm^{-1}, RNA phosphate symmetric stretching, an A-form RNA helix marker; 1,003 cm^{-1}, Phe; 1,096 cm^{-1}, a complex region of CC and CH vibrations of lipid, RNA, and protein capsid; 1,127 cm^{-1}, nonaromatic amino acids and lipids; 1,240 cm^{-1}, Am III; 1,335 cm^{-1}, RNA bases; 1,446 cm^{-1}, C-H vibrations from the proteins; 1,478 cm^{-1}, RNA bases; 1,572 cm^{-1}, Trp/RNA; 1,668 cm^{-1}, Am I, revealing information about the secondary structure of the proteins. Data acquisition was performed as described for Fig. 4, and the spectra represent mean signals of measurements from three different EV1 batches, all with a concentration of about 3.8 mg ml^{-1}.

Apart from major differences in the Raman signals, subtle signal variations along the spectra can reveal information from important details of the EV1 uncoating process. These changes along with the assignments are indicated in Tables 1 and 2. For example, a slight change in the signal at around 1,710 cm^{-1} in the spectra of the particles treated at 50°C can be observed (Fig. 5D). This signal increase could imply protonation changes of carboxylic groups of Glu residues (42). In ideal case, such increase of signal of the protonated forms of Glu should lead to a decrease in the signals of the COO^- population, found in the region between 1,390 cm^{-1} and 1,410 cm^{-1}, which, however, is hard to detect in Fig. 5C from the spectra of viruses that were heat treated at 50°C. Another small change, a shift to lower wave numbers, or a decrease in the signal at the higher-frequency side of the band, is seen in the peak at 1,122 to 1,128 cm^{-1} (Fig. 5B). This peak represents nonaromatic amino acid residues, but it might also include some fatty acid vibrations. There are two kinds of fatty acids in the EV1 capsid, myristate and palmitic acids, the first being covalently attached to VP4 and the second being buried in a VP1-formed pocket. No obvious fatty acid peaks can be detected from the spectra, but there are small decreases in signals of heat-treated viruses at the fatty acid signal sites at 1,063 cm^{-1}, 1,129 cm^{-1}, and 1,296 cm^{-1} (37) that could be consistent with heat-induced changes in the local environment of the fatty acid molecules or reduction of fatty acid molecule amounts at the measured spot of the sample.

The Fermi doublets of the aromatic amino acids Trp and Tyr are often used as indicators of indole environment hydrophobicity and phenolic hydrogen bonding. Neither of these doublets stands out very clearly from the spectra, but they can be assigned to specific signals nonetheless. Small changes are seen in signals assigned to the Tyr Fermi doublet at 829 and 854 cm^{-1} (Fig. 5A), where heat treatments reduce the Raman signal ratio I_{829}/I_{854}, indicative of a greater hydrogen bond acceptor role, or exposure to the solvent, of the average phenoxyl group after heat treatments (43). The Trp Fermi doublet at 1,340 and 1,360 cm^{-1} shows a small increase in the signal at 1,340 cm^{-1} after heat treatment (Fig. 5C), indicating an increasingly hydrophilic environment of Trp residues (44, 45), although the overlapping RNA signal assigned to the larger peak at 1,335 cm^{-1} might affect this as well. A Trp band at around 880 cm^{-1} has been considered a marker for Trp hydrogen bonding, with signals at 882 to 883 cm^{-1} indicating Trp residues with no hydrogen bonding and a signal at 871 cm^{-1} indicating residues with strong hydrogen bonding (44). In intact viruses, this Trp signal is a single peak centered at 877 cm^{-1}, and after heat treatments, the signal divides to two peaks at 873 and 881 cm^{-1}, indicating changes in Trp hydrogen bonding status. The frequency of the Trp signal near 1,550 cm^{-1} has been reported to be indicative of changes in side chain conformation (46–48), and there are heat-induced changes in this region in our data (Fig. 5D). Particularly, in the spectrum of the intact virus, this signal overlaps with the peak at 1,572 cm^{-1}, and after heat treatment, a new peak slightly under 1,550 cm^{-1} appears, suggesting a considerable change in conformation of some of the Trp residues. A similar change has been noticed for bovine enterovirus uncoating with resonance Raman spectroscopy (46). However, the RNA signal also appears relatively close at around 1,578 cm^{-1}. Yet another Trp peak, at 756 cm^{-1}, also shows apparent heat-induced changes, supporting the interpretation that Trp residues undergo significant changes upon virus uncoating.

Partially overlapping the Trp 756 cm^{-1} signal is an RNA signal at 783 cm^{-1}, coming from the C/U ring breathing modes (Fig. 5A). This signal has been reported to change in intensity due to changes in the environment, particularly in nonhelical regions of RNA (39, 49). In our experiment, there were heat-induced changes around this peak. A small increase is also seen in the symmetric phosphate stretching vibration signal at 811 cm^{-1},

considered a marker for the A-form RNA helix, suggesting a change in RNA backbone conformation. Most of the RNA signals somewhat overlap protein signals; however, RNA can be considered the main source of the peaks at 1,335 and 1,478 cm^{-1}. More detailed assignments of signals to RNA vibrations are presented in Table 2 (39). Most RNA-assigned signals above 1,200 cm^{-1} slightly increase in intensity after heat treatments, with one exception. The decrease at 1,300 cm^{-1} could come from changes in cytosine or adenine ring stretching vibrations, although it could also be due to fatty acids or changes in protein secondary structures. A signal just below 1,050 cm^{-1} that can be assigned to RNA P-O and sugar phosphate C-O stretching appears only after heat treatments.

DISCUSSION

Virus particles of various species or in different assembling or uncoating states deviate from each other in terms of structure and chemical content. In this study, EV1 viral particles, in three different states, were characterized in terms of both structural and chemical information. The intact virion, the uncoating intermediate produced after heating the virion at 50°C for 3 min, and the disrupted viral particle treated at 60°C for 10 min, all showed different types of structures obtained by TEM analysis. Also, the Raman spectroscopy of different states produced unique spectral features.

The Raman spectrum of a complex biological sample is a mixture of spectral contributions from all Raman active molecular groups contained in the sample, and therefore it enables simultaneous studying of all sections taking part in the biological processes and ultimately determining the sequence of the changes taking place in the molecule. As a result, the Raman spectrum of a virus consists of numerous, overlapping bands and peak shoulders. The most prominent spectral features, seen in the spectra of large polypeptides, are Am I, originating from the polypeptide chain C-O stretching, and Am III, mainly resulting from the coupled C-N and N-H bending motions. These are widely used as indicators of the secondary structure of proteins (17). Other informative Raman marker bands originate from the aromatic amino acids. Although Raman spectra of biological material are usually interpreted mainly as indicators of secondary structure conformation, other factors in the local environment strongly influence the position, size, and shape of the Raman signal. Local electric fields, polarity, and protonation state of the vibrators (50) play an important role, which means that Raman signals are sensitive to ions, charged amino acids, and even charged phosphates in the protein or in the genome. As shown in this and other studies (18–20, 22–27), Raman spectroscopy can provide a vast amount of information about the character and status of virion particles. In many cases, however, it is difficult to distill all information from a single set of data. Below, we condense the essential features of the Raman fingerprint of EV1 and discuss some of the crucial factors that must be considered when one attempts to determine the genuine Raman spectra from viral samples in an aqueous environment.

As Raman signals are relatively weak, in comparison with, for example, fluorescence signals of fluorophores, relatively high sample concentrations are needed. Typically, the reported Raman spectra of viral particles are measured with concentrations up to 100 mg ml^{-1} (18–27). Low sample concentrations are preferable when the viral particles in nonaggregated form are being measured. On many occasions, the scattering intensity of viruses is small, and the changes at low concentrations are hidden inside the overruling background spectra. This leads to challenges in detecting the Raman signal of the sample and accurately subtracting the solvent and other background from the weak viral spectra (41). It is also important to keep in mind that some buffers include groups that have vibrations similar to those of many biological samples or, at worst, are quite reactive (51) and therefore can, if not obscure the spectra, at least skew the interpretation. Other informative vibrations may be overwhelmed in a heterogeneous sample containing leftovers, such as sugars, from the purification procedure. The material besides the sample may then result in the biggest changes in the Raman spectra, overlapping the small changes taking place in the actual sample. Alternatively, they may influence the behavior of the sample; for example, sucrose is known to stabilize protein structure (52). In our measurements, the viral particles were clearly dominated by sucrose contamination even after dialysis with a molecular weight cutoff of 2,000 (data not shown) and were properly purified only with a higher-molecular-weight cutoff of 50,000. Also, in a recently published article on virus-like particles, there are clear and identified sucrose leftovers in the Raman spectra (53). It is important to note that because Raman spectroscopy "sees everything," the purity and homogeneity of the samples are crucial. Even smallest changes in the purification method used can cause additions to and interference with the spectra, which can lead to erroneous interpretations. This means that critical attention must be paid to the purification procedure, and as a result, better-quality spectra containing more information are achieved. Further, once a spectrum of a pure viral sample has been obtained, Raman spectroscopy could be used as a very sensitive probe for impurity studies for analytical purposes.

To the best of our knowledge, there are no previous Raman studies on EV1 and its close relatives. Bovine enterovirus and rhinovirus have been studied by means of surface enhanced Raman scattering (SERS) and UV resonance Raman spectroscopy (46, 54). It is notable that, in the case of SERS, the choice of the substrate material and, in the case of resonance Raman studies, the choice of the laser wavelength contribute to the intensity of each Raman transition. Our spectra of EV1 are especially similar to those obtained for the BPMV virion (20), which shares considerable structural similarity with picornaviruses (55). Li et al. also observed differences in the Raman spectra between crystalline and liquid BPMV viral particles and concluded that changes mainly originate from packed RNA molecules that have different electrostatic environments in the samples (56). It should be recognized, though, that one particular difference with most of the previously reported linear Raman data is that our Raman spectra were measured with much lower protein concentrations, i.e., less than 4 mg ml^{-1} in our study versus 80 mg ml^{-1} or more in other studies (for example, see references 19, 20, and 24). The amount of aggregation and interaction between viral particles at such concentrations could diminish the differences compared to the crystalline state. In our EV1 samples there are differences between spectra measured in solvated and dried states, for example, a broadening or a shift in the Am I band to higher wave numbers, indicating a larger amount of disordered secondary structures in the dried sample. On the other hand, the width of some bands originating from individual amino acids, like the Phe band at 1,003 cm^{-1}, is similar to the width in spectra of dried and solvated samples. Drying removes the stabilizing hydration shell (57) and can influence sta-

bility, cause aggregation, and hamper at least certain parts of capsid structures. This also implies that the SERS technique (54), where viral particles are attached to metallic surfaces or nanoparticles, can reveal somewhat different vibrational spectroscopic information than measurement of viral particles normally diffusing freely in a buffer solution.

Care was taken to remove the contribution of the wagging mode of water molecules from the Raman data of the diluted samples, which has been determined to be essential for a proper analysis of the Am I modes (41). The Raman Am I band centered at 1,668 cm^{-1} indicates β-sheets as the predominant secondary structure of the capsid, which is consistent with the known structure of the major capsid proteins, VP1, VP2, and VP3, in EV1 (58). However, temperature-induced alterations around 1,653 cm^{-1} reveal a decrease in α-helical secondary structure due to the partial unfolding of the shell subunits, especially at the intermediate state. The decreasing signal in the Am III area at around 1,300 cm^{-1} could also be due to reduced α-helical content of proteins. This indicates that the heat-induced uncoating is dominating in the α-helical regions of the protein. The signals assigned to β-sheets and coiled structures in Am I and III regions, at 1,668 and 1,240 cm^{-1}, respectively, increase in magnitude at the same time, suggesting that some of the α-helix structures are converted to β-sheets or coils. Flexible loops between structured domains are known to make protein dynamics less constrained and play a critical role in the uncoating process. For example, these mechanically uncoupled structures could enable the capsid expansion, which is clearly visible from the TEM image of the uncoated EV1 particle (Fig. 3C).

Signals of aromatic amino acids reveal information on hydrogen bonding, hydrophobicity, and side chain conformation of these residues (43–48). Many of these informative signals of EV1 change with heat treatments. Small changes are seen in the Fermi doublets of Tyr and Trp that change with hydrogen bonding of Tyr and hydrophobicity of Trp environment. Changes in the 877 cm^{-1} signal indicate variations in Trp hydrogen bonding status, and the appearance of a new Trp signal at around 1,550 cm^{-1} indicates changes in side chain conformations. All these signals point in the same direction as the changes seen in secondary structures of viral proteins and TEM-images, i.e., loosening of the capsid structure and subsequent exposure of these residues to water.

Obtaining Glu vibrations of protonated carboxyl group suggests that protonation processes take place in the heat-induced uncoating of EV1. In the unprotonated state, the negatively charged Glu may interact with positively charged residues (e.g., Lys and Arg) to form salt bridges, which have been shown to be important stabilizers of HIV, influenza virus, filamentous viruses, and bacteriophage hk97 (59–62). These salt bridges may be involved in a constrained network of interactions within one subunit or between two neighboring units, clamping the domains in a considerably more stable capsid structure. Our data suggest that salt bridges may be involved in fine-tuning the metastable capsid structure of EV1. By studying the EV1 structure, the distribution of possible salt bridges in the EV1 structure was shown to be in the interior of the capsid or buried within the capsid structure (Fig. 6A and B). Interestingly, the enterovirus uncoating intermediates reported were shown to have lost the internal protein VP4 (13), which mediates two interprotomer and one inter-VP salt bridge connection (Fig. 6C). It is thus tempting to speculate that the extraction of VP4 from the capsid particle might be controlled, at least partially, by salt bridges. In comparison to the native virion, the heat-induced uncoating intermediate of EV1 showed a small increase in protonated carboxylic acid stretching. Also, a small decrease in signals that could be assigned to fatty acids was detected. The disconnected salt bridges, together with the expelled fatty acid chains, are expected to shift the capsid dynamics into a more flexible motion as these constraints are removed.

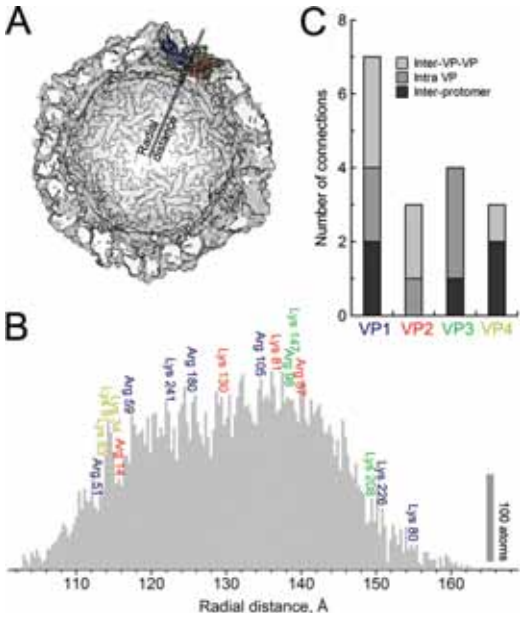

FIG 6 Radial distribution of salt bridge donors in EV1 protomer. (A) Single-protomer (colored) positioning with respect to the whole capsid (a half capsid is displayed). (B) The radial distribution of all atoms in EV1 protomer (PDB entry 1EV1) are depicted in the gray histogram to illustrate the density of the capsid shell. Colors indicate VP1 (blue), VP2 (red), VP3 (green), and VP4 (yellow), and the positioning of the salt bridge-forming amino acids (Lys and Arg) in a single protomer is shown, followed by their sequential positioning within these structural proteins. (C) The distribution of the salt bridge donors shows various degrees of connectivity within and between protomers. Interestingly, the inner protein VP4 forms connections mainly between protomers and one inner VP-VP connection.

In addition to the changes in the capsid proteins, several heat-induced changes in the RNA signals were observed. In general, the changes are difficult to interpret as particular structural changes but are more like a general change of the solute-solvent interactions of the RNA molecule. In particular, the signal variation at 783 cm^{-1} suggests that there are changes in the RNA solvation shell (39, 49). Both the ejection of genome and an increased permeability of the capsid structure could explain these changes in the signal sensitive to the environment of RNA. Still, a small increase in the A-form helix marker band at 811 cm^{-1} (39, 40) after heat treatment at 60°C also suggests that RNA is no longer bound by the intact capsid structure and refolds to the A-form double-helical structure.

In conclusion, we were able to acquire signature Raman spectra that distinguish between intact and uncoated EV1 diluted in

buffer at relatively low concentrations. Very few vibrational spectroscopic data on the conformational changes during viral uncoating are available as yet. The observed Raman signatures are in good agreement with the present knowledge of enteroviral uncoating. For example, a UV resonance Raman study comparing intact and empty bovine enterovirus particles (46) revealed increasing hydrophobicity of the virus, or moving of Trp residues to increasingly hydrophilic environment during the viral opening process, consistent with our measurements. However, the detected differences between the intact virion in dried phase and in the liquid state indicate that the natural environment is essential in order to retain all the information from the uncoating process. Most biological macromolecules are physiologically active in aqueous solutions, and water molecules are thought to play a crucial role in the function and structure of biomolecules.

The Raman signatures of EV1 virion particles consist of numerous signals, with the most pronounced features being the following. The first is amide bands. The Am I became less broad after the uncoating process and revealed a decrease of α-helical structures and an increase of irregular structures or β-sheets. The second such feature is aromatic amino acids. The vibration modes of tryptophan and tyrosine residues suggest loosening of the capsid structure with increasing hydrophilicity around these residues. Third is chemical changes in the virion particles. The carbonyl vibrations showed small changes between the native virion and the heated particles, which indicates at least partial disruption of salt bridges. The fourth feature is genome signals. RNA signatures indicate both changes in the environment of the genome and a change in RNA conformation.

The observed differences in the Raman spectra between the intact and uncoated virions give novel insight into the structural changes occurring during virus opening. Most probably, findings would be similar for the enteroviruses that are close relatives of EV1. The prominent Raman marker bands of the intact virion, intermediate uncoating state of the virion, and disrupted virion particles presented here also enable *in vivo* studies of factors leading to viral uncoating in cellular structures with Raman mapping and coherent anti-Stokes Raman scattering microscopy.

ACKNOWLEDGMENTS

This research was supported by the Academy of Finland (134061 and 257125) and the National Doctoral Programme in Nanoscience (NGS).

We thank Alli Liukkonen, Eila Korhonen, and Arja Mansikkaviita for practical help, together with Tommi Isoniemi for supportive studies. Thomas Huser, Mika Pettersson, Olli Pentikäinen, and Vesa Aho are warmly appreciated for valuable discussions.

REFERENCES

1. **Tuthill TJ, Groppelli E, Hogle JM, Rowlands DJ.** 2010. Picornaviruses. Curr. Top. Microbiol. Immunol. **343:**43–89. http://dx.doi.org/10.1007/82_2010_37.
2. **Hober D, Sauter P.** 2010. Pathogenesis of type 1 diabetes mellitus: interplay between enterovirus and host. Nat. Rev. Endocrinol. **6:**279–289. http://dx.doi.org/10.1038/nrendo.2010.27.
3. **Roivainen M, Alfthan G, Jousilahti P, Kimpimaki M, Hovi T, Tuomilehto J.** 1998. Enterovirus infections as a possible risk factor for myocardial infarction. Circulation **98:**2534–2537. http://dx.doi.org/10.1161/01.CIR.98.23.2534.
4. **Fry EE, Stuart DI.** 2010. Virion structure, p 59–71. *In* Ehrenfeld E, Domingo E, Roos RP (ed), The picornaviruses. ASM Press, Washington, DC.
5. **Brandenburg B, Lee LY, Lakadamyali M, Rust MJ, Zhuang X, Hogle JM.** 2007. Imaging poliovirus entry in live cells. PLoS Biol. **5:**1543–1555. http://dx.doi.org/10.1371/journal.pbio.0050183.
6. **Karjalainen M, Rintanen N, Lehkonen M, Kallio K, Mäki A, Hellström K, Siljamäki V, Upla P, Marjomäki V.** 2011. Echovirus 1 infection depends on biogenesis of novel multivesicular bodies. Cell. Microbiol. **13:**1975–1995. http://dx.doi.org/10.1111/j.1462-5822.2011.01685.x.
7. **Curry S, Chow M, Hogle JM.** 1996. The poliovirus 135S particle is infectious. J. Virol. **70:**7125–7131.
8. **Bubeck D, Filman DJ, Cheng N, Steven AC, Hogle JM, Belnap DM.** 2005. The structure of the poliovirus 135S cell entry intermediate at 10-angstrom resolution reveals the location of an externalized polypeptide that binds to membranes. J. Virol. **79:**7745–7755. http://dx.doi.org/10.1128/JVI.79.12.7745-7755.2005.
9. **Lin J, Cheng N, Chow M, Filman DJ, Steven AC, Hogle JM, Belnap DM.** 2011. An externalized polypeptide partitions between two distinct sites on genome-released poliovirus particles. J. Virol. **85:**9974–9983. http://dx.doi.org/10.1128/JVI.05013-11.
10. **Levy HC, Bostina M, Filman DJ, Hogle JM.** 2010. Catching a virus in the act of RNA release: a novel poliovirus uncoating intermediate characterized by cryo-electron microscopy. J. Virol. **84:**4426–4441. http://dx.doi.org/10.1128/JVI.02393-09.
11. **Bostina M, Levy H, Filman DJ, Hogle JM.** 2011. Poliovirus RNA is released from the capsid near a twofold symmetry axis. J. Virol. **85:**776–783. http://dx.doi.org/10.1128/JVI.00531-10.
12. **Chow M, Newman JFE, Filman D, Hogle JM, Rowlands DJ, Brown F.** 1987. Myristylation of picornavirus capsid protein VP4 and its structural significance. Nature **327:**482–486. http://dx.doi.org/10.1038/327482a0.
13. **Fricks CE, Hogle JM.** 1990. Cell-Induced conformational change in poliovirus: externalization of the amino terminus of VP1 is responsible for liposome binding. J. Virol. **64:**1934–1945.
14. **Racaniello VR.** 1996. Early events in poliovirus infection: virus-receptor interactions. Proc. Natl. Acad. Sci. U. S. A. **93:**11378–11381. http://dx.doi.org/10.1073/pnas.93.21.11378.
15. **Smyth M, Pettitt T, Symonds A, Martin J.** 2003. Identification of the pocket factors in a picornavirus. Arch. Virol. **148:**1225–1233. http://dx.doi.org/10.1007/s00705-002-0974-4.
16. **Smyth MS, Martin JH.** 2002. Picornavirus uncoating. Mol. Pathol. **55:**214–219. http://dx.doi.org/10.1136/mp.55.4.214.
17. **Tuma R.** 2005. Raman spectroscopy of proteins: from peptides to large assemblies. J. Raman Spectrosc. **36:**307–319. http://dx.doi.org/10.1002/jrs.1323.
18. **Hartman KA, McDonald-Ordzie PE, Kaper JM, Prescott B, Thomas GJ, Jr.** 1978. Studies of virus structure by laser-Raman spectroscopy. Turnip yellow mosaic virus and capsids. Biochemistry **17:**2118–2123.
19. **Li TS, Johnson JE, Thomas GJ, Jr.** 1993. Raman dynamic probe of hydrogen exchange in bean pod mottle virus: base-specific retardation of exchange in packaged ssRNA. Biophys. J. **65:**1963–1972.
20. **Li TS, Chen ZG, Johnson JE, Thomas GJ, Jr.** 1990. Structural studies of bean pod mottle virus, capsid, and RNA in crystal and solution states by laser Raman spectroscopy. Biochemistry **29:**5018–5026. http://dx.doi.org/10.1021/bi00473a004.
21. **Prescott B, Sitaraman K, Argos P, Thomas GJ, Jr.** 1985. Protein-RNA interactions in belladonna mottle virus investigated by laser Raman spectroscopy. Biochemistry **24:**1226–1231. http://dx.doi.org/10.1021/bi00326a026.
22. **Overman SA, Aubrey KL, Vispo NS, Cesareni G, Thomas GJ, Jr.** 1994. Novel tyrosine markers in Raman spectra of wild-type and mutant (Y21M and Y24M) Ff virions indicate unusual environments for coat protein phenoxyls. Biochemistry **33:**1037–1042. http://dx.doi.org/10.1021/bi00171a001.
23. **Overman SA, Thomas GJ, Jr.** 1995. Raman spectroscopy of the filamentous virus Ff (fd, fl, M13): structural interpretation for coat protein aromatics. Biochemistry **34:**5440–5451. http://dx.doi.org/10.1021/bi00016a015.
24. **Tuma R, Bamford J, Bamford D, Russell M, Thomas GJ, Jr.** 1996. Structure, interactions and dynamics of PRD1 virus II. Organization of the viral membrane and DNA. J. Mol. Biol. **257:**102–115. http://dx.doi.org/10.1006/jmbi.1996.0150.
25. **Fish SR, Hartman KA, Fuller MT, King J, Thomas GJ.** 1980. Investigation of secondary structures and macromolecular interactions in bacteriophage p22 by laser Raman spectroscopy. Biophys. J. **32:**234–327. http://dx.doi.org/10.1016/S0006-3495(80)84945-9.
26. **Aubrey KL, Casjens SR, Thomas GJ, Jr.** 1992. Secondary structure and interactions of the packaged dsDNA genome of bacteriophage P22 inves-

tigated by Raman difference spectroscopy. Biochemistry **31:**11835–11842. http://dx.doi.org/10.1021/bi00162a023.
27. **Reilly KE, Thomas GJ, Jr.** 1994. Hydrogen exchange dynamics of the P22 virion determined by time-resolved Raman spectroscopy. Effects of chromosome packaging on the kinetics of nucleotide exchanges. J. Mol. Biol. **241:**68–82.
28. **Hogle JM, Chow M, Filman DJ.** 1985. Three-dimensional structure of poliovirus at 2.9 Å resolution. Science **229:**1358–1365. http://dx.doi.org/10.1126/science.2994218.
29. **Walter TS, Ren J, Tuthill TJ, Rowlands DJ, Stuart DI, Fry EE.** 2012. A plate-based high-throughput assay for virus stability and vaccine formulation. J. Virol. Methods **185:**166–170. http://dx.doi.org/10.1016/j.jviromet.2012.06.014.
30. **Abraham G, Colonno RJ.** 1984. Many rhinovirus stereotypes share the same cellular receptor. J. Virol. **51:**340–345.
31. **Reed LJ, Muench H.** 1938. A simple method of estimating fifty percent endpoints. Am. J. Hyg. **27:**493–497.
32. **Porterfield JZ, Zlotnick A.** 2010. A simple and general method for determining the protein and nucleic acid content of viruses by UV absorbance. Virology **407:**281–288. http://dx.doi.org/10.1016/j.virol.2010.08.015.
33. **Pettersen EF, Goddard TD, Huang CC, Couch GS, Greenblatt DM, Meng EC, Ferrin TE.** 2004. UCSF Chimera—a visualization system for exploratory research and analysis. J. Comput. Chem. **13:**1605–1612. http://dx.doi.org/10.1002/jcc.20084.
34. **McGregor S, Mayer HD.** 1968. Biophysical studies on rhinovirus and poliovirus. I. Morphology of viral ribonucleoprotein. J. Virol. **2:**149–154.
35. **Ren J, Wang X, Hu Z, Gao Q, Sun Y, Li X, Porta C, Walter TS, Gilbert RJ, Zhao Y, Axford D, Williams M, McAuley K, Rowlands DJ, Yin W, Wang J, Stuart DI, Rao Z, Fry EE.** 2013. Picornavirus uncoating intermediate captured in atomic detail. Nat. Commun. **4:**1929. http://dx.doi.org/10.1038/ncomms2889.
36. **Wang X, Peng W, Ren J, Hu Z, Xu J, Lou Z, Li X, Yin W, Shen X, Porta C, Walter TS, Evans G, Axford D, Owen R, Rowlands DJ, Wang J, Stuart DI, Fry EE, Rao Z.** 2012. A sensor-adaptor mechanism for enterovirus uncoating from structures of EV71. Nat. Struct. Mol. Biol. **19:**424–429. http://dx.doi.org/10.1038/nsmb.2255.
37. **De Gelder J, De Gussem K, Vandenabeele P, Moens L.** 2007. Reference database of Raman spectra of biological molecules. J. Raman Spectrosc. **38:**1133–1147. http://dx.doi.org/10.1002/jrs.1734.
38. **Matthäus C, Bird B, Miljkovic M, Chernenko T, Romeo M, Diem M.** 2008. Infrared and Raman microscopy in cell biology. Methods Cell Biol. **89:**275–308. http://dx.doi.org/10.1016/S0091-679X(08)00610-9.
39. **Hobro AJ, Rouhi M, Blanch EW, Conn GL.** 2007. Raman and Raman optical activity (ROA) analysis of RNA structural motifs in domain I of the EMCV IRES. Nucleic Acids Res. **35:**1169–1177. http://dx.doi.org/10.1093/nar/gkm012.
40. **Hobro AJ, Standley DM, Ahmad S, Smith NI.** 2013. Deconstructing RNA: optical measurement of composition and structure. Phys. Chem. Chem. Phys. **15:**13199–13208. http://dx.doi.org/10.1039/c3cp52406j.
41. **Sane SA, Cramer SM, Przybycien TM.** 1999. A holistic approach to protein secondary structure characterization using amide I band Raman spectroscopy. Anal. Biochem. **269:**255–272. http://dx.doi.org/10.1006/abio.1999.4034.
42. **Barth A, Zscherp C.** 2002. What vibrations tell about proteins. Q. Rev. Biophys. **35:**369–430. http://dx.doi.org/10.1017/S0033583502003815.
43. **Siamwiza MN, Lord RC, Chen MC, Takamatsu T, Harada I, Matsuura H, Shimanouchi T.** 1975. Interpretation of the doublet at 850 and 830 cm-1 in the Raman spectra of tyrosyl residues in proteins and certain model compounds. Biochemistry **14:**4870–4876. http://dx.doi.org/10.1021/bi00693a014.
44. **Miura T, Takeuchi H, Harada I.** 1988. Characterization of individual tryptophan side chains in proteins using Raman spectroscopy and hydrogen-deuterium exchange kinetics. Biochemistry **27:**88–94. http://dx.doi.org/10.1021/bi00401a015.
45. **Schlamadinger DE, Gable JE, Kim JE.** 2009. Hydrogen bonding and solvent polarity markers in the UV resonance Raman spectrum of tryptophan: application to membrane proteins. J. Phys. Chem. B **113:**14769–14778. http://dx.doi.org/10.1021/jp905473y.
46. **Kaminaka S, Imamura Y, Shingu M, Kitagawa T, Toyoda T.** 1999. Studies of bovine enterovirus structure by ultraviolet resonance Raman spectroscopy. J. Virol. Methods **77:**117–123. http://dx.doi.org/10.1016/S0166-0934(98)00153-0.
47. **Miura T, Takeuchi H, Harada I.** 1989. Tryptophan Raman bands sensitive to hydrogen bonding and side-chain conformation. J. Raman Spectrosc. **20:**667–671. http://dx.doi.org/10.1002/jrs.1250201007.
48. **Takeuchi H.** 2003. Raman structural markers of tryptophan and histidine side chains in proteins. Biopolymers **72:**305–317. http://dx.doi.org/10.1002/bip.10440.
49. **Hernández B, Baumruk V, Leulliot N, Gouyette C, Huynh-Dinh T, Ghomi M.** 2003. Thermodynamic and structural features of ultrastable DNA and RNA hairpins. J. Mol. Struct. **651–653:**67–74. http://dx.doi.org/10.1016/S002202860(02)00627-0.
50. **Park ES, Boxer SG.** 2002. Origins of the sensitivity of molecular vibrations to electric fields: carbonyl and nitrosyl stretches in model compounds and proteins. J. Phys. Chem. B **106:**5800–5806. http://dx.doi.org/10.1021/jp0203043.
51. **Taha M, Ming-Jer L.** 2010. Interactions of TRIS [tris(hydroxymethyl) aminomethane] and related buffers with peptide backbone: thermodynamic characterization. Chem. Phys. **12:**12840–12850. http://dx.doi.org/10.1039/c0cp00253d.
52. **Allison SD, Dong A, Carpenter JF.** 1996. Counteracting effects of thiocyanate and sucrose on chymotrypsinogen secondary structure and aggregation during freezing, drying, and rehydration. Biophys. J. **71:**2022–2032. http://dx.doi.org/10.1016/S0006-3495(96)79400-6.
53. **Lu X, Liu Q, Benavides-Montano JA, Nicola AV, Aston DE, Rasco BA, Aguilar HC.** 2013. Detection of receptor-induced glycoprotein conformational changes on enveloped virions by using confocal micro-Raman spectroscopy. J. Virol. **87:**3130–3142. http://dx.doi.org/10.1128/JVI.03220-12.
54. **Shanmukh S, Jones L, Driskell J, Zhao Y, Dluhy R, Tripp RA.** 2006. Rapid and sensitive detection of respiratory virus molecular signatures using a silver nanorod array SERS substrate. Nano Lett. **6:**2630–2636. http://dx.doi.org/10.1021/nl061666f.
55. **Joisson C, Kuster F, Plaué S, Van Regenmortel MH.** 1993. Antigenic analysis of bean pod mottle virus using linear and cyclized synthetic peptides. Arch. Virol. **128:**299–317. http://dx.doi.org/10.1007/BF01309441.
56. **Li TS, Chen ZG, Johnson JE, Thomas GJ, Jr.** 1992. Conformations, interactions, and thermostabilities of RNA and proteins in bean pod mottle virus: investigation of solution and crystal structures by laser Raman spectroscopy. Biochemistry **31:**6673–6682. http://dx.doi.org/10.1021/bi00144a006.
57. **Prestrelski SJ, Tedeschi N, Arakawa T, Carpenter JF.** 1993. Dehydration-induced conformational transitions in proteins and their inhibition by stabilizers. Biophys. J. **65:**661–671. http://dx.doi.org/10.1016/S0006-3495(93)81120-2.
58. **Filman DJ, Wien MW, Cunningham JA, Bergelson JM, Hogle JM.** 1998. Structure determination of echovirus 1. Acta Crystallogr. **54:**1261–1272.
59. **He Y, Liu S, Li J, Lu H, Qi Z, Liu Z, Debnath AK, Jiang S.** 2008. Conserved salt bridge between the N- and C-terminal heptad repeat regions of the human immunodeficiency virus type 1 gp41 core structure is critical for virus entry and inhibition. J. Virol. **82:**11129–11139. http://dx.doi.org/10.1128/JVI.01060-08.
60. **Rachakonda PS, Veit M, Korte T, Ludwig K, Böttcher C, Huang Q, Schmidt MF, Herrmann A.** 2007. The relevance of salt bridges for the stability of the influenza virus hemagglutinin. FASEB J. **21:**995–1002. http://dx.doi.org/10.1096/fj.06-7052hyp.
61. **Dolja VV, Boyko VP, Agranovsky AA, Koonin EV.** 1991. Phylogeny of capsid proteins of rod-shaped and filamentous RNA plant viruses: two families with distinct patterns of sequence and probably structure conservation. Virology **184:**79–86. http://dx.doi.org/10.1016/0042-6822(91)90823-T.
62. **Gertsman I, Fu CY, Huang R, Komives EA, Johnson JE.** 2010. Critical salt bridges guide capsid assembly, stability, and maturation behavior in bacteriophage HK97. Mol. Cell. Proteomics **9:**1752–1763. http://dx.doi.org/10.1074/mcp.M000039-MCP201.